Title

Command Modification Using Input Shaping for Automated Highway Systems with Heavy Trucks

Authors

Bae, Hong S.
Gerdes, J. Christian

Publication Date

2004-12-01

CALIFORNIA PATH PROGRAM
INSTITUTE OF TRANSPORTATION STUDIES
UNIVERSITY OF CALIFORNIA, BERKELEY

Command Modification Using Input Shaping for Automated Highway Systems with Heavy Trucks

Hong S. Bae, J. Christian Gerdes
Stanford University

California PATH Research Report
UCB-ITS-PRR-2004-48

This work was performed as part of the California PATH Program of the University of California, in cooperation with the State of California Business, Transportation, and Housing Agency, Department of Transportation; and the United States Department of Transportation, Federal Highway Administration.

Final Report for Task Order 4202

December 2004

ISSN 1055-1425

COMMAND MODIFICATION USING INPUT SHAPING FOR AUTOMATED HIGHWAY SYSTEMS WITH HEAVY TRUCKS

Hong S. Bae
J. Christian Gerdes
Department of Mechanical Engineering
Stanford University
Stanford, California 94305
August 2004

Contents

List of Tables

List of Figures

Abstract

Automated vehicles require sufficiently accurate system models in order to achieve a desired level of closed-loop performance in, for example, automated highways systems or smart cruise control systems. Parameters of the models are one of the important factors that determine the accuracy of system modeling and, eventually, the overall performance of the closed-loop system.

Current GPS sensing technology enables estimation of road grade and, consequently, simple treatment of parameter estimation from a static force balance. This work has demonstrated that road grade can be reliably estimated using synchronized two antennae GPS system or the vertical to horizontal velocity ratio from GPS speed measurements. While both methods provide similar performance in road grade estimation with comparable errors, the velocity-ratio based, single-antenna system is a better choice since it is more economical to implement than two-antenna system. Accurate estimation of road grade enables the estimations of other important vehicle parameters. With reliable and accurate road grade estimates and the assumption of low frequency dynamics, the vehicle mass estimates have been shown to converge quickly within $\pm 2\%$ and $\pm 5\%$ of the measured values for a passenger car and a heavy truck, respectively.

This work also presented a new method for maintaining and improving string stability by preventing actuator saturation in automated vehicles on highways. Instead of relying on feedback controllers to deal with the issue of actuator saturation after the fact, reference commands are fed through an FIR filter called an input shaper so that harmful components in the reference commands are reduced or removed. Input shaping is a command modification technique in which a reference command to a system is modified or shaped through convolution with an FIR filter. Original (unmodified) reference signals are passed through the input shaper and the shaped (modified) signals are then fed to the system. The purpose of this modification is to remove frequency content from the reference command that can produce oscillations in the closed-loop system due to lightly damped, flexible modes. With properly chosen impulses, the effect can be very significant.

Automated highway systems can benefit from input shaping. A platoon of automated vehicles can be thought of as a series of spring-mass-damper systems where vibration must be controlled for stable operation. For such systems, acceleration can be used for reference commands, but ideal signals must be modified to reflect performance limitations of a platoon of vehicles. A convex optimization approach to input shaper design that can capture time and frequency domain constraints such as engine saturation, maneuver end-point or ride quality is therefore quite useful. Input shapers designed with time and frequency domain constraints in convex optimization framework have been shown to prevent actuator saturation by dynamically bounding reference commands, and therefore, generating smooth trajectories that ultimately guarantee string stability.

Keywords

Advanced Vehicle Control Systems, Automated Highway Systems, Global Positioning Systems, Intelligent Vehicle Highway Systems, Longitudinal Control, Vehicle Follower control, Parameter Estimation, Command Modification, Input Shaping, String stability

Acknowledgements

This report is part of a large effort to develop control systems for automated highways systems under MOU 4202, 4211 and 4235. The authors would like to thank PATH research staff at Richmond Field Station and California Department of Transportation for hardware support in heavy truck testing.

Executive Summary

Automated vehicles require sufficiently accurate system models in order to achieve a desired level of closed-loop performance in, for example, automated highways systems or smart cruise control systems. Parameters of the models are one of the important factors that determine the accuracy of system modeling and, eventually, the overall performance of the closed-loop system.

Current GPS sensing technology enables estimation of road grade and, consequently, simple treatment of parameter estimation from a static force balance. This work has demonstrated that road grade can be reliably estimated using synchronized two antennae GPS system or the vertical to horizontal velocity ratio from GPS speed measurements. While both methods provide similar performance in road grade estimation with comparable errors, the velocity-ratio based, single-antenna system is a better choice since it is more economical to implement than two-antenna system.

In addition, GPS is used to generate an accurate elevation and/or road grade maps for future reference. Results show that these maps are comparable in accuracy to offline maps. When combined with inertial navigation sensors through Kalman filtering, GPS may also be used for dead reckoning purpose. This GPS/INS integration has been demonstrated experimentally to eliminate the problem of GPS signal loss due to the difficulty associated with maintaining the line of sight to satellites inherent in GPS navigation around urban environment.

Accurate estimation of road grade enables the estimations of other important vehicle parameters. With reliable and accurate road grade estimates and the assumption of low frequency dynamics, the vehicle mass estimates have been shown to converge quickly within $\pm 2\%$ and $\pm 5\%$ of the measured values for a passenger car and a heavy truck, respectively. Sum of drag force and rolling resistance has also been reliably estimated. However, separate estimation of them proved less successful.

This work also presented a new method for maintaining and improving string stability by preventing actuator saturation in automated vehicles on highways. Instead of relying on feedback controllers to deal with the issue of actuator saturation after the fact, reference commands are fed through an FIR filter called an input shaper

so that harmful components in the reference commands are reduced or removed. Input shaping is a command modification technique in which a reference command to a system is modified or shaped through convolution with an FIR filter. Original (unmodified) reference signals are passed through the input shaper and the shaped (modified) signals are then fed to the system. The purpose of this modification is to remove frequency content from the reference command that can produce oscillations in the closed-loop system due to lightly damped, flexible modes. With properly chosen impulses, the effect can be very significant.

Automated highway systems can benefit from input shaping. A platoon of automated vehicles can be thought of as a series of spring-mass-damper systems where vibration must be controlled for stable operation. For such systems, acceleration can be used for reference commands, but ideal signals must be modified to reflect performance limitations of a platoon of vehicles. A convex optimization approach to input shaper design that can capture time domain constraints such as engine saturation or maneuver end-point is therefore quite useful.

These previous formulations for designing input shapers, however, have included only time domain constraints such as acceleration or position requirements. It is sometimes desirable to have constraints specified in the frequency domain, for instance limiting input shaper gain at high frequencies. In other cases, constraints can only be effectively expressed in the frequency domain. A good example in the context of automated highways is ride quality, which is strongly frequency dependent. This work showed how such constraints can be added to the convex optimization framework in a systematic way.

Input shapers designed with time and frequency domain constraints in convex optimization framework have been shown to prevent actuator saturation by dynamically bounding reference commands, and therefore, generating smooth trajectories that ultimately guarantee string stability.

Chapter 1

Introduction

1.1 Overview of Automated Highways

The traffic congestion has long been a serious problem in most of cities in the world. The economic loss due to congestion problem was $66 billion in 1996 and $72 billion in 1999 [2]. This figure has grown to $80+ billion in 2004. This loss is combination of about 6.8 billion gallons of fuel wasted per year in idle (more than twice the amount 15 years ago) and 2.5 billion hours of potential productivity lost. In a more tangible numbers, a typical driver in Los Angeles, California is estimated to lose $1,370 through wasted fuel and increased travel time. The problem is that there is not enough land space to build more roads to relieve traffic congestion problem. Instead, more vehicles can be packed on existing roads if vehicles can travel closer to each other and safely, which can be achieved with automated highway systems.

Automated Highways Systems (AHS) is a general concept that ranges from enabling the autonomous intelligence in the vehicle [57, 17], to allowing the highway infrastructure to have full control over the vehicles [10]. The California Partners for Advanced Transit and Highways (PATH) Program aims for a compromise between these two extremes [34]. It envisions platoons or convoys of vehicles coordinated by the highway infrastructure. Each platoon will receive information such as speed, lane assignment, maximum number of vehicles in the platoon, etc. The cars in each platoon are linked electronically with range and range-rate sensors and inter-vehicle

communications. Each vehicle is then responsible for maintaining a certain speed and distance from the vehicles in front of and behind it through actuators (brake and throttle).

The idea of automated highway systems has been around for a while. One of the first concepts was presented by General Motors at 1939 World's Fair in New York [39]. In 1940's, the idea of multi-vehicle pallets was conceived which is essentially conveyor belt systems or, moving sidewalk systems and suffers from the same characteristics such as inflexibility and inefficiency. In 1960's, mechanical entrainment was tried, which also proved time-consuming, inefficient and inflexible to mechanically link vehicles. Other studies performed in the 1960s were intended to investigate the feasibility of an automated highway system and the potential benefits over human drivers [7, 24]. Interest in this area, however, saw a decline in the following decade due to lack of enabling technologies.

In recent years (1980-90's), the interest in automated highways has resurrected thanks to the advancements in electronics. The automated highway has the potential to increase the highway capacity from today's 2000 passenger cars per lane per hour (pcplph) to 6000 pcplph, a 200% improvement. This increase is primarily due to the fact that by automating driving (little or no human driver duties), vehicles can be packed more closely. Furthermore, since most accidents (90%) are due to human error [9], relieving vehicle control from a human driver is also expected to reduce the number of accidents. This in turn will reduce accident-related congestions. Additionally, traffic congestion is expected to be reduced because lane changing will be reduced and optimized.

The idea of having platoons of closely packed vehicles with large inter-platoon distances is driven by the goal to increase capacity and improve safety. As Figure 1.1 shows, low relative-speed impacts occur either at very small or very large inter-vehicle distances [33]. It is interesting to notice that current inter-vehicle distances result in the highest relative-speed impact.

Operating the vehicles at the engine's optimum performance point is also expected to reduce both emissions and fuel usage. Reduced emissions and lower fuel consumption will also be the result of lower drag forced experienced by vehicles in a platoon

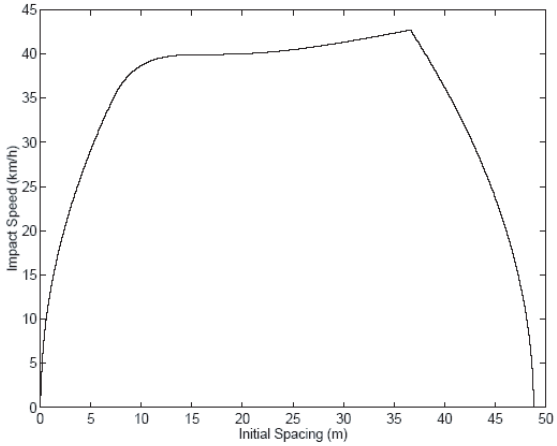

Figure 1.1: Collision speed relative to spacing at braking initiation.

[63]. According to [21], heavy trucks traveling in tandem may enjoy substantial benefits in terms of reduced drag. For steady travel (no acceleration/deceleration, no braking), a 25% overall drag saving would results in 15-20% fuel saving, depending on the truck loading. While these predictions are probably overly optimistic, some savings are certain.

Although this concept may seem futuristic, most of the actuators and sensors required for the longitudinal and lateral vehicle control are already commercially available on most vehicles. A complete survey of the work in this area can be found in [23, 50, 49].

1.1.1 AHS Research in the World

The United States and Japan have several programs aimed at developing the technology and cooperation among industries and government. In 1994, the U.S. Department of Transportation formed the National Automated Highway Systems Consortium (NAHSC) to investigate alternative AHS designs and to test some key elements of AHS technology [25]. In Japan the Vehicle, Road and Traffic Intelligent Society (VERTIS) was created in January 1994 with the participation of academia and industries and backed by five government organizations [29, 54].

In Europe, the emphasis has been mostly on driver's aides. The Program for European Traffic of Highest Efficiency and Unprecedented Safety (PROMETHEUS) was stared in October 1997 by 18 European car makers [15]. The project has currently evolved into a program called Dedicated Road Infrastructure for Vehicle Safely in Europe (DRIVE) and is sponsored by the 19-country consortium (Organization for European Research and Technological Cooperation). Automated highways, in different incarnations, is thus seen as the next logical step in improving personal and cargo transit.

1.1.2 Different Research Areas in AHS

The collective ideas in AHS is called Intelligent Vehicle Highway Systems (IHVS). There are mainly 5 different areas of research in IHVS:

- Advanced traffic management systems (ATMS) that aim to increase traffic flow through real-time traffic monitoring and ramp management.
- Advanced public transportation systems (APTS) that aim to increase efficiency of public transportation systems through intelligent planning of buses, trains, subways and taxies.
- Advanced traveler information systems (ATIS) that help travelers with pre-trip planning, route guidance, navigation, real-time traffic information and service information such as restaurants.
- Advanced vehicle control systems (AVCS) that utilize sensors and actuators on vehicles for some sort of automatic operation such as smart cruise control, collision avoidance, platooning and auto-pilot.
- Commercial vehicle operations (CVO), in conjunction with AVCS improve large commercial vehicle fleet operations with real-time vehicle tracking, routing, distribution planning and weigh-in-motion.

This report focuses on AVCS and CVO.

1.2 AHS and Heavy Vehicles

Commercial heavy vehicles, unlike passenger vehicles, display huge variation in parameters such as vehicle mass. Coupled with lower actuation authorities (engine and brake capabilities), these variations can induce actuator saturation even in moderately demanding maneuvers. Thus, variations in the open-loop vehicle performance present a challenge to the task of maintaining string stability in a platoon formation. A new control scheme is proposed to put on-line bounds, or artificial saturation, on command signals via parameter estimation such that all members in a platoon can follow the reference commands without saturating actuators. This paper describes the rationale, structure and potential benefits behind such a scheme.

Advanced vehicle control systems (AVCS) and automated highway systems (AHS) – with the goal of increasing traffic capacity of existing roads through intelligent coordination of vehicles and highway automation – have seen significant progresses in the past decade. While previous efforts have been focused on automation of passenger cars, the efforts of AVCS and AHS research and development activity are now shifting towards commercial heavy trucks due to feasibility of implementation and economic benefits.

As mentioned earlier, one of the most promising strategies for AHS is the concept of platoon operation [38, 37, 22]. A platoon consists of a number of vehicles traveling at a high speed, with a small inter-vehicle spacing. In addition to reduced driver fatigue due to automation, platoon operation of heavy trucks also provides an economic incentive in the form of lower fuel cost due to lower air drag resistance in a long stream of trucks. Moreover, the concept of a platoon is more feasible with heavy trucks than passenger cars since heavy trucks tend to spend a majority of travel time on highways and follow well-established routes [62].

In order for the platoon operation to be useful, the vehicles in the platoon should travel with a small inter-vehicle spacing for higher traffic throughput. Therefore, the longitudinal controller has to provide not only asymptotic stability - where relative speed and inter-vehicle spacing are ensured to go to zero - but also guarantee a property known as string stability. With string stability, disturbances in inter-vehicle

spacing upstream in the platoon will be attenuated as they propagate downstream. Since it was established that constant inter-vehicle spacing cannot provide string stability without additional information [38], many inter-vehicle spacing policies have been devised. For example, inter-vehicle communication has been used to ensure string stability by transmitting the velocity and acceleration of the lead vehicle to followers [37]. Speed dependent spacing policies where time headway term provides more spacing at higher speeds have also been used [12]. Nonlinear spacing policies that place different weights on control gains based on measurements of relative speed or spacing have been suggested [62].

Controller design methods such as fixed or adaptive gain PID have proven useful in highway automation [37]-[62]. However, these are based on the assumption that the system to be controlled is constant, i.e. plant parameters are known and do not change much over time. Although controllers can be designed to tolerate some variances in vehicle parameters, typical ranges of parameter variations in commercial heavy vehicles are well beyond what conventional controllers are capable of handling and may saturate actuation capabilities (engine and brake) to the point where the platoon operation results in instability. The issue of actuator saturation is of a particular concern if the concept of highway automation is to be useful in the real world where a platoon is composed of heavy vehicles that may have different open loop capabilities. Such a situation arises fairly easily if the leading vehicle in a platoon has a larger engine than the following vehicles and/or the following vehicles are hauling heavier cargo.

It is proposed that a better way of implementing longitudinal control is to incorporate the knowledge of physical actuation limits in all members of a platoon through parameter estimation so that string stability is preserved by avoiding actuator saturation.

On-line Parameter Estimation Four parameters play significant roles in the longitudinal dynamics of highway automation: vehicle mass, road grade, aerodynamic drag, and rolling resistance. Their qualitative characteristics are shown in Table 1. The first column lists the four parameters. The second column indicates the extent to which parameter change produce performance variations and the third column lists

Table 1.1: Vehicle parameters and Loads

Parameter	Impact	Over time
Vehicle Mass	Large	Slow
road Grade	Medium/large (0.14g)	Fast
Air Drag ($C_d = 0.85 \sim 1.5$, Area $= 12m^2$)	Medium (0.02-0.04g)	Fast
Rolling Resistance	Small (0.01g)	Medium
Engine output at 55 mph (25 m/s)	0.035g	

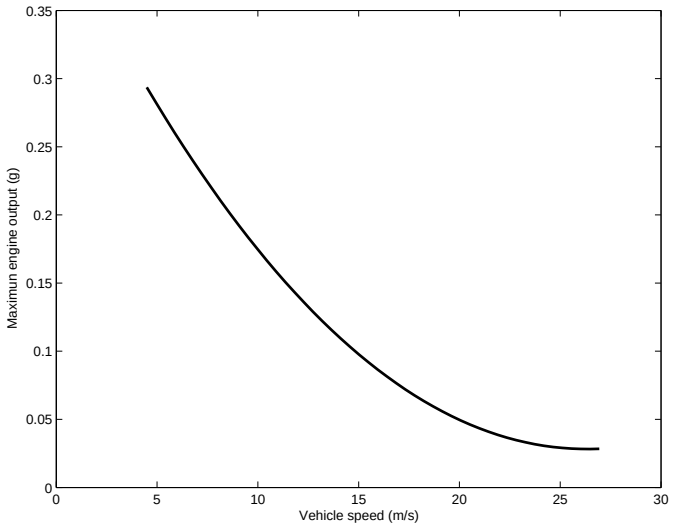

Figure 1.2: Typical maximum output of a heavy truck engine (500 hp) vs. vehicle speed. Note the low acceleration level at highway speeds ($20 \sim 25m/s$).

parameter variation over time during the course of a trip. For example, the vehicle mass, while not changing very much once on the road, has a strong influence on the longitudinal dynamics. In comparison, road grade variations have a similar effect and may change quickly over time.

Among these parameters, vehicle mass is of the most importance since it has the most impact in longitudinal performance and potentially very large changes. It is not unusual to see the variation up to 500 % in operating mass (from unloaded mass of 7500 kg to fully loaded mass of 37000 kg, or from low density cargo to high density cargo). On the other hand, it is easiest to estimate the vehicle mass due to its slowly time-varying nature.

Road grade changes are the second most important parameter to be estimated. For example, if the road grade information is not taken into account, the leading vehicle may out-accelerate the followers on an uphill road. Then, platoon formation may break down since the followers cannot maintain desired spacing from the leader. A modest road grade (4deg uphill) can be a dominant load source compared to air drag and rolling resistance. An 8deg uphill (maximum allowable grade in California highway construction) presents even stronger challenges [35]. This is equivalent to having a load of 0.14g (normalized to units of acceleration). Since the maximum acceleration of a typical loaded heavy vehicle is roughly 0.3g at low speed, road grade can be problematic in terms of avoiding engine output saturation, especially combined with uncertainty in the vehicle mass.

The loads on heavy vehicles mentioned above are important issues because of relatively low reserve powers on heavy truck. When traveling at highway speed, loaded heavy trucks often have 0.05g or less of acceleration capability as shown in Figure 1.2 [19] and approximated by the simple relationship:

$$P_{engine} = F_{engine} V \tag{1.1}$$

where

$$P_{engine} = \text{engine power output} \tag{1.2}$$

$$F_{engine} = \text{engine force output} \tag{1.3}$$

$$V = \text{vehicle speed} \tag{1.4}$$

Because of this low actuation authority, loading conditions that are not issues to passenger cars become a challenge for heavy trucks. The amount of variation in the road loads can exceed the overall actuation capability of the engine at highway speeds. Engine outputs can thus be easily saturated if commands are not properly generated or maneuvers not carefully coordinated to reflect these limits. When actuators saturate, the followers may not be able to keep with the leader, dropping back significantly. This in turn would cause overshoots in relative spacing and velocity,

resulting in string instability and possibly a collision. Therefore, avoiding actuator saturation is especially important in heavy truck platooning. Although smart nonlinear control schemes such as in [61, 62] may reduce integrator windup and controller overshoot, actuator saturation cannot be systematically avoided without careful planning of vehicle maneuvers.

In short, heavy trucks are more susceptible to actuator saturations that may cause instability in platooning. Parameter estimation can provide a better understanding of the system limits and loads, enabling the modification of raw trajectory commands into a reachable set of commands.

1.3 Report Overview

Chapter 2 describes parameter identification techniques and experimental results.

Chapter 3 lists platoon models, spacing and control laws used and other assumptions.

Chapter 4 discusses a new input shaping method for command modification through convex optimization technique.

Chapter 5 summarizes the work and discusses future research directions.

Appendix lists notations used in this report and includes relevant information.

Chapter 2

Parameter Estimation

2.1 Introduction

Longitudinal control systems such as adaptive cruise control [61], predictive cruise control system [1] [30], or spacing control on an automated highway [62] require accurate models of a vehicle's longitudinal dynamics to achieve desired levels of safety and closed-loop performance. While basic models of longitudinal dynamics are well established and straightforward, the exact parameters of the models are rarely known. This uncertainty limits the accuracy of the system models and, ultimately, overall performance of closed-loop system. Since these parameters are many times not known in advance, they must be successfully identified while the vehicles are in operation in order to prevent such limitations. This is particularly important for automated highways where a number of vehicles may form a platoon and uncertainties can propagate as disturbances migrate down the platoon.

Parameter variation plays an even larger role in automated control of heavy commercial vehicles (trucks, tractor-trailers and buses). Heavy vehicles generally exhibit larger variations in parameters such as vehicle mass (up to 500% differences between loaded and unloaded configurations) and aerodynamic drag than do passenger cars [13, 14, 53]. These facts highlight the need for estimation of mass and drag forces on

[1] A predictive cruise control system varies the vehicle speed around the cruise control set speed within a defined speed band in an effort to, for example, reduce fuel consumption.

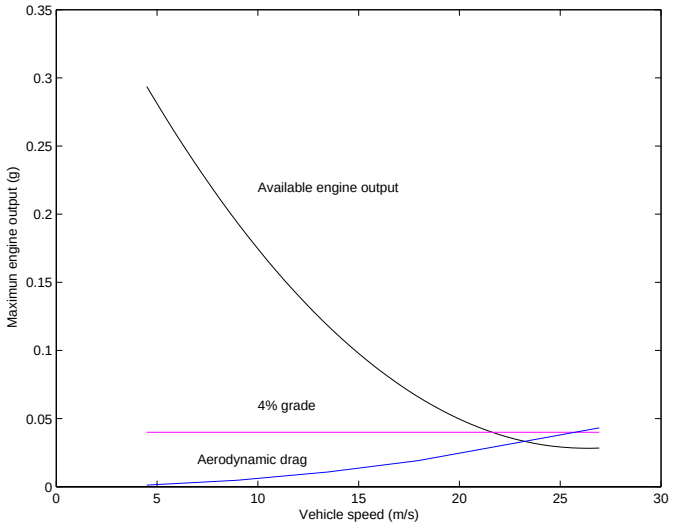

Figure 2.1: Comparison of forces in longitudinal heavy truck dynamics. Forces are normalized by weight and presented in units of acceleration for intuition.

a heavy vehicle.

Another variable that has a profound effect on vehicle performance is the road grade. Modest road grades may prove to be quite a challenge for vehicles with low power-to-weight ratio such as automated commercial heavy vehicles. Figure 2.1 shows the relative capability of a heavy truck engine and the demands from grade and aerodynamics as a function of speed. At highway speeds (about 20 m/s), a typical commercial heavy vehicle has little capability for acceleration in reserve since most of the engine output must go to counteract aerodynamic drag and rolling resistance. A 4% road grade can be a severe loading to such vehicles. This is why, in most cases, heavy vehicles have to slow down considerably going up steep grades, sacrificing speed in order to get more power from the engine. A map-based system such as lookup table format could be used to get road grade information. However, disadvantages are 1) such systems are typically not available, 2) if available, such systems may require a rather large database storage and constant update of database, 3) and sometimes available maps are not accurate enough to be useful.

The need for parameter identification can be further emphasized by considering the reserve acceleration available to heavy vehicles [3]. The acceleration capability of

a heavy vehicle can be used for several purposes: overcoming road loads (grade, rolling resistance and aerodynamic drag), maneuvering (trajectory following) and correcting for spacing or parameter errors (control authority). Since grade is set by the road, the vehicle has no choice but to devote sufficient capacity to overcome this load. If the vehicle capabilities are not known with sufficient accuracy, vehicle maneuvers may be planned based on the incorrect knowledge of vehicle performance. For example, imagine that a platoon of automated vehicles is traveling in a pack on a highway with close inter-vehicle spacing. If most of vehicle acceleration is used for maintaining tight inter-vehicle spacing in a platoon, vehicles in the platoon will certainly not be able to go up a hill due to lack of any reserve engine power. Such poor planning can have devastating effects in case of incorrect assumption of braking performance, which may lead to vehicle collisions in a platoon. Therefore, the vehicle would cope better with road grade changes if acceleration and deceleration capabilities of the vehicle through parameter estimation are known with sufficient accuracy.

This chapter presents a system for estimating road grade, mass, rolling resistance and aerodynamic drag of a ground vehicle using values of engine torque calculated by the engine map, a Global Positioning System (GPS) receiver and, optionally, wheel speed or inertial sensors. Two approaches for obtaining the grade measurement are presented: using two GPS antennae with a synchronizing receiver to calculate the pitch angle of the vehicle and using a single GPS antenna to calculate the ratio of the vehicle's vertical velocity to its horizontal velocity. Both methods are demonstrated to produce reasonable measures for road grade variations experimentally. Integration of GPS and INS (Inertial Navigation Sensors such as accelerometers in this work) through Kalman filtering is then employed to circumvent GPS outage problems due to loss of GPS signal (e.g. overpass structures). Using this grade estimate, it is straightforward to estimate mass and drag terms and separate this latter term further into aerodynamic drag and rolling resistance.

Evidence in the following section shows that GPS alone can be a reliable source for road grade estimation, or could be used to create maps for elevation and grade. Once accurate road grade information is available in a timely manner, other vehicle parameters such as mass can be accurately estimated.

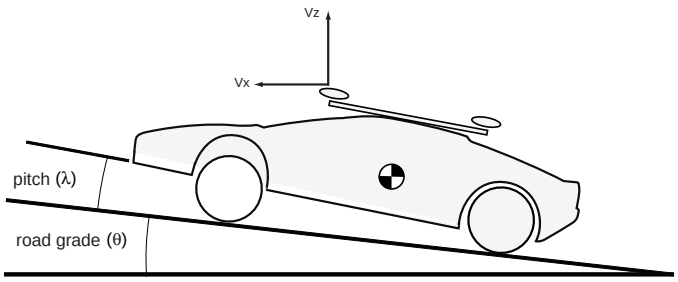

Figure 2.2: Two-antenna GPS setup on a car to measure vehicle pitch angle. Note two-antenna system measures combined quantity of road grade, θ and vehicle pitch angle, λ.

2.2 Road Grade Estimation

2.2.1 Estimation with GPS

GPS can be used to estimate road grade in two different ways, depending upon whether the system has a single antenna or two antennae. Figure 2.2 illustrates two GPS antennae mounted longitudinally on the roof of a vehicle, with a fixed baseline between antennae. By tracking the carrier phase at each antenna, the angle of this baseline relative to the horizontal can be measured. Since the antennae are fixed to the roof of the vehicle, the angle measured by the antenna is the sum of road grade (angle θ) and the pitch of the car (angle λ) which changes in response to acceleration, deceleration and high frequency road irregularities. Since the road grade changes much less rapidly than the pitch motion of the vehicle, the low frequency part of this signal can be assumed to be grade (with a constant bias due to antenna orientation). This method is called "two-antenna method" in this work. Alternately, the ratio of vertical velocity to horizontal velocity - both obtained from the GPS receiver - can be used to estimate grade. Equation 2.1 shows the relationship between road grade estimate and the velocity ratio. x and z refer to longitudinal and vertical directions, respectively. While the same low frequency assumptions hold, the velocity method is unbiased and can be implemented with a conventional GPS system using a single antenna. This method is called "single-antenna method".

$$\theta = \arctan\left(\frac{V_z}{V_x}\right) \tag{2.1}$$

Figure 2.3 shows estimates of road grade for a section of Highway 280 in California using both of these methods. Several things can be clearly seen in this plot. First, the characteristic frequency at which road grade is changing is substantially slower than the frequencies associated with motion of the suspension. Hence, this data supports the claim that grade information can be obtained from the low frequency content of either of two grade estimation methods. The two methods also produce rather similar results overall, though they differ in terms of how much oscillation in the measurement is produced by vehicle motion. During the first 45 seconds, the grade estimate from vehicle pitch measurement shows more pronounced oscillations than the estimate based upon velocity. This is a function of the large amount of vehicle pitch in the first part of this test produced by rapid periods of acceleration and deceleration. The second plot shows that the oscillations in pitch correlate with the acceleration of the vehicle. Since the single antenna method is based upon velocity measurement, it exhibits much less sensitivity to these motions. However, after the acceleration commands become more moderate (from 50 to 100s), the estimate based on velocity exhibits more variability. This is more clearly illustrated in Figure 4, which shows a Fourier transform of both signals during another test run representing normal driving. As can be seen, there is more power associated with higher frequency motions (0.5 - 2.5 Hz) in the grade estimate using single-antenna method. This follows from the fact that the pitch based measurement is insensitive to vertical motions of the vehicle, which appear as common mode disturbances, while the velocity based measurement assumes such motions are actually grade changes. From a performance standpoint, the choice of method represents a tradeoff between rejecting disturbances caused by vehicle bounce and those caused by vehicle pitch.

In addition, there are several other considerations in the choice of grade estimation approach. First, a single GPS antenna can be positioned anywhere on the roof while restrictions exist for a two-antenna system due to the fixed baseline requirement between two GPS antennae. Second, a single antenna system is more robust to

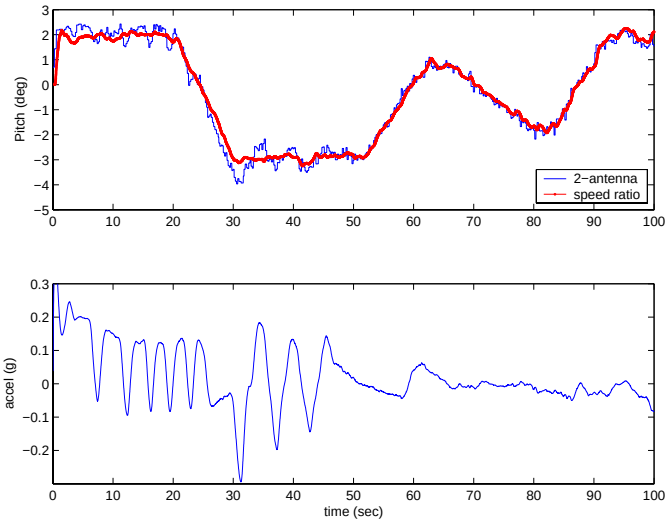

Figure 2.3: Plot of filtered (2-pole, 0.5 Hz Butterworth) pitch-derived road grade (Highway 280) using two-antenna GPS setup and speed ratio-derived road grade on a passenger car. Velocity ratio-based grade estimation shows less influence from contamination by pitch.

problems with multipath [2] or loss of satellite visibility since it does not need to resolve integer ambiguity [3] like a two-antenna system. Third, a single antenna system is more cost effective not only because merely one antenna is required, but also since a lower cost receiver can be used. In comparison, two-antenna method requires either differential GPS or synchronization of GPS signals collected at two antennae, which means, as used in this work, a more expensive receiver capable of such task is necessary. Finally, calculating grade from a single antenna using velocity eliminates the bias that arises from the installation of the two antennae (e.g. a heavy load in a wagon which causes a constant tilt along the pitch axis). Of course, both methods could be combined (e.g. through Kalman filters) to produce a measurement which balances sensitivity to pitch and bounce motions. Furthermore, if higher frequency grade information is desired, a Kalman filter structure could also be used to decouple

[2]Multipath is the corruption of the direct GPS signal by one or more signals reflected from the local surroundings. It occurs when GPS signal arrives at the receiving antenna from ore than one propagation route (multiple propagation paths).

[3]The unknown number of whole wavelengths of the carrier signal contained in an unbroken set of measurements from a single satellite at a single receiver.

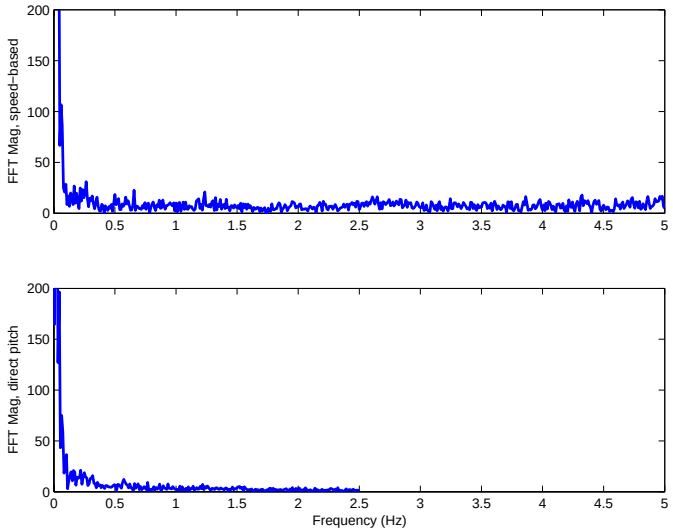

Figure 2.4: Frequency contents of road grade estimation (velocity-based, sampled at 10Hz and direct pitch, sampled at 5Hz) from GPS readings before filtering. Note that, as expected, most energy is concentrated at low frequencies (below 0.5 Hz).

the pitch motion from the longitudinal acceleration. As Figure 2.4 demonstrates, however, the road grade variation is concentrated at low frequencies below 0.5 Hz. Thus, simple low frequency filtering was deemed sufficient for this work.

2.2.2 Error Analysis of Grade Estimation Methods

Manufacturer-claimed and observed errors from the two-antenna GPS system in the work are about 0.4 deg and 0.2 deg, respectively. This section shows how velocity ratio based, single-antenna method fares, compared to two-antenna method.

Manufacturer-claimed and observed velocity errors from the single-antenna system are about $0.15m/s$ and $0.1m/s$, respectively. Applying the standard error analysis formula [4] on Equation 2.1,

[4] A useful fact: $\frac{d}{dx}\arctan(u) = \frac{1}{1+u^2}\frac{du}{dx}, -\frac{\pi}{2} < \arctan(u) < \frac{\pi}{2}$

$$\begin{aligned}\epsilon_\theta^2 &= \epsilon_{V_z}^2\left(\frac{d\theta}{dV_z}\right)^2 + \epsilon_{V_x}^2\left(\frac{d\theta}{dV_x}\right)^2 \\ &= \epsilon_{V_z}^2\left[\frac{1}{1+(V_z/V_x)^2}\cdot\frac{1}{V_x}\right]^2 + \epsilon_{V_x}^2\left[\frac{1}{1+(V_z/V_x)^2}\cdot\left(-\frac{V_z}{V_x^2}\right)\right]^2\end{aligned} \tag{2.2}$$

Given the observed performance data of $\epsilon_{V_x}, \epsilon_{V_x} \approx 0.1m/s$, $V_x \approx 20m/s$ and $V_z \approx 1m/s$,

$$\epsilon_{\theta,velocity} \approx 0.29\,\text{deg} \tag{2.3}$$

Thus, the single-antenna system has comparable grade estimation performance to more expensive two-antennae system.

Another potentially useful method to estimate road grade is to use the ratio of vertical-to-horizontal positions as opposed to velocity ratio, both using a single-antenna system. However, as the following error analysis shows, the position based estimation has a much bigger error. For a position based grade estimation,

$$\begin{aligned}\theta &= \arctan\left(\frac{z_\Delta}{x_\Delta}\right) \\ z_\Delta &= z(k+1) - z(k) \\ x_\Delta &= x(k+1) - x(k)\end{aligned} \tag{2.4}$$

Applying the same error analysis formula on Equation 2.4,

$$\begin{aligned}\epsilon_\theta^2 &= \epsilon_{z_\Delta}^2\left(\frac{d\theta}{dz_\Delta}\right)^2 + \epsilon_{x_\Delta}^2\left(\frac{d\theta}{dx_\Delta}\right)^2 \\ &= \epsilon_{z_\Delta}^2\left[\frac{1}{1+(z_\Delta/x_\Delta)^2}\cdot\frac{1}{x_\Delta}\right]^2 + \epsilon_{x_\Delta}^2\left[\frac{1}{1+(z_\Delta/x_\Delta)^2}\cdot\left(-\frac{z_\Delta}{x_\Delta^2}\right)\right]^2\end{aligned}$$

In this case, differential correction for position measurements is a must since the error in single position measurement from GPS is in the range of a few meters if not differentially corrected. Even with position measurements with good differential correction (DGPS) $\epsilon_{x_\Delta} \approx 0.02m, \epsilon_{z_\Delta} \approx 0.04m$, $x_\Delta \approx 2m$ (traveling at $20m/s$, sampled

at $10Hz$) and $z_\Delta \approx 0.10m$ (for about 3 deg of road grade),

$$\epsilon_{\theta,position} \approx 1.14\,\text{deg} \tag{2.5}$$

The error in road grade estimation using consecutive, differentially corrected position measurements is roughly three times larger than the error based on velocity ratio. Obviously, the velocity based road grade estimation does not need differential correction and is better than position based grade estimation.

2.2.3 Integration of GPS and Inertial Navigation Sensors for Dead Reckoning

Using the ratio of vertical to horizontal speeds has been shown as a reliable and accurate method to estimate road grade for highway automation as described in previous sections and in [5]. However, as discussed earlier and on highways in general, loss of GPS signals due to blockage of line of sight to GPS satellites by nearby structures such as overpasses at an intersection poses a challenge for longitudinal control in highway automation. Experiments performed in [55] show that, in urban conditions, the availability of GPS can be less than 50% of total time. Degradation of GPS can range from the error introduced by reflection of the satellite signals from the buildings (called multipath) to total unavailability in tunnels. Figure 2.5 shows that in the longitudinal speed measurement from GPS, taken on I-15 in San Diego, California, the longest outage lasts about 5 seconds (t = 432 to 438 seconds) before the GPS receiver reacquires the satellites.

2.2.4 Methodology

There are a few ways to deal with GPS outage. First, GPS data during outage may be just ignored and substituted with previous values before the outage. This is a viable option only when road grade is constant. Second, a simple moving average during the past set time period could be implemented. While this approach may be able to deal with slowly changing road grades, the advantage of simplicity disappears when used

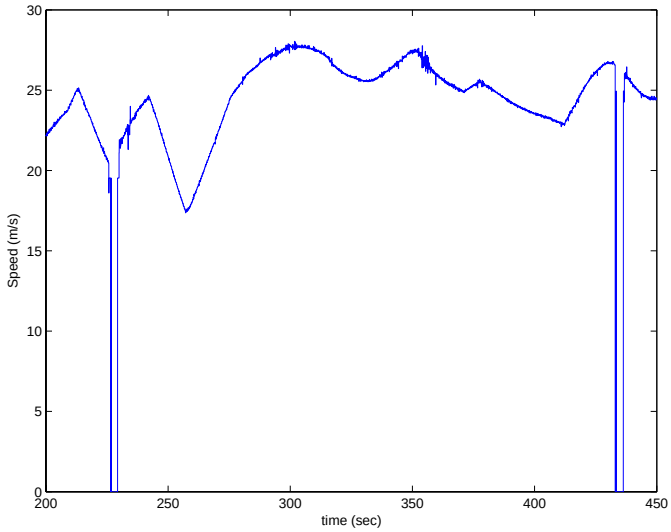

Figure 2.5: GPS outages on a highway (I-15 in California). The longest outage lasts as long as 5 seconds before reacquisition.

with a number of conditional statements to get around GPS outages. In addition, a long moving average to smooth out large jumps in GPS measurements would slow down road grade estimation significantly. Third, as in other GPS applications [28], INS (inertial navigation sensors) can be merged with GPS to sail through outages. This last method is described in detail.

2.2.5 GPS and INS Integration with Kalman Filter

A conventional Kalman filter framework is used in this research [18]. Vehicle velocity is calculated from integration of accelerometer measurements, recorded at a high sampling rate (250Hz). A Kalman filter is then used to correct the inherent errors in velocity estimates due to integration of the bias in accelerometer measurements with GPS updates which are sampled at a lower sampling rate (10 Hz).

The continuous time kinematic relationship between acceleration measurements and velocity can be modeled as

$$a_{z,m} = \dot{V}_z + a_{z,bias} + noise \tag{2.6}$$

where

$$\begin{aligned} V_z &= \text{Vertical speed} \\ a_{z,m},\ a_{z,bias} &= \text{Vertical accelerometer measurement and bias.} \end{aligned}$$

Therefore, the system model for time update is,

$$\begin{bmatrix} \dot{V}_z \\ \dot{a}_{z,bias} \end{bmatrix} = \begin{bmatrix} 0 & -1 \\ 0 & 0 \end{bmatrix} \begin{bmatrix} V_z \\ a_{z,bias} \end{bmatrix} + \begin{bmatrix} 1 \\ 0 \end{bmatrix} a_{z,m} \tag{2.7}$$

with

$$Q_k = Q = \begin{bmatrix} q_1 & 0 \\ 0 & q_4 \end{bmatrix}, \quad q_1, q_4 = \text{Variances in } V_z, a_{z,bias} \tag{2.8}$$

and, the measurement update is,

$$V_{z,m}^{GPS} = \begin{bmatrix} 1 & 0 \end{bmatrix} \begin{bmatrix} V_z \\ a_{z,bias} \end{bmatrix} + noise \tag{2.9}$$

where $V_{z,m}^{GPS}$ is vertical speed measurement from GPS.

This structure can be expanded to estimate longitudinal and lateral speed if necessary. However, they are omitted in this report since wheel speed is available and provides better information regarding longitudinal velocity. Details on expanding the Kalman filter structure for longitudinal and lateral speed estimation can be found in [36].

The design knobs are Q and R matrices. Actual inertial sensor and GPS measurement variances are used as a starting point. Then, these matrices are adjusted to get desired integration performance. For example, taking advantage of the special structure in the kinematic relationship in vertical accelerometer bias ($a_{z,bias}$) and Q, the vertical accelerometer bias can be adjusted to change slowly in time by lowering q_4. In addition, Q and R can also made varying if different weighting or confidence levels in measurement are desired, depending on GPS availability. In this work, the

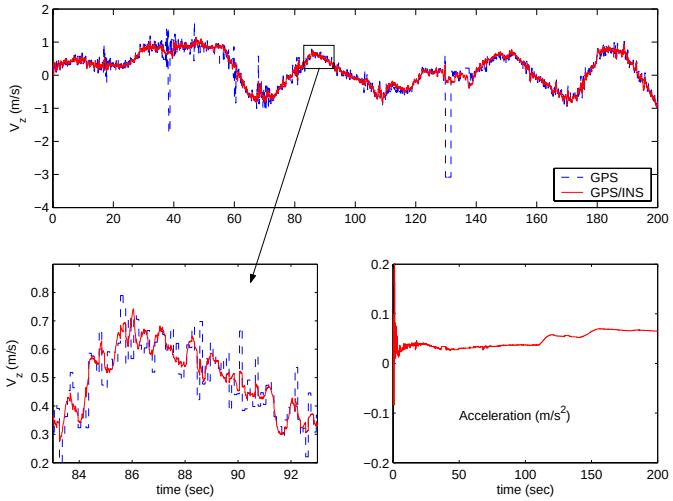

Figure 2.6: Estimation of V_z and $a_{z,bias}$. Raw GPS measurements (shown in lower left) are used for integration with inertial navigation sensors.

following values are used. Entries in Q matrix are smaller than R since the noise for time update (accelerometer) is actually smaller than the measurement update noise (GPS).

$$Q = \begin{bmatrix} 7.5 \times 10^{-4} & 0 \\ 0 & 1 \times 10^{-7} \end{bmatrix}, \quad R = 0.1$$

Results are shown in Figures 2.6 and 2.7 for a passenger car with a NovAtel OEM4 MiLLennium receiver on Highway 280 in northern California. Vertical acceleration and wheel speed are measured at 250 Hz while vertical speed from GPS is recorded at 10 Hz. Figure 2.6 also shows the Kalman filter output compared to the raw GPS vertical speed (zoomed-in raw GPS speed in the lower left plot). Jumps in vertical speed have now disappeared. Finally, road grade estimation from the ratio of vertical and longitudinal speeds (from wheel speed sensor) is shown in Figure 2.7. Most of high frequency, large magnitude spikes are now eliminated. Note that raw (instead of low-pass filtered) GPS measurements are used in the integration of sensors.

Once the GPS outage problem has been corrected, a road map for elevation or road grade can be created from GPS information. Figure 2.8 shows a plot of altitude

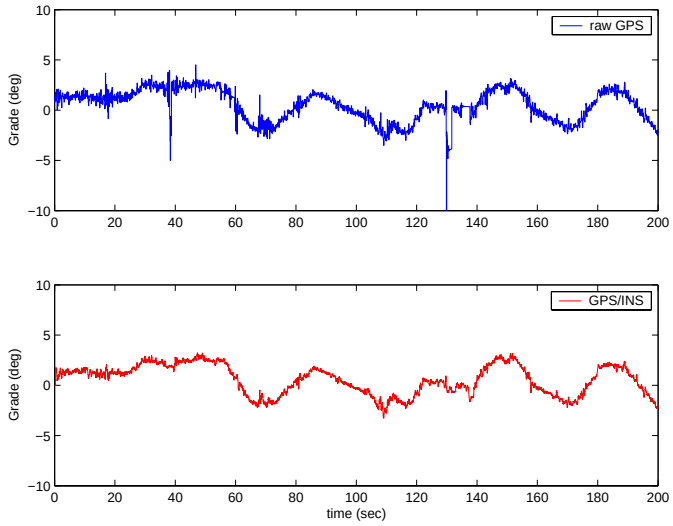

Figure 2.7: Grade estimations without and with INS integration. Spikes in GPS measurements (thus, in grade estimation) have been smoothed out.

changes for a section of a highway obtained by integrating the road grade from vertical and horizontal GPS velocity measurements over time. Comparison with available altitude measurements verifies that GPS can be a invaluable tool to create a map. Similarly, comparison of a known map and digital map created with grade estimation method described in previous sections is shown in Figure 2.9. It is important to note, however, that maps created with GPS represent the actual altitude information. In other words, the GPS-created maps are immune from discrepancy between the designed and the actual altitudes or grade after construction has finished.

In summary, combining inertial sensors and GPS signals presents a solution to GPS outage problem and errors due to drift in integrating inertial sensors. The integration structure is formulated in a Kalman filter framework. Disruptions in vertical speed measurements are eliminated through integration of GPS and inertial navigation sensors (vertical accelerometer) in Kalman filtering. Road grade can then be reliably estimated from the ratio of vertical speed (integration of GPS and inertial navigation sensors) to longitudinal speed (integration of GPS, inertial sensors and/or wheel speed sensor). Experimental work shows the road grade estimation with 0.3

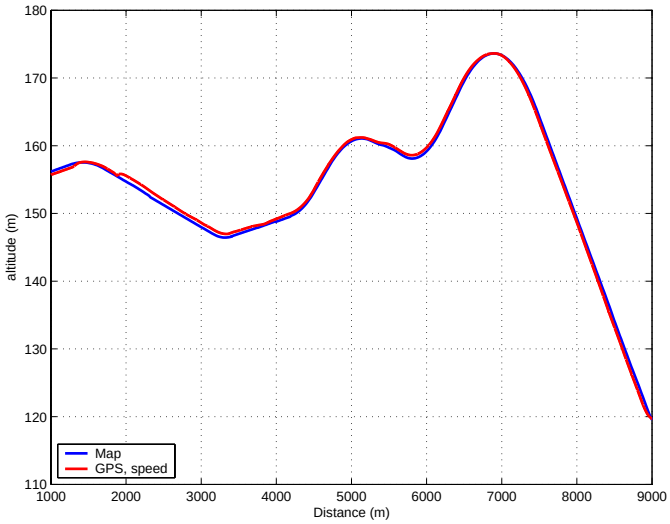

Figure 2.8: Comparison of GPS-integrated altitude with CalTrans map.

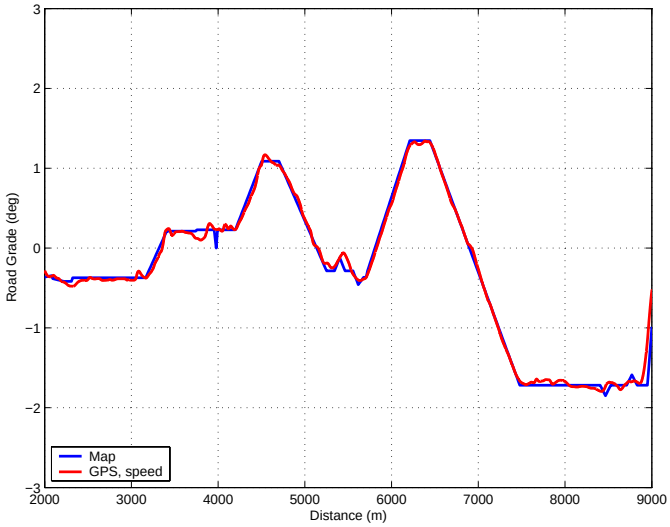

Figure 2.9: Comparison of GPS-integrated road grade with CalTrans map.

deg accuracy in a vehicle traveling at 50 mph.

2.3 Parameter Identification

2.3.1 Estimation Outline

The longitudinal vehicle dynamics can be modeled as in Equation 2.10.

$$m\ddot{x} = F_{engine} - F_{drag} - F_{\substack{rolling \\ resistance}} - F_{\substack{road \\ grade}} \tag{2.10}$$

Given measurements of longitudinal acceleration, engine output and road grade, the mass and the sum of the drag and rolling resistance can be identified by a simple least-squares fit to the experimental data. Acceleration can be obtained from an accelerometer or – in regions of low tire slip – through numerical differentiation of wheel speed sensors. As described in previous sections, GPS velocity is used for road grade estimation and numerical differencing may also be used to obtain acceleration directly from the GPS measurement. The measurement of the force produced by the engine is obtained directly from the engine map inside the engine controller and represents the "stock" estimate available on the vehicle.

Aerodynamic drag and rolling resistance cannot be distinguished in this approach if the vehicle moves at a constant speed. Since aerodynamic drag is a function of velocity, some variation in velocity is necessary to obtain an accurate estimation of drag coefficient. This would, in turn, produce a better estimate of rolling resistance.

Isermann demonstrated that the vehicle mass, aerodynamic drag and rolling resistance could be obtained on flat ground from measurements of acceleration and engine output [60]. However, the remaining unknown, road grade, has been mainly ignored in previous research. An exception to this has been an estimation scheme by [13] which estimates mass and grade while the vehicle is braking. As shown in Figure 1, forces from road grade play a major role in uphill sections, particularly for heavy trucks. Since road grade has the potential of completely overwhelming the engine capability of heavy trucks, particularly at highway speeds, knowledge of the grade is crucial in its own right for control of longitudinal vehicle dynamics in addition to

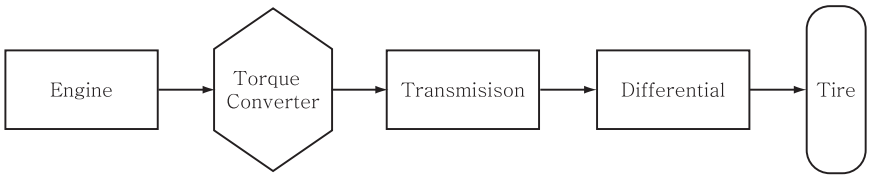

Figure 2.10: Engine torque flow diagram. Force on car is determined by several cascaded components.

being necessary for parameter estimation.

2.3.2 Estimation of Individual Unknowns

In this work, acceleration is derived through numerical differentiation of longitudinal velocity from GPS as well as front wheel speed. The engine force is calculated from the engine output torque as in Equation 2.11.

$$F_{engine} = \frac{T_{engine} \cdot N_{\substack{torque \\ converter}} \cdot N_{transmisison} \cdot N_{differential} \cdot f_{\substack{mechanical \\ loss}}}{R_{tire}} \tag{2.11}$$

The output torque should be adjusted with torque converter amplification ratio, transmission ratio, final differential ratio, tire radius and total mechanical efficiency, as illustrated in Figure 2.10, to find the force exerted on the car. The test vehicle used in this research had the torque converter ratio and the current gear available on the databus. The remaining ratios were determined from the vehicle specifications while the mechanical efficiency was adjusted experimentally, as described later.

To separate effects of aerodynamic drag from rolling resistance, aerodynamic drag is modeled as in Equation 2.12 where constants (air density, frontal area, and coefficient of drag) are lumped in C_{df} (drag factor),

$$F_{drag} = \frac{1}{2}\rho A C_d V^2 = C_{df} V^2 \tag{2.12}$$

Force from road grade is based on the GPS grade angle:

$$F_{\substack{road \\ grade}} = mg\theta \tag{2.13}$$

Rearranging the equations in a linear estimation format for one data point yields

$$F_{engine} = \begin{bmatrix} \ddot{x} + g\theta & V^2 & 1 \end{bmatrix} \begin{bmatrix} \hat{m} \\ \hat{C}_{df} \\ \hat{F}_{roll} \end{bmatrix} \tag{2.14}$$

For n data points, therefore,

$$z = H\hat{x} + noise \tag{2.15}$$

Then, z is $n \times 1$ vector of F_{engine} and H is $n \times 3$ matrix of acceleration, road grade and speed squared. In the current setup, m, C_{df} (drag factor), and F_{roll} are estimated, while the road grade angle is measured directly with a GPS receiver. The estimates is calculated in a batch process where a pseudo inverse of H is multiplied to z. A recursive method is used since it translates to on-line estimation of the parameters easily.

Parameters are assumed to be constants and the H matrix be noise free. While the vehicle mass and the drag factor are constants, rolling resistance is a nonlinear function of speed [1]. However, the estimation results show little effect from this simplification. Note also that F_{roll} in Equation 1 contains not only the rolling resistance forces but also any unmodeled dynamics such as aerodynamic forces from wind gust, engine friction, etc.

2.3.3 Experiments with Passenger Cars

Engine-related information (F_{engine}) is essential to parameter estimation. A Mercedes-Benz E320 wagon is used for this experiment. Since this vehicle incorporates various sensors for advanced vehicle stability control system, the information necessary for this work is available through the CAN (Control Area Network) databus. In this experiment, engine torque (T_{engine}), torque converter amplification ratio, front wheel speeds, and gear number (converted to gear ratio) are read from CAN. A NovAtel MiLLennium receiver is used for GPS measurements.

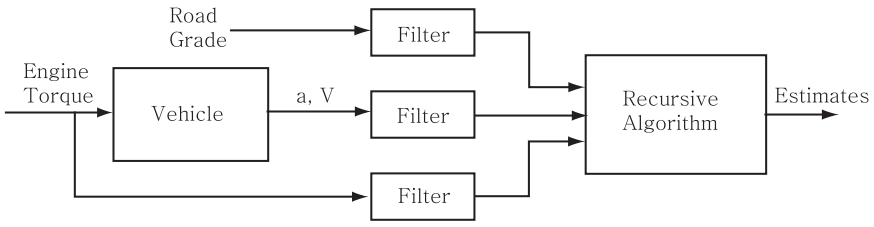

Figure 2.11: Input-output representation of signal flow.

2.3.4 Experimental Procedures and Assumptions

The experiments were performed under typical driving conditions. The vehicles were driven on relatively straight roads because the engine torque was assumed to be used only for longitudinal motion. Excessive wheel spins, such as tire slip during hard acceleration, were also avoided. Deceleration by pressing the brake pedal was avoided since the measurement of braking force was not available.

2.3.5 Algorithm and Data Processing

The signal flow is shown in Figure 2.11. Engine torque is the input to the system to be identified while speed and acceleration are the outputs. Using a typical engine map in a vehicle for transient operation could be problematic since it is steady-state data. Therefore, all engine map measurements are filtered through a second order Butterworth low pass filter with the cut-off frequency at 0.5 Hz in order to remove any unmodeled high frequency dynamics such as hydrodynamic coupling in torque converter. This is consistent with the understanding that the engine map is really only valid in steady-state operation. A recursive algorithm estimates vehicle mass, drag factor and rolling resistance based on the filtered version of input/output data and road grade.

2.3.6 Results and Discussion

The speed profile for parameter estimation is shown in Figure 2.12. A mix of acceleration of the vehicle followed by deceleration (letting the accelerator pedal up without

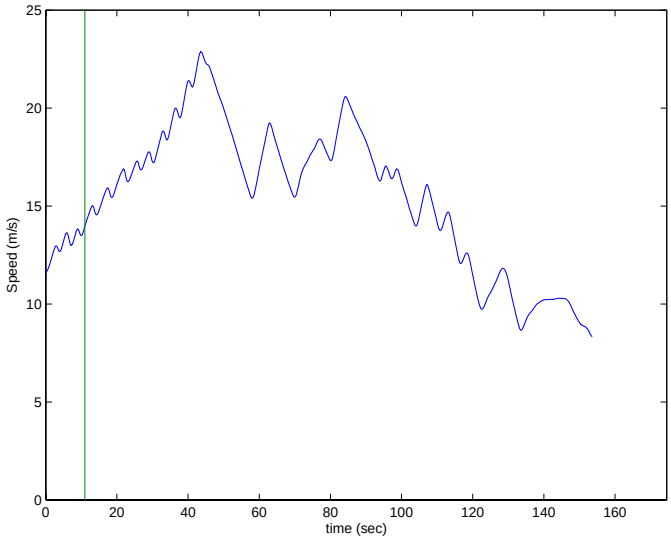

Figure 2.12: Horizontal speed profile for mass estimation. Note the repetition of acceleration and deceleration although estimated vehicle mass converged quickly (by t = 12 s) through recursive estimation algorithm.

engaging foot brake pedal) was repeated to simulate real world situations and generate excitation for judging the stability of the estimate. As Figure 2.13 illustrates, the mass estimate converged to a final value very quickly by t = 12 s as shown by a vertical line, negating the need for long periods of persistent excitation in the vehicle. The maneuver executed during the first 12 seconds would be similar to merging on a highway. This shows that mass estimation can be performed successfully with normal operation of a vehicle.

As Figure 2.13 shows, the estimated mass converges to within ± 2% error of the measured mass value. The 2% error range was chosen to be the threshold for good estimation since mechanical losses such as torque converter loss, transmission loss, or errors in engine map data cannot be accounted for perfectly. Obtaining this level of accuracy required scaling the mechanical loss factor to match the overall efficiency of the drivetrain, which would be known at least approximately by the manufacturer. To determine the amount of error that could arise due to changes in this value, the total mechanical loss factor was varied from 0.9 to 0.98 and a final value of 0.96 chosen. Different data sets with a fixed mechanical loss factor showed strong consistency with

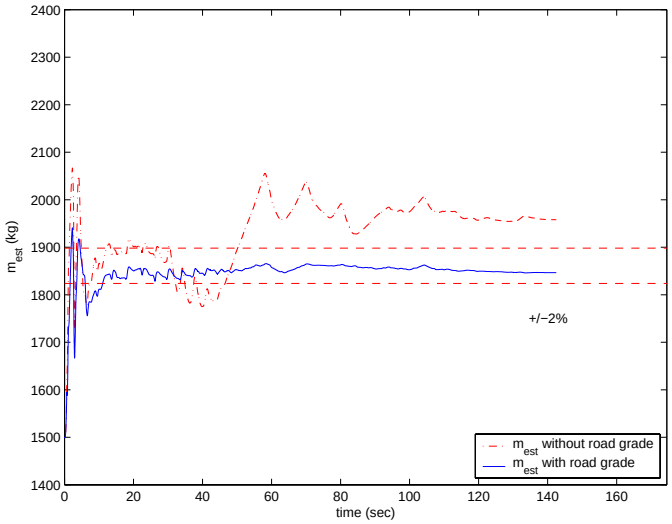

Figure 2.13: Recursive estimation of vehicle mass. The mass estimate converged to 2% of final value in 12 s.

standard deviation in errors of less than 1%. Furthermore, the total estimation errors stayed within ± 5% as the loss factor was varied within this range. The conclusion based upon this test vehicle is that mass estimation within 5% is clearly feasible with this method and that results within 2% are possible if some estimation of overall efficiency is available (from design data or periodic calibration with actual vehicle weight, for instance).

On the same plot, vehicle mass estimation without road grade information is also shown. Even the modest road slopes (maximum magnitude of 3 deg in Figure 2.3) were large enough to cause significant errors in mass estimation of a passenger vehicle. Without grade information, estimation of vehicle parameters using this method would contain an unacceptable level of error for control, or converge very slowly.

Unlike mass, estimates of drag factor and rolling resistance did not converge to constant values in Figure 2.15 although the estimates have the right orders of magnitude. With C_{df} of 0.7, C_d (drag coefficient) for the experimental vehicle with two GPS antennae on the roof is about 0.42 while C_d provided by the manufacturer is 0.34 [5]. As noted before, it is difficult to separate the drag and rolling resistance terms when

[5] $A_{frontal} = 1.7 \times 1.5m^2$, $\rho = 1.25kg/m^3$

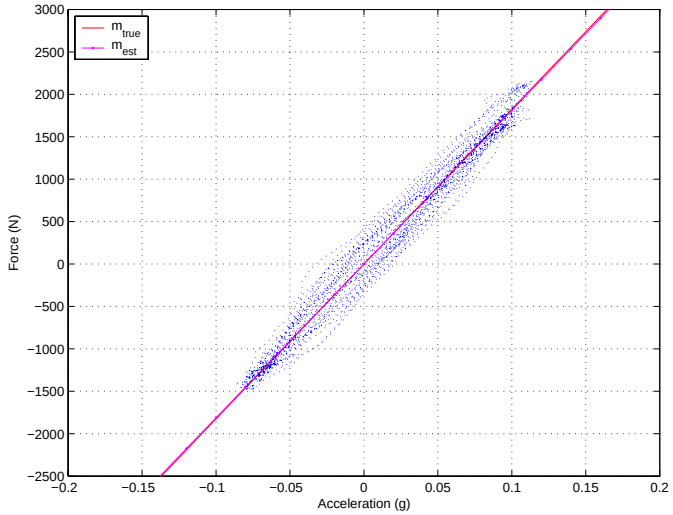

Figure 2.14: Plot of F_{engine} vs. acceleration. The filtered data are scattered in a cigar-like shape. The best fit in the sense of least squares is shown as a line going through the data points. The estimation error is about 2%.

the vehicle operates in a narrow speed range so these values will not exhibit the same accuracy as mass estimation under this approach. Obtaining more accurate measurement of the aerodynamic drag and rolling resistance by incorporating additional models represents an avenue for future work. In addition to factors affecting vehicles such as rolling resistance and drag forces, the ambient wind speed can affect truck loads, which may be estimated as well. However, it is typically of high frequency, and hence, estimating and trying to adapt to ambient wind variation is generally not very useful.

2.3.7 Experiments with Heavy Trucks

The same estimation scheme was tested on a tractor-trailer heavy truck. Since torque converter data was not accessible, a torque converter model is derived from one set of data runs. Only high (fourth and fifth) gear accelerations from different data runs are used in order to minimize the potentially unmodeled dynamics in the empirical torque converter model.

Unlike passenger cars, the vehicle mass of heavy trucks can certainly be measured

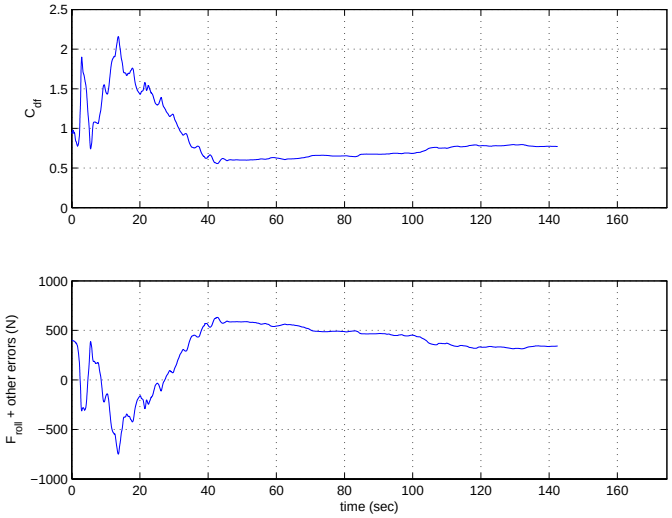

Figure 2.15: Plots of C_{df} and F_{roll} estimations. Note the complementary nature of two plots.

directly by other means such as scales at weigh-in-motion stations. However, there are cases where a heavy truck, departing from a distribution center located near a highway, wants to join a platoon of automated vehicles before passing through a weigh station. In such cases, the vehicle mass has to be known in order to join the platoon of automated trucks for a proper execution of platooning. Therefore, the capability to estimate the truck mass online quickly is very useful.

The results are exceptionally promising in that the mass estimation of a heavy truck converges to 5% of the final value within 25 seconds (Figure 2.16). The estimate takes longer to converge, possibly because of low excitation level feasible in heavy trucks, which could result in larger errors in final estimate. However, authors are confident that estimation of truck mass would converge within 10% under widely varying conditions in a real world environment.

Figure 2.17 shows force vs. acceleration in a heavy truck. While the ranges are narrower due to low power-to-weight ratio in heavy trucks, data points form a slender ellipse after high frequency dynamics have been filtered out.

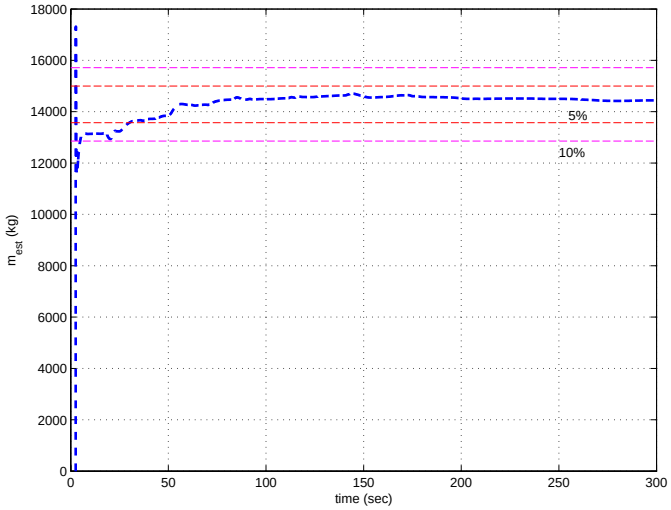

Figure 2.16: Estimation of heavy truck mass. Estimation converges to 5% of the final value within 25 seconds.

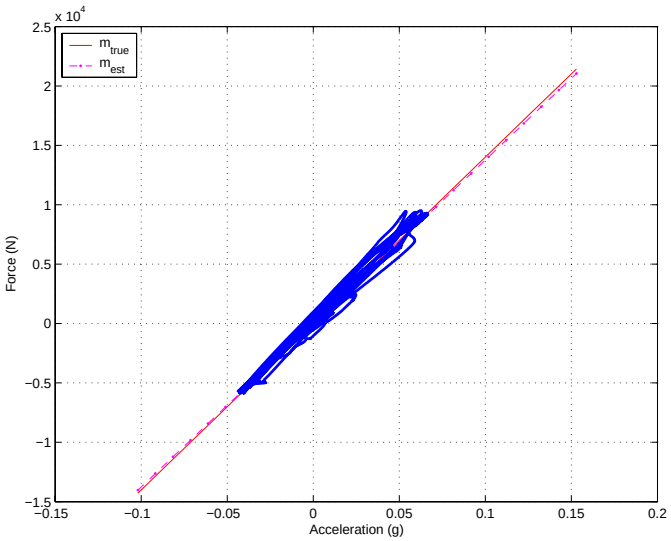

Figure 2.17: Plot of F_{engine} vs. acceleration in a heavy truck. The estimation error is about 5 %.

2.4 Summary

Automated vehicles require sufficiently accurate system models in order to achieve a desired level of closed-loop performance in, for example, automated highways systems or smart cruise control systems. Parameters of the models are one of the important factors that determine the accuracy of system modeling and, eventually, the overall performance of the closed-loop system.

Current GPS sensing technology enables estimation of road grade and, consequently, simple treatment of parameter estimation from a static force balance. This work has demonstrated that road grade can be reliably estimated using synchronized two antennae GPS system or the vertical to horizontal velocity ratio from GPS speed measurements. While both methods provide similar performance in road grade estimation with comparable errors, the velocity-ratio based, single-antenna system is a better choice since it is more economical to implement than two-antenna system.

In addition, GPS is used to generate an accurate elevation and/or road grade maps for future reference. Results show that these maps are comparable in accuracy to offline maps. When combined with inertial navigation sensors through Kalman filtering, GPS may also be used for dead reckoning purpose. This GPS/INS integration has been demonstrated experimentally to eliminate the problem of GPS signal loss due to the difficulty associated with maintaining the line of sight to satellites inherent in GPS navigation around urban environment.

Accurate estimation of road grade enables the estimations of other important vehicle parameters. With reliable and accurate road grade estimates and the assumption of low frequency dynamics, the vehicle mass estimates have been shown to converge quickly within $\pm 2\%$ and $\pm 5\%$ of the measured values for a passenger car and a heavy truck, respectively. Sum of drag force and rolling resistance has also been reliably estimated. However, separate estimation of them proved less successful. Future work will include separation of drag coefficient and rolling resistance using more detailed models. Given accurate estimate of important vehicle parameters, high performance closed-loop systems are possible.

Chapter 3

Platoon Model

3.1 Introduction

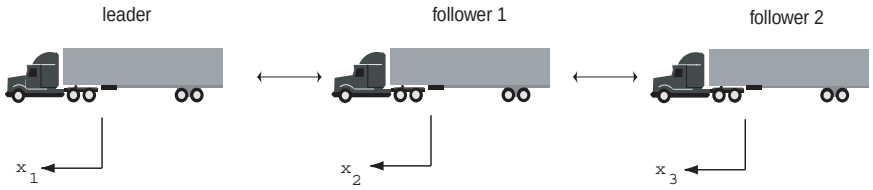

Figure 3.1: 3-vehicle Platoon.

In a platoon of automated vehicles, the longitudinal controller has to provide not only asymptotic stability - where relative speed and inter-vehicle spacing are ensured to go to zero - but also guarantee a property known as string stability. With string stability, disturbances in inter-vehicle spacing upstream in the platoon will be attenuated as they propagate downstream. Since it was established that constant inter-vehicle spacing cannot provide string stability without additional information [16], many inter-vehicle spacing policies have been devised. For example, inter-vehicle communication has been used to ensure string stability by transmitting the velocity and acceleration of the lead vehicle to followers [37]. Speed dependent spacing policies where time headway term provides more spacing at higher speeds have also been used. Nonlinear adaptive spacing policies that place different weights on control gains have also been suggested [62]. All of these spacing polices developed to date are based on

the assumption that engine and brake actuators can actually follow reference trajectories without saturation. The efforts of automated highway systems (AHS) research and development activity are now shifting towards platoon formation of commercial heavy trucks due to feasibility of implementation and economic benefits. The issue of actuator saturation is of particular concern in heavy truck AHS since 1) normal maneuvers use most of the control authority in heavy trucks; hence, little reserve is left for disturbance rejection 2) typical ranges of parameter variations in commercial heavy vehicles are well beyond what conventional (adaptive) controllers are capable of handling and may saturate actuators so that the platoon operation results in instability, 3) members in a heavy truck platoon may have different open loop capabilities and 4) such a situation arises fairly easily if the leading vehicle in a platoon has a higher power-to-weight ratio. Therefore, a better way of implementing longitudinal control is to incorporate the knowledge of physical actuation limits in all members of a platoon through estimation of important parameters such as vehicle mass and road grade changes and to modify incoming commands accordingly [3, 5]. The concept of command modification is beneficial in the sense that undesirable components in command signals are removed before they enter the system, thus less work for feedback controllers. Command modification techniques such as input shaping can guarantee that actuators stay out of saturation range and, therefore, string stability is preserved. In this work, a linear model is derived for a 3-vehicle platoon and effects of reference commands on actuator saturation are explicitly analyzed. Two input shapers design techniques are discussed, zero-placement and convex optimization, and their benefits of saturation prevention and smoothed trajectories are shown with simulations. ll closed-loop platoon is,

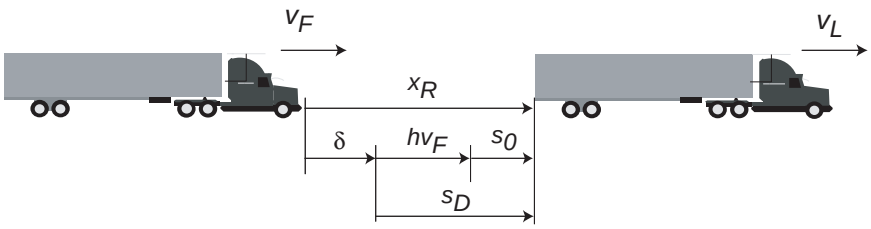

Figure 3.2: Coordinate definitions.

3.2 Platoon Model

Following the same notion and control law in [62] and as shown in Figure 3.2,

$$\begin{aligned}
s_0 &: \text{minimum spacing} \\
h &: \text{time headway} \\
v_L &: \text{velocity of leading vehicle} \\
v_F &: \text{velocity of following vehicle} \\
v_r &: \text{relative vehicle velocity} \\
x_r = x_L - x_F &: \text{relative vehicle spacing} \\
s_d = s_0 + hv_F &: \text{desired spacing} \\
\delta = x_r - s_d &: \text{separation error} \\
e = v_r + k\delta &: \text{error signal for control} \\
u = k_p e + ki\frac{1}{s}e &: \text{PI control law}
\end{aligned}$$

For vehicles #2 and #3, the followers use spacing information relative to immediately preceding vehicles only. Actuation commands with constant K_i are then,

$$\begin{aligned}
u_i &= K_{P,i}e + K_{I,i}\frac{1}{s}e && (3.1) \\
&= K_{P,i}(v_r + k\delta) + K_{I,i}\,(v_r + k\delta) \quad i = 2, \ldots, N. && (3.2)
\end{aligned}$$

Closed loop systems for the followers are then,

$$\begin{aligned}
\dot{X}_i &= \begin{bmatrix} 0 & 1 & 0 & 0 \\ 0 & 0 & 1 & 0 \\ 0 & 0 & 0 & 1 \\ -b_i K_{I,i} k & \begin{matrix} -b_i(K_{P,i}k \\ -K_{I,i}(1+kh)) \end{matrix} & -b_i(K_{P,i}+kh) & -a_i \end{bmatrix} \begin{bmatrix} x_i \\ \dot{x}_i \\ \ddot{x}_i \\ \dddot{x}_i \end{bmatrix} \\
&+ \begin{bmatrix} 0 & 0 & 0 \\ 0 & 0 & 0 \\ 0 & 0 & 0 \\ b_i K_{I,i} k & b_i(K_{Pi}k + K_{I,i}) & b_i K_{P,i} \end{bmatrix} \begin{bmatrix} x_{i-1} \\ \dot{x}_{i-1} \\ \ddot{x}_{i-1} \end{bmatrix} + \begin{bmatrix} 0 \\ 0 \\ 0 \\ -K_{I,i} k s_0 \end{bmatrix} \\
&= A_i X_i + B_i X_{i-1} \qquad (3.3) \\
y_i &= \begin{bmatrix} I_{3\times 3} & 0_{3\times 1} \end{bmatrix} X_i
\end{aligned}$$

Additional followers can be easily added in this format since the inputs to the new follower are the states (system coordinates) from the preceding vehicle.

Putting it all together, the overall closed-loop platoon is,

$$\begin{aligned}
X &= [X_1\ X_2\ X_3\ ]^T \\
\dot{X}_{cl} &= AX_{cl} + Ba_r \qquad (3.4) \\
A &= \begin{bmatrix} A_1 & 0 & 0 \\ B_2C_1 & A_2 & 0 \\ 0 & B_3C_2 & A_3 \end{bmatrix}, \quad B = \begin{bmatrix} B_1 \\ 0 \\ 0 \end{bmatrix}
\end{aligned}$$

The expression for actuation dynamics($\ddot{x}_i = Gu_i$) is then,

$$\begin{bmatrix} u_1 \\ u_2 \\ u_3 \end{bmatrix} = \left[\begin{array}{cccc|cccc|cccc} 0 & -K_1 & 0 & K_1 & 0 & 0 & 0 & 0 & 0 & 0 & 0 & 0 \\ \hline 0 & 0 & 0 & 0 & 0 & 0 & \frac{a}{b} & \frac{1}{b} & 0 & 0 & 0 & 0 \\ \hline 0 & 0 & 0 & 0 & 0 & 0 & 0 & 0 & 0 & 0 & \frac{a}{b} & \frac{1}{b} \end{array}\right] X_{new} \qquad (3.5)$$

Vehicle parameters and controller gains are listed in Table 3.1.

Vehicle #	a	b	k	h	K_P	K_I
1	31.4	11	N/A	0	0	0
2	31.4	7	4	0	0	0
3	31.4	10	4	0	0	0

Table 3.1: Vehicle and controller parameters

Representing the system in the frequency domain, transfer functions from reference acceleration, $a_{ref}(t)$, to control effort, $u(t)$, or vehicle acceleration, $\ddot{x}(t)$, are denoted respectively by,

$$\frac{U(s)}{A_{ref}(s)} \quad or \quad \frac{s^2X(s)}{A_{ref}(s)}$$

Each vehicle is modelled as a stable, 1st order plant representing actuator delay,

$$G_i(s) = \frac{s^2X_i(s)}{U_i(s)} = \frac{b_i}{s+a_i} \tag{3.6}$$

The transfer function from reference acceleration to actuation for vehicle #1 is

$$\frac{u_1(s)}{a_r(s)} = \frac{s+K_1}{s+K_1G_1} \tag{3.7}$$

and, for vehicle #2 and #3, it is

$$\frac{u_i(s)}{a_r(s)} = \frac{K_iH_{i-1}G_{i-1}\,(s+w_i)}{s^2+K_iG_is+K_iw_iG_i}, \qquad i=2,3 \tag{3.8}$$

Similarly,

$$\begin{aligned}\frac{x_i}{x_{i-1}} &= \frac{b(K_ps^2+(K_pk+K_i)s+kK_i)}{s^4+as^3+bK_p(1+kh)s^2+b(K_pk+K_i(1+kh))s+bK_ik}, \quad i=2,3,\ldots,N \\ &= \frac{G(s)}{s^2}\frac{u_i}{x_{i-1}}\end{aligned}$$

3.2.1 Individual Stability

Stability of the closed-loop platoon model is verified with Routh's stability criteria.

$$
\begin{aligned}
A &= \begin{bmatrix} 0 & 1 & 0 & 0 \\ 0 & 0 & 1 & 0 \\ 0 & 0 & 0 & 1 \\ -K_{I,i}k & \substack{-b_iK_{P,i}k \\ -K_{I,i}(1+kh)} & -b_iK_{P,i} - kh & -a_i \end{bmatrix} \\
&= \begin{bmatrix} 0 & 1 & 0 & 0 \\ 0 & 0 & 1 & 0 \\ 0 & 0 & 0 & 1 \\ a & b & c & d \end{bmatrix} \\
\det(A - sI) &= s^4 - ds^3 - cs^2 - bs - a
\end{aligned}
$$

All coefficients are positive. Thus, it satisfies the first Routh's stability.

$$
\begin{array}{cccc}
s^4 & 1 & -c & -a \\
s^3 & -d & -b & 0 \\
s^2 & q_1 & -a & 0 \\
s^1 & \frac{ad-bq_1}{q_1} & 0 & \\
s^0 & -a & &
\end{array}
$$

$$
\left(q_1 = \frac{b - dc}{d} \right)
$$

There is no change of sign as long as $h, k, K_{P,i}, K_{I,i} \geq 0$. Therefore, all poles are in the left hand plane, hence a stable system.

3.2.2 Asymptotic Stability and Spacing Error

A generalized spacing error, δ_i, is defined [48], if the zero steady state spacing error specification is relaxed.

$$u_1 = a_{ref} + K_1(v_{ref} - v_1) \tag{3.9}$$
$$a_1 = G_1 u_1 \tag{3.10}$$

$$u_i = K_P e + K_I \frac{1}{s} e \tag{3.11}$$
$$e = v_r + k\delta \tag{3.12}$$
$$= \dot{x}_{i-1} - \dot{x}_i + k\delta \tag{3.13}$$

From the equations above,

$$\frac{a_2}{a_1} = \frac{K_P s^2 + (K_P k + K_I)s + K_I k}{\frac{1}{b}s^4 + \frac{a}{b}s^3 + K_P(1+kh)s^2 + (K_P k + K_I(1+kh))s + K_I k} \tag{3.14}$$
$$\frac{v_1 - v_2}{a_1} = \frac{\frac{1}{b}s^3 + \frac{a}{b}s^2 + K_P(kh)s + K_I(kh)}{\frac{1}{b}s^4 + \frac{a}{b}s^3 + K_P(1+kh)s^2 + (K_P k + K_I(1+kh))s + K_I k} \tag{3.15}$$

At steady state,

$$\left.\frac{v_1 - v_2}{a_1}\right|_{t\to\infty} = \lim_{s\to 0} \frac{1}{s} \frac{\frac{1}{b}s^3 + \frac{a}{b}s^2 + K_P(kh)s + K_I(kh)}{\frac{1}{b}s^4 + \frac{a}{b}s^3 + K_P(1+kh)s^2 + (K_P k + K_I(1+kh))s + K_I k} s = h$$

Therefore, it is clear that h should be zero for zero steady spacing (velocity) error for any step change in lead vehicle velocity (acceleration). However, in order to ensure string stability, $h \neq 0$. Zero spacing error requirement is relaxed in favor of string stability.

3.2.3 String Stability using Autonomous Spacing Strategies

An autonomous platoon is under consideration in this work. In other words, only on-board sensors are used for control: the current vehicle's spacing and speed relative to immediately preceding vehicle.

$$\epsilon_i = x_{i-1} - x_i - s_0 \tag{3.16}$$

$$\delta_i = \epsilon_i - h\dot{x}_i \tag{3.17}$$

Using relative spacing and speed information only, consider the following error signal:

$$e_i = v_r + k\delta \tag{3.18}$$

$$= \dot{x}_{i-1} - \dot{x}_i + k\delta \tag{3.19}$$

And, the control law:

$$u_i = k_P e_i + k_I \int e_i \, \mathrm{d}t \tag{3.20}$$

The spacing error dynamics, with a first order individual vehicle model ($\ddot{x}_i = \frac{b}{s+a}u_i$), is given by:

$$\frac{\delta_i(s)}{\delta_{i-1}(s)} = \frac{\overbrace{k_P}^{D} s^2 + (\overbrace{kk_P + k_I}^{E})s + kk_I}{s^4/b + (a/b)s^3 + (\underbrace{k_P + kk_P}_{A})s^2 + (\underbrace{kk_P + k_I + kk_I h}_{B})s + \underbrace{kk_I}_{C}} \tag{3.21}$$

For string stability,

$$\left|\frac{\delta_i(s)}{\delta_{i-1}(s)}\right| = \left|\frac{Ds^2 + Es + C}{s^4/b + (a/b)s^3 + As^2 + Bs + C}\right|_{s=jw} \tag{3.22}$$

$$= \left|\frac{C - Dw^2 + jEw}{C - Aw^2 + w^4/b + j(Bw - (a/b)w^3)}\right| \tag{3.23}$$

$$\leq 1 \tag{3.24}$$

Therefore,

$$(C - Dw^2)^2 + (Ew)^2 \leq (C - Aw^2 + w^4/b)^2 + (Bw - (a/b)w^3)^2 \tag{3.25}$$

$$\Rightarrow w^6 + w^4(a^2 - 2Ab) + w^2(b^2A^2 - b^2D^2 - 2Cb - 2Bab) \tag{3.26}$$

$$+b^2(B^2 - 2CA + 2CD - E^2) \geq 0 \quad \forall\ w \geq 0 \tag{3.27}$$

The last equation is then,

$$F(w) = w^6 + \alpha w^4 + \beta w^2 + \gamma \geq 0 \tag{3.28}$$

where

$$\alpha = a^2 - 2Ab \tag{3.29}$$

$$\beta = b^2A^2 - b^2D^2 - 2Cb - 2Bab \tag{3.30}$$

$$\gamma = b^2(B^2 - 2CA + 2CD - E^2) \tag{3.31}$$

From the theory of quadratic equations, the above inequality holds if and only if one of the following holds:

$$w = 0,\ \gamma \geq 0$$

or

$$w^2 = \tfrac{-\alpha \pm \sqrt{\alpha^2 - 3\beta}}{3},\ \alpha < 0,\ \alpha^2 - 3\beta \geq 0$$

$$\alpha < 0 \Rightarrow k_P \geq \frac{a^2}{2b(1-k)}$$

$$F\left(w^2 = \frac{-\alpha \pm \sqrt{\alpha^2 - 3\beta}}{3}\right) \geq 0$$

For the following values used in this work ($a = b = 4\pi,\ k = 2,\ k_P = 6,\ k_I = 5,\ h = 0.1$),

$$h = 0.1$$

3.2.4 Constant Spacing and Need for Inter-vehicle Communication

The following shows why inter-vehicle communication is necessary for constant spacing law. Assuming a point mass for each vehicle, without inter-vehicle communication,

$$\begin{aligned}
\epsilon_i &= x_{i-1} - x_i - s_0 \\
u_i &= K_v\dot{\epsilon}_i + K_p\epsilon_i \\
\ddot{\epsilon}_i &= u_{i-1} - u_i \\
&= K_v\dot{\epsilon}_{i-1} + K_p\epsilon_{i-1} - K_v\dot{\epsilon}_i - K_p\epsilon_i \\
\left|\frac{\epsilon_i(s)}{\epsilon_{i-1}(s)}\right| &= \left|\frac{K_v s + K_p}{s^2 + K_v s + K_p}\right| \\
&= \frac{\sqrt{K_v^2 w^2 + K_p^2}}{\sqrt{K_v^2 w^2 + (K_p - w^2)^2}}
\end{aligned}$$

Thus, it is obvious that for some K_v and K_p, the ratio is larger than 1 [48]. Now, with inter-vehicle communication (leading vehicle position information),

$$\begin{aligned}
\epsilon_i &= x_{i-1} - x_i - s_0 \\
u_i &= K_v\dot{\epsilon}_i + K_p\epsilon_i + K_l(x_l - x_i) \\
\ddot{\epsilon}_i &= u_{i-1} - u_i \\
&= K_v\dot{\epsilon}_{i-1} + K_p\epsilon_{i-1} + K_l(x_l - x_{i-1}) - K_v\dot{\epsilon}_i - K_p\epsilon_i - K_l(x_l - x_i) \\
&= K_v\dot{\epsilon}_{i-1} + K_p\epsilon_{i-1} - K_v\dot{\epsilon}_i - K_p\epsilon_i - K_l\epsilon_i \\
\left|\frac{\epsilon_i(s)}{\epsilon_{i-1}(s)}\right| &= \left|\frac{K_v s + K_p}{s^2 + K_v s + K_p + K_l}\right| \\
&= \frac{\sqrt{K_v^2 w^2 + K_p^2}}{\sqrt{K_v^2 w^2 + (K_p + K_l - w^2)^2}}
\end{aligned}$$

Now, it's obvious that having leading vehicle information is useful to bring the magnitude below 1.

3.3 Model Analysis and Responses

Control effort (u)over time in response to step acceleration input are shown in Figures 3.3 and 3.4. Delay in control response for vehicles further in the platoon is obvious. A more important observation is that each vehicle produces some overshoot which cumulates for later vehicles in the platoon. This is precisely why changing characteristics in input command that may excite undesirable dynamics in a platoon is very important.

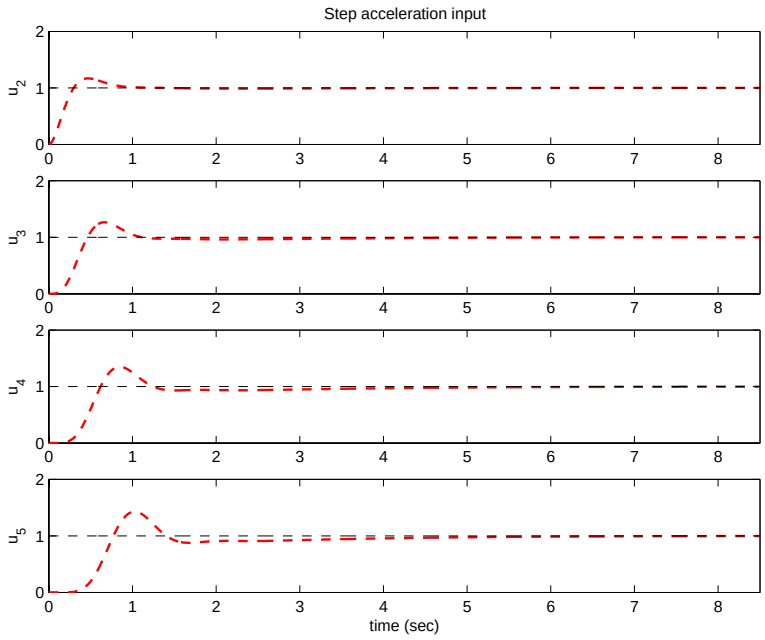

Figure 3.3: Controls (u_2 to u_5) to step acceleration input.

Low damping and associated overshoot/gain amplification are clearly seen in frequency response analysis of $|U_i(s)/A_{ref}(s)|$ in Figure 3.5. $|U_2(s)/A_{ref}(s)|$ has the most high frequency content and the least amplification while $|U_9(s)/A_{ref}(s)|$ has the least high frequency content and the most amplification. Intermediate vehicles fall somewhere between these two end cases. Therefore, it is obvious that at minimum, the

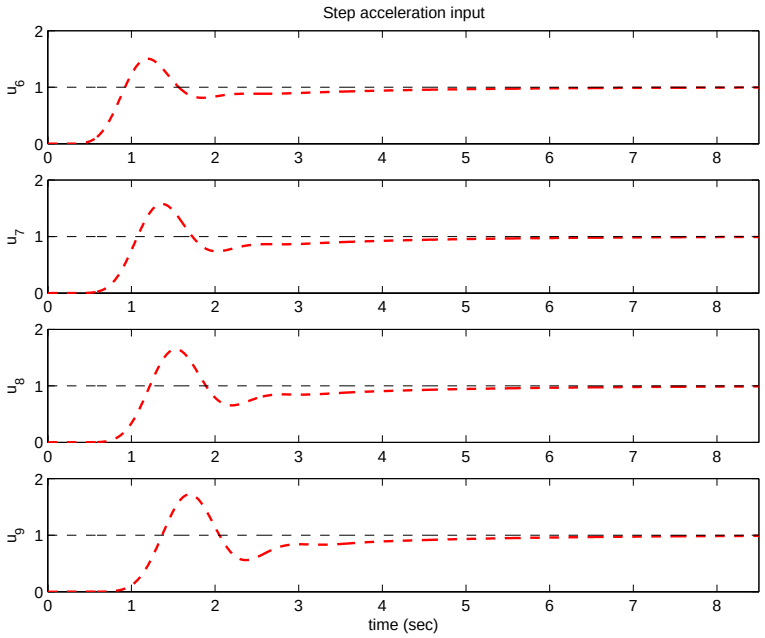

Figure 3.4: Controls (u_2 to u_5) to step acceleration input.

amplification in the magnitude of $|U_i(s)/A_{ref}(s)|$ for all i has to be lowered below 1, and perhaps more for sufficient damping. Using ramp acceleration inputs introduces some damping into the system. However, the question is how much damping is necessary and how to do it in a systematic way. The next chapter addresses this question. Figure 3.6 shows $|A_i(s)/A_{ref}(s)|$ for comparison, which is similar to $|U_i(s)/A_{ref}(s)|$ in Figure 3.5 due to current models used in analysis.

A representative profiles of acceleration and speed for automated highways are shown in Figure 3.7. Reference acceleration commands may be thought of as a series of step acceleration changes (in blue) or ramped acceleration changes (in red). Step acceleration changes correspond to sharp corners in speed profile while ramp acceleration changes produce smooth corners in speed profile. Ramp acceleration changes also have the effect of introducing damping into the platoon dynamics, which explains less overshoot in control effort response in Figure 3.9 than in Figure 3.8. The question is then how to pick the right "ramping" input in reference signals in a systematic way. The following chapter discusses this question in detail.

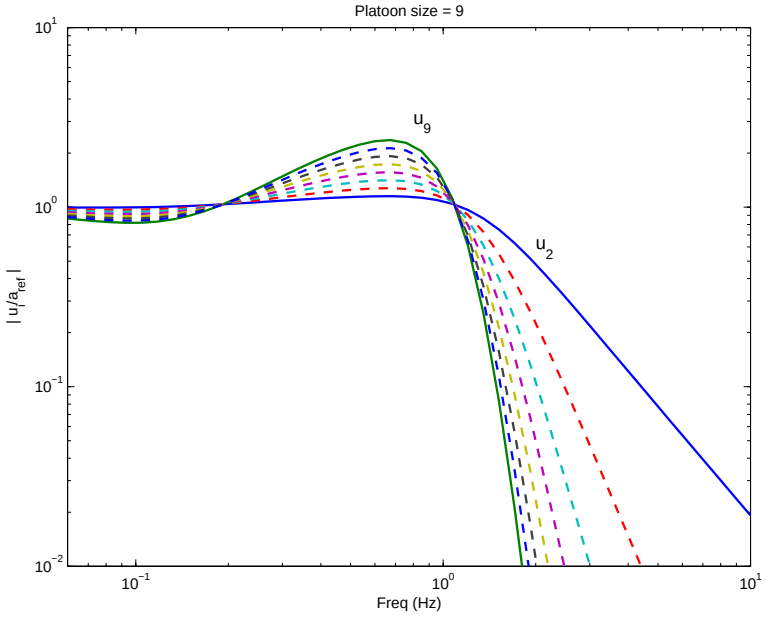

Figure 3.5: Magnitude of reference acceleration input to control efforts: $|U_i(s)/A_{ref}(s)|$.

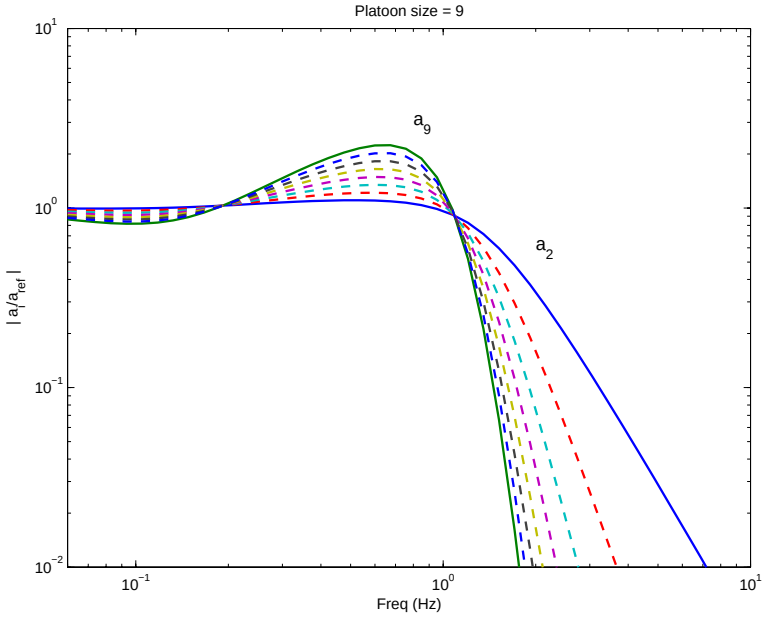

Figure 3.6: Magnitude of reference acceleration input to accelerations: $|A_i(s)/A_{ref}(s)|$.

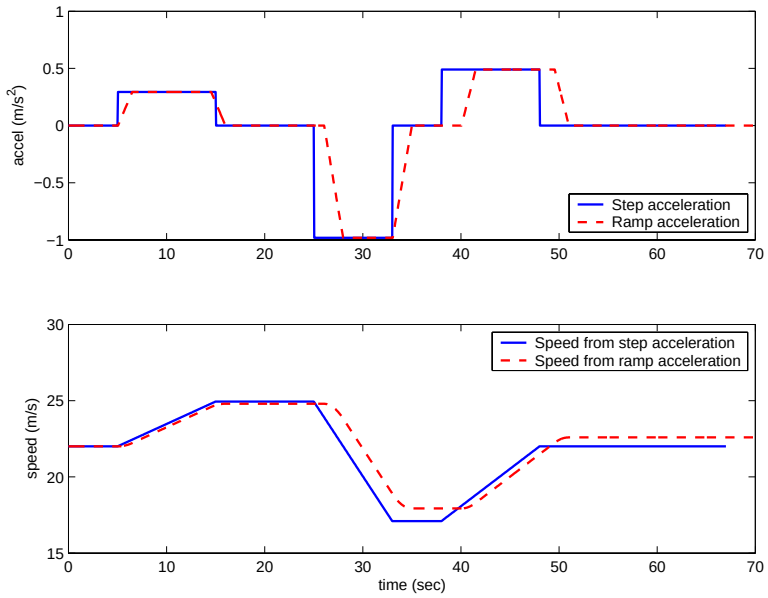

Figure 3.7: Realistic acceleration and speed profiles. Acceleration inputs can be a series of step changes or ramped.

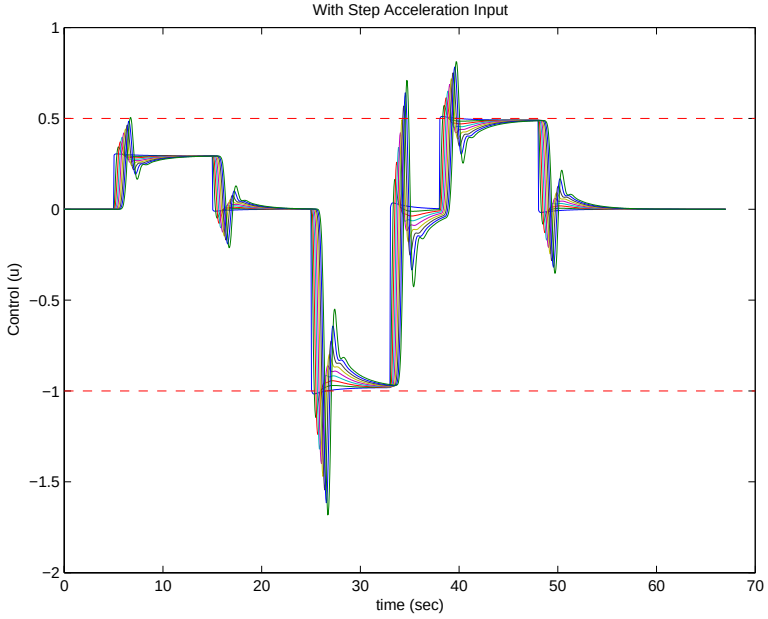

Figure 3.8: Controls (u_1 to u_9) to step acceleration inputs. Overshoot leads to control saturation.

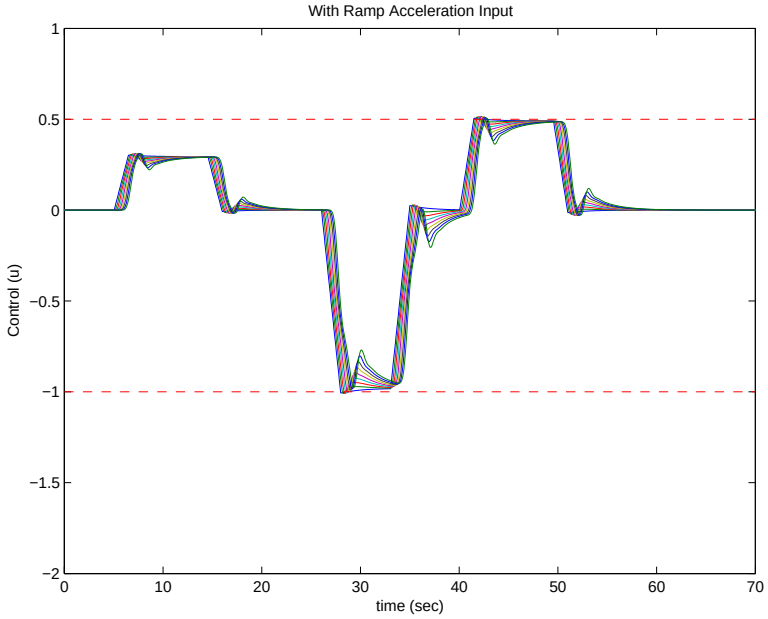

Figure 3.9: Controls (u_1 to u_9) to ramp acceleration inputs. Ramped inputs produce less overshoot, hence little saturation.

Chapter 4

Command Modification

This chapter presents a new method for maintaining and improving string stability by preventing actuator saturation in automated vehicles on highways. Instead of relying on feedback controllers to deal with the issue of actuator saturation after the fact, reference commands are feed through an FIR filter called an input shaper so that harmful components in the reference commands are reduced or removed.

4.1 Input Shaping for Command Modification

Input shaping is a command modification technique in which a reference command to a system is modified or shaped through convolution with an FIR filter (input shaper in Figure 4.1). Original (unmodified) reference signals are passed through the input shaper and the shaped (modified) signals are then fed to the system. The purpose of this modification is to remove frequency content from the reference command that can produce oscillations in the closed-loop system due to lightly damped, flexible modes. With properly chosen impulses, the effect can be very significant. In practice, input shaping has been used in areas where zero vibration of an object after a maneuver is required, for example, a reader arm in a hard disk drive or a cargo crane [52, 42].

Automated highway systems [62] are another interesting application that can benefit from input shaping. A platoon of automated vehicles can be thought of as a series

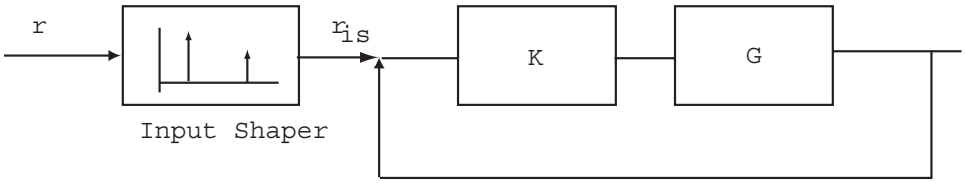

Figure 4.1: Input shaping. Reference command is convolved with an input shaper.

of spring-mass-damper systems where vibration must be controlled for stable operation. For such systems, acceleration can be used for reference commands, but ideal signals must be modified to reflect performance limitations of a platoon of vehicles. A convex optimization approach to input shaper design that can capture time domain constraints such as engine saturation or maneuver end-point [32] is therefore quite useful. Previous work [4] has demonstrated that this approach can be successfully applied to automated highways.

These previous formulations for designing input shapers, however, have included only time domain constraints such as acceleration or position requirements. It is sometimes desirable to have constraints specified in the frequency domain, for instance limiting input shaper gain at high frequencies. In other cases, constraints can only be effectively expressed in the frequency domain. A good example in the context of automated highways is ride quality, which is strongly frequency dependent. This chapter shows how such constraints can be added to the convex optimization framework.

4.2 Previous Work in Input Shaping

The zero-placement technique is first summarized since it captures essential idea of input shaping. Then, input shaping design with direct manipulation of impulses is discussed.

4.2.1 Zero-placement for Input Shaping

A frequency domain approach to input shaping provides insights into input shaping design for systems with complicated dynamics since specific system poles can be explicitly targeted. A zero-placement design procedure has been developed to cancel undesired system dynamics from poles with low damping by placing zeros around the undesired system poles [51]. Robustness can be added with additional $n_i - 1$ zeros at the same or nearby frequencies. The zero-placement technique is used in this work for its simplicity and the resulting input shaper is a fourth order FIR filter with positive coefficient impulse sequences. First order robustness is chosen since it provides adequate performance while keeping the input shaper length low. In the discrete domain, the input shaper can be represented as follows.

$$\begin{aligned} H(z) &= \frac{C}{z^{\alpha}}(z-p_1)^{n_1}(z-p_1^*)^{n_1}(z-p_2)^{n_2}(z-p_2^*)^{n_2} \\ &\quad \cdots (z-p_m)^{n_m}(z-p_m^*)^{n_m} \end{aligned} \tag{4.1}$$

where n_i is the multiplicity of pole p_i and $\alpha = 2\sum_{i=1}^{m} n_i$ is the number of poles added to make the filter causal. The constant C makes DC gain of the input shaper unity and frequency response of the resulting input shaper designed for the transfer function in Equation 4.2 is shown in Figure 4.2.

$$\frac{U_2(s)}{A_r(s)} = \frac{U_2(s)}{s^2 R(s)} = \frac{K_2 G_1 (s+w_2)\frac{s+K_1}{s+K_1 G_1}}{s^2 + K_2 G_2 (s+w_2)} \tag{4.2}$$

Figure 4.2 also shows frequency response of Equation 4.2 with and without the input shaper. The figure shows that amplification around 1 Hz has been reduced by a factor of 5. This means that reference command with input shaping will not saturate actuators, which is particularly important in maintaining string stability in a platoon of heavy trucks. A smaller magnitude in control effort also means that less energy is used for control actuators, and, therefore, fuel economy and ride quality/driver comfort will improve. Note that, if minimum distortion (i.e. less phase distortion, or shorter response time) of original command signals is required, the depth of valley from input shaper (extent of notching effect) can be reduced so that the gain at the

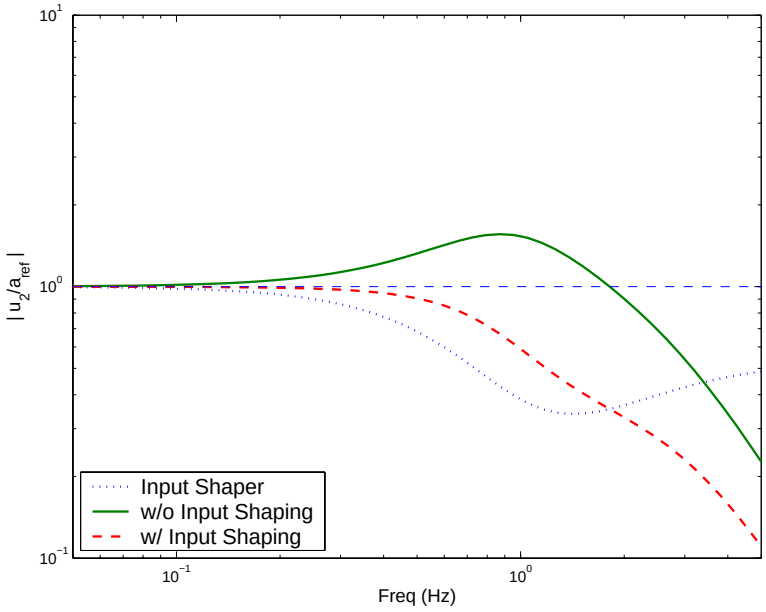

Figure 4.2: Frequency response of transfer function, Equation 4.2, with and without input shaper. Input shaper is similar to a notch filter.

undesired system pole frequency is just below unity, instead of much below unity.

4.2.2 Impulse Design for Input Shaping

A typical method of design input shapers is presented here. More detailed discussion can be found in [41]. A reference command can be decomposed into a function convolved with an impulse sequence . First, a non-dimensional measure of the residual vibration is defined as an expression for the amplitude of residual vibration caused by the impulse sequence and then dividing by the amplitude of residual vibration from a single unity-magnitude impulse. For example, if the system is a second-order

harmonic oscillator with natural frequency w and damping ration ζ, then this non-dimensional residual vibration is:

$$V = e^{-\zeta w t_n}\sqrt{C_w^2 + S_w^2} \tag{4.3}$$

$$C_w = \sum_{i=1}^{n} A_i e^{\zeta w t_i} cos\left[w\sqrt{1-\zeta^2}t_i\right] \tag{4.4}$$

$$S_w = \sum_{i=1}^{n} A_i e^{\zeta w t_i} sin\left[w\sqrt{1-\zeta^2}t_i\right] \tag{4.5}$$

A_i and t_i are the amplitudes and time locations of the impulses and n is the number of impulses.

Equation 4.3 provides an easy method for evaluating the residual vibration from a command profile. The value given by Equation 4.3 is the amplitude of residual vibration caused by the shaped command divided by the amplitude of residual caused by the unshaped command. The increase in rise time associated with the shaping process is simply the time duration of the input shaper. Furthermore, the settling time is also equal to the duration of the shaper, assuming that the shaping performs as expected.

Equation 4.3 can also be used for designing input shapers. Such input shapers should generate impulse sequences that yield zero residual vibration. This requires that Equation 4.3 be zero at the frequency and the damping of the system under consideration. In this case, both the cosine and sine summations must be zero independently.

$$C_w = \sum_{i=1}^{n} A_i e^{\zeta w t_i} cos\left[w\sqrt{1-\zeta^2}t_i\right] = 0 \tag{4.6}$$

$$S_w = \sum_{i=1}^{n} A_i e^{\zeta w t_i} sin\left[w\sqrt{1-\zeta^2}t_i\right] = 0 \tag{4.7}$$

To minimize the time delay, the first impulse must be placed at time zero.

$$t_1 = 0 \tag{4.8}$$

Furthermore, the impulse amplitudes must sum to one:

$$\sum_{i=1}^{n} A_i = 1 \tag{4.9}$$

The solution to Equation 4.7 to 4.9 that minimizes the shaper duration is undefined because the impulse amplitudes go to positive and negative infinity as the shaper duration decreases. To avoid this difficulty, the impulse amplitudes can be restricted to positive values.

There are four equations to be satisfied. Therefore, an input shaper with two impulses is desired because two impulses give four unknowns (two amplitudes and two time locations). In this case, $i = 2$ and substituting into yields:

$$0 = A_1 + A_2 e^{\zeta w t_2} cos\left[w\sqrt{1-\zeta^2}t_2\right] \tag{4.10}$$

$$0 = A_2 e^{\zeta w t_2} sin\left[w\sqrt{1-\zeta^2}t_2\right] \tag{4.11}$$

$$1 = A_1 + A_2 \tag{4.12}$$

To satisfy Equation 4.11 and keep the impulse sequence at minimum, the argument of the sine term must equal π. Therefore,

$$t_2 = \frac{\pi}{w\sqrt{1-\zeta^2}} \tag{4.13}$$

Substitution yields,

$$0 = A_1 + (1 - A_1) e^{\frac{\zeta w}{\sqrt{1-\zeta^2}}} \tag{4.14}$$

Solving for A_1 and A_2, we get:

$$A_1 = \frac{1}{1 - exp\left\{\frac{-\zeta w}{\sqrt{1-\zeta^2}}\right\}} \tag{4.15}$$

$$A_2 = 1 - \frac{1}{1 - exp\left\{\frac{-\zeta w}{\sqrt{1-\zeta^2}}\right\}} \tag{4.16}$$

The derivation above is the simplest example of how the impulse response can be used to design an input shaper. Other types of shapers are derived by including additional constraint equations such as robustness constraints. In many cases, these input shapers cannot be obtained in a closed form, rather a numerical optimization is performed to obtain the impulse amplitudes and time locations.

The two-impulse sequence given above is called a zero vibration (ZV) shaper because it satisfies the constraint that the residual vibration must be zero when the model is known perfectly. When the model contains uncertainty, robustness to such variations can be factored into, and such methods are summarized in the following section.

4.2.3 Robust Input Shaping Design

- ZV (Zero Vibration): To limit he amount of residual vibration that occurs when the system reaches its desired setpoint, the amplitude of residual vibration when the system is given a series of impulses is required to be less than a particular level at time t_f. ZV shapers have zeros at the flexible poles of the system [6, 51].

- ZVD (Zero Vibration, Zero Derivative): he major drawback of ZV input shaper is that it is extremely sensitive to modeling errors. There are several ways to make a shaped command less sensitive to modeling errors [43, 45, 40]. One simple way is to differentiate each vibration equation with respect to each flexible mode frequency and set the result to zero (hence, the name ZVD). This has the effect of putting double zeros at the location of system poles. A ZVDD shaper provides additional robustness with three zeros at the system poles. It should be noted, however, that the robustness does not come free: each addition of zeros makes the shaper longer, which means system response will be longer as well.

- EI (Extra Insensitive): Another method of increasing robustness to parameter uncertainty is called the extra-insensitive (EI) shaper design [41]. The main idea is to allow some finite residual vibration at each of the modeled structural frequencies but to constrain zero residual vibration at frequencies slightly above

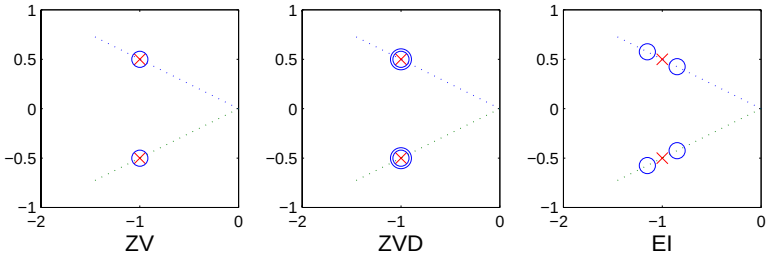

Figure 4.3: Pole-zero maps of ZV, ZVD and EI shapers in the s-plane.

and below each modeling frequency; and the derivative of the residual vibration is still constrained to be zero at each modeling frequency. This has the effect of broadening the sensitivity curve about each modeling frequency and hence increasing the insensitivity. EI shapers have been shown to give larger insensitivities than the ZVD shapers with approximately the same maneuver times.

Methods for controlling flexible modes in a system are usually feedback and feedforward approaches. Feedback control uses measurements and estimated of the system states to reduce vibration from the flexible modes. While feedback techniques have demonstrated good control of flexible modes, the performance of control system can often be improved by addition of a feedforward controller that alters reference commands. Furthermore, a properly designed feedforward controller can drastically reduce the complexity of the required feedback controllers for a given level of performance requirements.

One feedforward approach, known as input shaping, has been successfully applied for controlling flexible structures, and the technique has been shown to allow flexible structures to be maneuvered with little residual vibration, even in the presence of modeling uncertainties. In this method, an input command is convolved with a sequence of impulses designed to produce a resulting input command that causes less residual vibration than the original unshaped command [43, 44, 58]. The goal of input shaping is to determine the amplitudes and timing of the impulses to eliminate or reduce residual vibration.

4.3 Input Shaping in Convex Optimization

The input shaping design techniques discussed in preceding sections lack two important characteristics necessary in any good design synthesis in that 1) optimality is hard to capture, hence, hard to compare one input shaper with another, 2) adding more constraints in a systematic way is very difficult. In the following sections, a new input shaping design technique is discussed in the framework of convex optimization.

4.3.1 System Propagation through Time Steps

A more sophisticated method using convex optimization has been developed to extend input shaping techniques for multi-input systems and additional constraints such as slew rate and transient response [32]. It has been shown that objectives associated with input shaper design can be approximately reformulated as quasi-convex optimization problems in the discrete domain [59]. The input shaper design is then a special case of FIR filter design problem. In this framework, a filter with the minimum length and minimum number of non-zero impulses is designed to shape reference commands so that a system tracks the shaped reference command with little residual while satisfying performance constraints such as bounded control effort [32].

Defining an input shaping filter $H(z)$ as an FIR filter with length N,

$$H(z) = \sum_{j=0}^{N-1} h_j z^{-j} \tag{4.17}$$

The *modified* or *shaped* reference command for step input is

$$q_k = \begin{cases} \left[\sum_{j=0}^{k} h_j\right] r & \text{when} \quad k \leq N-1 \\ r & \text{when} \quad k \geq N \end{cases} \tag{4.18}$$

Discretizing the closed loop system (Equation **??**) with T_s (a design variable) and

propagating through time steps,

$$\begin{aligned} x_0 &= 0 \\ x_k &= Fx_{k-1} + Gq_{k-1}, \quad F \in \mathbf{R}^{n\times n}, \quad G \in \mathbf{R}^{n\times m} \\ &= Fx_{k-1} + G\left[\sum_{i=0}^{k-1} h_i\right] r \\ &= \left(\sum_{i=0}^{k-1} F^j G h_0 + \sum_{i=0}^{k-2} F^j G h_1 + \cdots + FGh_{k-2} + Gh_{k-1}\right) r \\ &= \left[\sum_{i=0}^{k-1} F^j G \;\; \sum_{i=0}^{k-2} F^j G \;\; \cdots \;\; FG \;\; G \;\; 0_{n\times(N-k)}\right] Hr \end{aligned} \tag{4.19}$$

where

$$H = [h_0 \;\; h_1 \;\; \cdots \;\; h_{N-1}]^T \tag{4.20}$$

For notational simplicity, let

$$S_k = \left[\sum_{j=0}^{k-1} F^j G \;\; \sum_{j=0}^{k-2} F^j G \;\; \cdots \;\; FG \;\; G \;\; 0_{n\times(N-k)}\right] \tag{4.21}$$

Then,

$$x_k = S_k H r \tag{4.22}$$

$$y_k = C_y S_k H r \tag{4.23}$$

where C_y extracts the appropriate variables.

$$y_{af} = C_{af} S_N H r = \begin{bmatrix} a_{1,\ final} \\ a_{2,\ final} \\ a_{3,\ final} \end{bmatrix} \tag{4.24}$$

$$y_{ae} = C_{ae}S_kHr = \begin{bmatrix} a_1 - a_2 \\ a_2 - a_3 \\ a_1 - a_3 \end{bmatrix} \tag{4.25}$$

$$y_{xe} = C_{xe}S_kHr = \begin{bmatrix} x_1 - x_2 \\ x_2 - x_3 \\ x_1 - x_3 \end{bmatrix} \tag{4.26}$$

$$y_{ve} = C_{ve}S_kHr = \begin{bmatrix} v_1 - v_2 \\ v_2 - v_3 \\ v_1 - v_3 \end{bmatrix} \tag{4.27}$$

$$y_u = C_uS_kHr = \begin{bmatrix} u_1 & u_2 & u_3 \end{bmatrix} \tag{4.28}$$

Some combination of these variable will be used in input shaping design.

4.3.2 ℓ_1-norm Cost Function

For a system with m inputs, the objective of an input shaper design can be to find an FIR filter with the minimum number of non-zero impulses for a given N. This is a non-convex l_0-norm[1]. This optimization problem is approximated with a weighted l_1-norm (convex) optimization.

$$\min_{H_j} \left[\sum_{j=1}^{m} \|W_j H_j\|_1 \right] \tag{4.29}$$

Two-step algorithm

In this work, a single-input system is considered ($m = 1$). Therefore, the cost function is,

$$\min_{H} \ \|WH\|_1 \tag{4.30}$$

[1]See Appendix C.5.1 for the definition of l_0-norm.

The weighting matrix W is to make smaller impulses even smaller (practically zero) in order to approximate l_0-norm as much as possible. In the two-step algorithm, the design routine is run once to calculate impulses. Then, W is a diagonal matrix whose elements are the reciprocal of impulses from the first step. This step is not always necessary.

4.3.3 ℓ_2-norm Cost function

Instead of ℓ_0/ℓ_1-norm for cost function, other forms of cost function may also be used. A common example is the minimum energy requirement. The ℓ_2-norm of control effort u can be used to quantify energy used to generate input commands. Square of ℓ_2-norm solves the same problem while simplifying formulation. In such cases, the cost function is then:

$$\text{minimize} \quad ||U||_2^2 \tag{4.31}$$

where, for a platoon of 9 vehicles and an input shaper of N impulses,

$$U = [u_1^T \quad u_2^T \quad \dots \quad u_9^T]^T \tag{4.32}$$

$$u_i = \begin{bmatrix} Cu_iS_1 \\ Cu_iS_2 \\ \vdots \\ Cu_iS_N \end{bmatrix} H = E_iH \tag{4.33}$$

$$\tag{4.34}$$

Therefore,

$$||U||_2^2 = U^TU = H^TMH \tag{4.35}$$

$$M = [\ E_1 \quad E_2 \quad \dots \quad E_9\ ] \begin{bmatrix} E_1 \\ E_2 \\ \vdots \\ E_9 \end{bmatrix} \succeq 0 \tag{4.36}$$

$$\begin{array}{ll} \text{minimize} & H^T M H \\ \text{subject to} & FH \preceq B \end{array} \tag{4.37}$$

which is a special case of quadratic program (C.3).

4.3.4 Constraint Functions in Time Domain

The convex framework provides much a more flexible platform for including various performance objectives as compared to zero-placement technique. In addition, expansion to multi-input, multi-output (MIMO) systems is quite easy. A few of the objectives, relevant to automated highways, are listed below [32]. In the following, ϵ's are design variables that allow tight/loose control, depending on acceptable compromise between performance and cost.

Final State Constraint

Final states (accelerations) should be as close to the final desired states a as possible, $X_f = [a_1\ a_2\ a_3]^T_{final}$.

$$\mid C_{af} S_N H r - X_f \mid \ \leq \ \epsilon_x$$

In a matrix form,

$$\left[\begin{array}{c} C_{af} S_N \\ -C_{af} S_N \end{array} \right] Hr \leq \left[\begin{array}{c} \epsilon_x + X_f \\ \epsilon_x - X_f \end{array} \right] \tag{4.38}$$

Transient Response Constraint

En route to the final states, in a platoon where only information from the preceding vehicles is used (compared to using information from the leader and vehicles behind), relative position, speed and acceleration errors between *i-th* and $(i-1)$*-th* vehicles should be small. The matrices C_{xe}, C_{ve} and C_{ae} extract relative position, speed and

acceleration error information of interest, respectively.

$$\begin{aligned} |\, C_{xe} S_k H r \,| &\leq \epsilon_{xe} \\ |\, C_{ve} S_k H r \,| &\leq \epsilon_{ve} \\ |\, C_{ae} S_k H r \,| &\leq \epsilon_{ae} \end{aligned}$$

Control Magnitude Constraint

Control effort should be bounded in order to avoid actuator saturation while reaching the final destination. This constraint is very useful in many applications where certain outputs would result in undesirable consequences and direct handle on controller outputs is crucial. This is easily expressed in MATLAB format as before.

$$u_{min} \leq C_u S_k H r \leq u_{max} \tag{4.39}$$

Unity DC Gain Constraint

The impulses in the input shaper should sum to 1, i.e. DC gain of 1, in order to eliminate any steady-state offset between the original reference (before input shaper, r in Figure 4.1) and modified (after input shaper, r_{is}) commands.

$$1 - \epsilon_0 \leq \sum_{j=0}^{N-1} h_j \leq 1 + \epsilon_0 \tag{4.40}$$

which can be written as:

$$1 - \epsilon_0 \leq \mathbf{1}^T H \leq 1 + \epsilon_0 \tag{4.41}$$

where $\mathbf{1}^T = [1 \quad 1 \quad \cdots \quad 1\ ]^T$. In a matrix form,

$$\begin{bmatrix} \mathbf{1}^T \\ -\mathbf{1}^T \end{bmatrix} H r \leq \begin{bmatrix} 1 + \epsilon_0 \\ -1 + \epsilon_0 \end{bmatrix}$$

Impulse Magnitude Constraint

Magnitudes of individual impulses can also be constrained. This effectively introduces high frequency roll-off in input shaper since, for a fixed sampling time, smaller impulses means lower frequency content.

$$h_{min} \leq h_j \leq h_{max} \qquad j = 0, 1, \cdots, N-1 \tag{4.42}$$

which, with identity matrix, I, can be written as

$$\begin{bmatrix} \mathbf{I} \\ -\mathbf{I} \end{bmatrix} Hr \leq \begin{bmatrix} \mathbf{1}h_{max} \\ -\mathbf{1}h_{min} \end{bmatrix}$$

Jerk Limit Constraint

"Jerk" is a concise term used to denote the time rate of change of acceleration of a point [46]. In some applications, it is useful to limit the rate of change in acceleration. For example, in the case of automated highways, it is better to have ramp acceleration changes, instead of step changes. Suppose the jerk is represented as follows:

$$\dddot{x} = \dot{a} = C_{jerk} S_N H r$$

Then, the jerk constraint is:

$$\dddot{x}_{min} \quad \leq \quad C_{jerk} S_N H r \quad \leq \quad \dddot{x}_{max}$$

Putting it all together, one example of the constraint matrix is,

$$\begin{bmatrix} C_{af}S_N \\ -C_{af}S_N \\ C_{xe}S_k \\ -C_{xe}S_k \\ C_{ve}S_k \\ -C_{ve}S_k \\ C_{ae}S_k \\ -C_{ae}S_k \\ C_uS_k \\ -C_uS_k \\ \mathbf{1}^T \\ -\mathbf{1}^T \\ \mathbf{I} \\ -\mathbf{I} \end{bmatrix} Hr \leq \begin{bmatrix} \epsilon_x + X_f \\ \epsilon_x - X_f \\ \epsilon_{xe} \\ -\epsilon_{xe} \\ \epsilon_{ve} \\ -\epsilon_{ve} \\ \epsilon_{ae} \\ -\epsilon_{ae} \\ u_{max} \\ -u_{min} \\ 1+\epsilon_0 \\ -1+\epsilon_0 \\ \mathbf{1}h_{max} \\ -\mathbf{1}h_{min} \end{bmatrix} \tag{4.43}$$

This constraint matrix example says, among other things, that inter-vehicle parameters such as relative spacing, speed, and acceleration at the step k are important. If a tight inter-vehicle spacing is required for all times, the relative spacing constraints for all k should be included. Other requirements could be easily added or removed from the constraint matrix.

4.3.5 Constraint Functions in Frequency Domain

It is well known that an input shaper with positive and negative impulses (as opposed to only positive impulses) may have magnitude amplification at high frequencies [27]. While this may be acceptable for real systems since most physical systems have a high frequency roll-off, a capability of frequency shaping is useful. This section summarizes how to incorporate frequency shaping when designing input shapers using convex optimization.

Expressing (4.17) in the frequency domain,

$$\begin{aligned} H(w) &= \sum_{i=0}^{N-1} h_i e^{-jw(iT_s)}, \quad j = \sqrt{-1} \\ &= \sum_{i=0}^{N-1} \{h_i \cos(iwT_s) - jh_i \sin(iwT_s)\} \end{aligned} \tag{4.44}$$

Some FIR filter design problems assume linear phase (symmetric impulses about the midpoint). This assumption simplifies the formulation of FIR filter design in a convex optimization framework since only real parts of (4.44) are used. However, input shapers in this work are not assumed to have a linear phase, which gives the input shaper more freedom to achieve the best performance.

Since the phase linearity is not assumed, manipulating the magnitude of the input shaper frequency response is essentially taking the magnitude of a series of complex numbers in (4.44). This makes formulating the filter magnitude shaping as a linear combination of h_i quite difficult. A number of techniques have been developed when the magnitude of a nonlinear phase FIR filter needs to be bounded in a form,

$$L(w) \leq |H(w)| \leq U(w), \tag{4.45}$$

such as reformulating the problem using power spectrum of $H(w)$ and retrieving impulse coefficients through spectral factorization [59]. However, most such formulations usually mean a nonlinear convex problem since they work with magnitude squared, instead of magnitude itself. Therefore, they cannot be added directly to the existing linear time domain constraints nor can such problems take advantage of the speed of a linear optimization solver [4].

However, methods for approximating these constraints in a linear form do exist [11, 56]. These methods, described in the following section, can be quite easily adapted to the input shaper problem.

Complex to Real Approximation

The magnitude of a complex number can be represented with a corresponding real number [20]. For any complex number $z = x + jy$,

$$|z| = \sqrt{x^2 + y^2} = \max\{Re(z\eta) \mid \eta \in S\} \tag{4.46}$$

$$S = \{\eta \in \mathbf{C} \mid |\eta| = \mathbf{1}\} \tag{4.47}$$

Choosing $\eta = e^{j2\pi\theta}$ [11], for any complex number z,

$$|z| = \max_{\theta \in T}\{Re(ze^{j2\pi\theta})\} \tag{4.48}$$

$$T = \{\theta \mid -0.5 \leq \theta \leq 0.5\} \tag{4.49}$$

Suppose that an FIR filter with amplitude bounds over frequency points is desired. This is achieved by putting an upper bound on the magnitude of an FIR filter.

$$|H(w)| \leq Z(w), \;\; Z(w) \in \Re_+ \tag{4.50}$$

Since the frequency response of an FIR filter is a complex number at a given frequency, (4.50) can be written as

$$|H(w)| = \max_{\theta \in T}[Re\{H(w)e^{j2\pi\theta}\}] \leq Z(w) \tag{4.51}$$

Solving (4.51) is a semi-infinite problem since the constraint is continuous. Discretizing the constraint by checking $2p$ points over the 2π radius range turns the problem into a semi-definite problem [11],

$$A(w) = \max_{\Delta_r}[Re\{H(w)e^{j\Delta_r}\}] \leq Z(w) \tag{4.52}$$

$$\Delta_r = \frac{(r-1)}{2p}, \quad r = 1, 2, \ldots, 2p \;\; (p \geq 2) \tag{4.53}$$

With the discretized constraints, the discretization error can be bounded as shown in

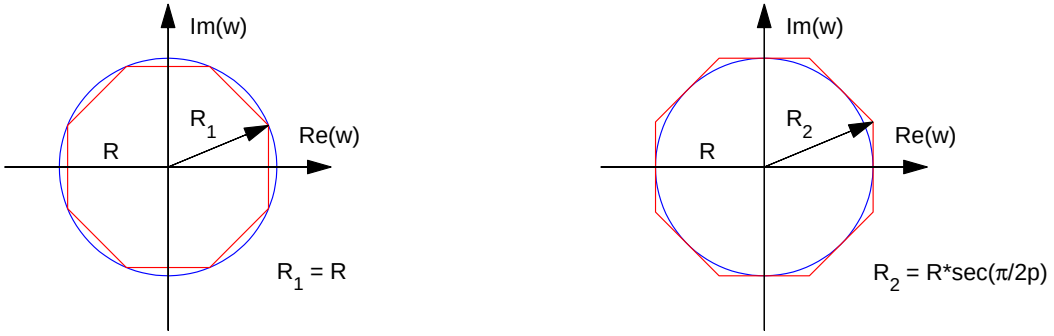

Figure 4.4: A polygon approximation of a unit circle ($p = 8$). The distance from origin to a vertex of the polygon is R in the left plot and $R \cdot sec(\pi/2p)$ in the right plot.

[11, 47], giving

$$A(w) \leq |H(w)| \leq A(w) \sec\left(\frac{\pi}{2p}\right) \tag{4.54}$$

As p gets larger, the discretized constraints more closely resemble the continuous constraints as shown in Figure 4.4. For example, $p = 4$ is used in this work giving an error magnitude bound of about 8% ($sec(\pi/2p) = 1.08$). However, p has to be chosen carefully as it adds complexity and cost in optimization process. Also, smaller p means discrete/approximated gain is much larger than continuous/actual value. This may cause infeasibility which can only be solved with longer impulses, thus slower response.

Frequency Domain Constraints in Convex Optimization

From (4.54),

$$\begin{aligned} |H(w_k)| \leq \max_{\Delta_r} Re\Bigg\{ \sum_{i=0}^{N-1} h_i[\cos(w_k i T_s) - j\sin(w_k i T_s)] \\ \cdot [\cos(\Delta_r) + j\sin(\Delta_r)] \Bigg\} \sec\left(\frac{\pi}{2p}\right) \\ = \max_{\Delta_r} \left[\sum_{i=0}^{N-1} h_i[\cos(w_k i T_s - \Delta_r)]\right] \sec\left(\frac{\pi}{2p}\right) \end{aligned} \tag{4.55}$$

where $k = 1, 2, \cdots, M$ is the number of frequency points for constraints to be matched at. As a rule of thumb, $M \approx 10N$ [59].

Note that the constraint in (4.55) is linear in h_i. Therefore, (4.55) and, hence, (4.51) at $w = w_k$ are satisfied, for all Δ_r if,

$$\sec\left(\frac{\pi}{2p}\right) C_k H \leq Z(w_k)\mathbf{1} \tag{4.56}$$

where

$$\begin{aligned} \mathbf{1}^T &= [1 \cdots 1]_{1\times 2p} \\ C_k &= \begin{bmatrix} 1 & \cos(w_k T_s - \Delta_1) & \cdots & \cos(w_k(N-1)T_s - \Delta_1) \\ \vdots & \vdots & \vdots & \vdots \\ 1 & \cos(w_k T_s - \Delta_{2p}) & \cdots & \cos(w_k(N-1)T_s - \Delta_{2p}) \end{bmatrix}_{2p\times N} \end{aligned}$$

Then, for all frequency points, w_k, $k = 1, 2, \ldots, M$,

$$\sec\left(\frac{\pi}{2p}\right) \begin{bmatrix} C_1 \\ \vdots \\ C_k \\ \vdots \\ C_M \end{bmatrix} H \leq \begin{bmatrix} Z(w_1)\mathbf{1} \\ \vdots \\ Z(w_k)\mathbf{1} \\ \vdots \\ Z(w_M)\mathbf{1} \end{bmatrix} \tag{4.57}$$

Now, Equation 4.57 can be easily added to the existing linear constraint matrices in time domain (Equation 4.43).

Ride Quality Constraint

Ride quality or comfort is a subjective perception that is the cumulative effect of many factors such as seating position, interior volume, tactile inputs, duration of exposure and sound/visual vibration inputs. As a simple proxy, however, the human tolerance to fore/aft vibration can be used to give a measure of the impact of the truck acceleration on ride quality. Tolerance to vibration varies as a function of frequency, reflecting resonances in the torso in the 1-4 Hz range [31]. A sample curve representing human tolerance limits over frequency for fore/aft motion is shown in Figure 4.5 [26].

This plot can be used to generate a weighting function in the form of a frequency domain constraint. For example, if the maximum reference acceleration for a heavy truck is 0.16g, the gain amplification between 1 Hz and 10 Hz should be less than 0.5 ($= 0.08g/0.16g$). Otherwise, the human tolerance limit would be violated (0.08g in that frequency range).

4.3.6 Comparison of Time and Frequency Domain Constraints

Some connections can be made between time and frequency domain constraints. Manipulating impulse magnitudes is one obvious example. In the frequency domain, an input shaper can be designed for little high frequency activity with inclusion of a high frequency roll-off in the constraint magnitude function. Similar effect may also be achieved by limiting the magnitude of each impulse and spreading out the times at which impulses occur. In other words, desired performance may be realized through either method. In most cases, however, one method is preferable to another since it may be much easier to express performance goals in one method, such as ride quality constraint.

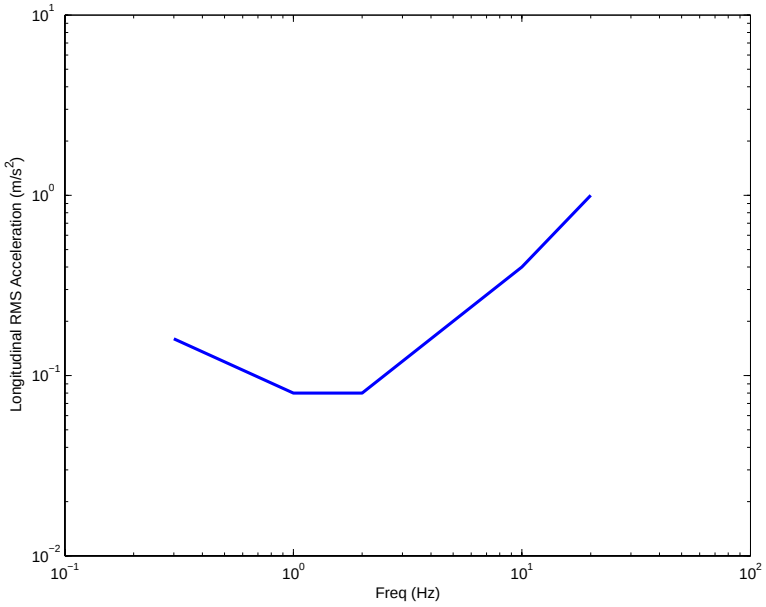

Figure 4.5: Human tolerance limits for fore/aft vibrations.

4.4 Robust Input Shaping Design

Robustness can be added to input shaper design through frequency domain constraint idea. An input shaper is a form of a notch filter. A notch filter "notches" out undesired low damping poles with zeros at that particular frequency. The deeper the notch is , the better the effect of notching is. Obviously, a notch filter with deep notching valley has narrow width. Therefore, it's very susceptible to modeling error or parameter variation (uncertainty in pole location in this case). Adding more zeros around the particular frequency makes the notch filter less sensitive to parameter variation.

The same idea can be used in input shaper design with convex framework. Given system poles in a platoon, a set of constraints for notching effect can be added using methods discussed in Section **??**. For example, robustness constraint may be combined with other frequency domain constraints to form a new constraint. Constraints for a nominal system has been expressed in the following form:

$$|F(w)H(w)| \leq B(w) \tag{4.58}$$

where $F(w)$ is a function of nominal system dynamic matrix. On the other hand, constraints for robust input shaper is the maximum of possible $F(w)$.

$$|F_{robust}(w)H(w)| \leq B(w) \tag{4.59}$$

$$F_{robust}(w) = \sup\{F_i(w) \mid F_i(w) = \text{model variation}\} \tag{4.60}$$

Suppose that some uncertainty lies in mass of the vehicle model and is represented as follows:

$$G(s) = \frac{\hat{m}}{m}\frac{a}{s+a} \tag{4.61}$$

Assuming 10% change in vehicle mass, for a platoon of 9 vehicles, magnitude vari-

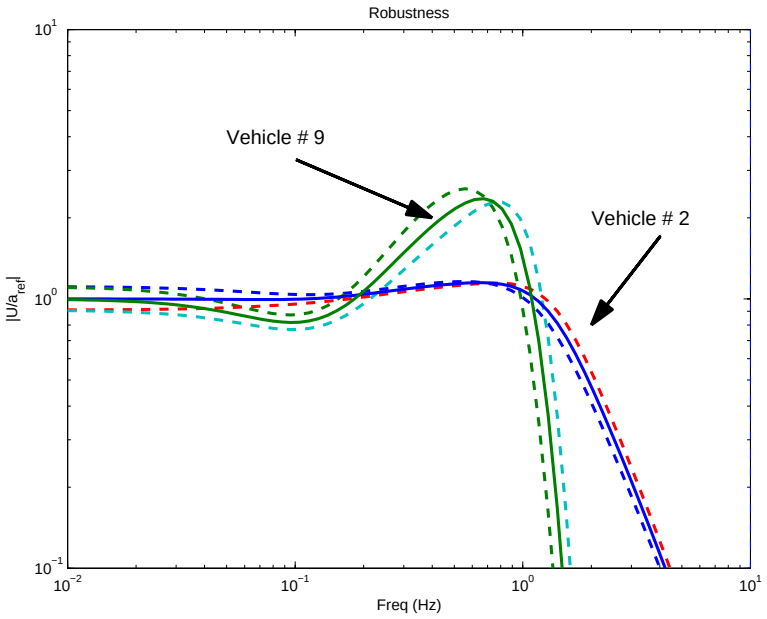

Figure 4.6: Magnitude variation in $|U(s)/a_{ref}(s)|$ due to 10% change in vehicle mass. Dotted lines are uncertain model responses and solid lines between dotted lines are nominal model responses.

ations in boundary cases are shown in Figure 4.6. Dotted lines correspond to model response variation due to ± 10% changes in vehicle mass. The response of Vehicle # 9 peaks around 1 Hz while vehicle # 2's response is more important below 0.2

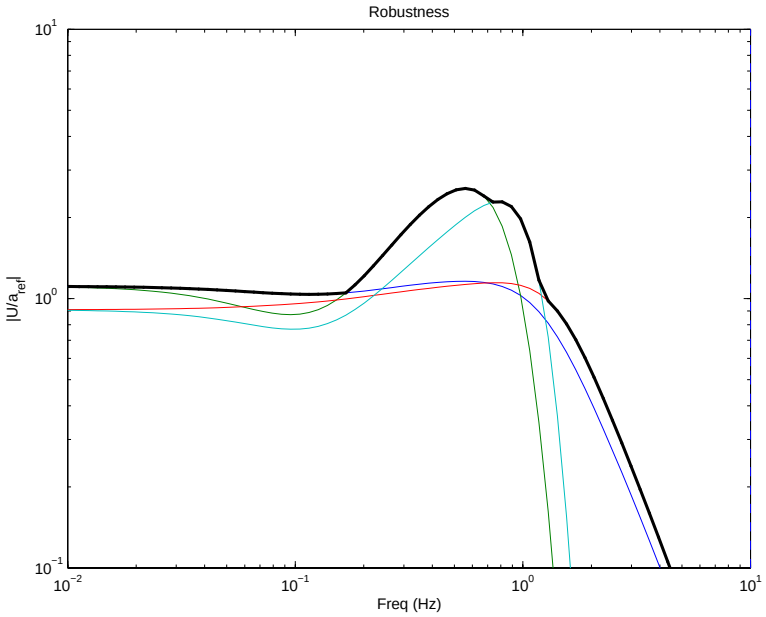

Figure 4.7: Maximum gains over range of models for robustness boundary.

Hz and above 2 Hz. The is because the largest magnitude at each frequency point has to be used such that the convolution of the largest magnitude (call it "robust magnitude") and input shaper magnitude would be below other specified magnitude constraint. The "robust magnitude" is shown in Figure 4.7 as black line. This black line is $|F_{robust}(w)|$ in Equation 4.59. If this line is below $B(w)$ line, then, input shaper is robust to plant variations.

Many factors come into play for determining $B(w)$ in Equation 4.59. For example, as discussed before, ride quality is a constraint that is effectively expressed in frequency domain. Figure 4.8 shows additional frequency domain constraint that puts more damping in $|U(s)/a_{ref}(s)|$ such that the response would not overshoot. As shown, the ride quality constraint is redundant in the presence of damping constraint since the higher magnitude response is a subset of the lower magnitude response. Choosing the lower magnitude response for $B(w)$,

$$B(w) \quad = \quad \inf\{1, b_i(w) \mid b_i(w) = \text{constraint with lower magnitude}\} \qquad (4.62)$$

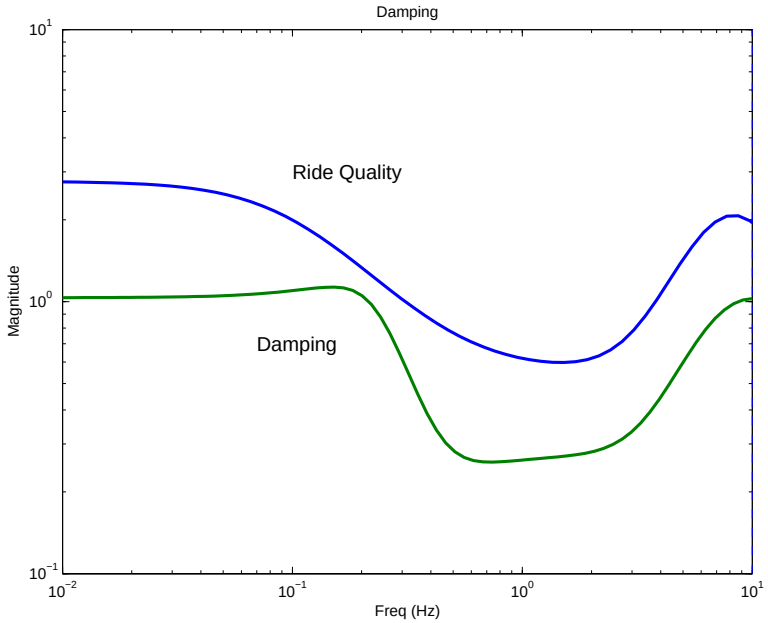

Figure 4.8: Ride quality and damping.

which is shown in red in Figure 4.9.

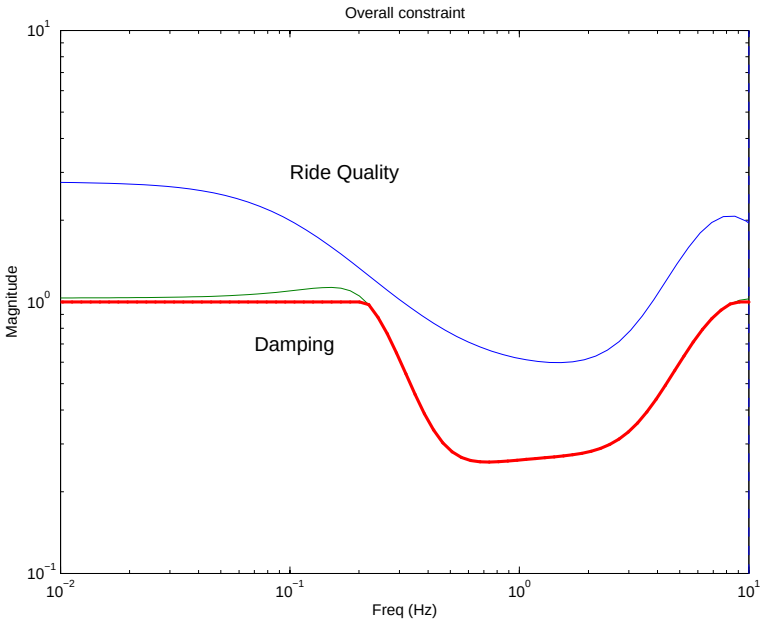

Figure 4.9: Minimum of various magnitude constraints is used for gain constraint.

4.5 Results and Discussion

In the results shown below, input shaper length (N) of 50 and sampling time of 0.05 seconds are used. Results also include robustness constraints as will be discussed wih appropriate figures.

4.5.1 Input Shaper Impulses

With ℓ_1-norm Cost Function

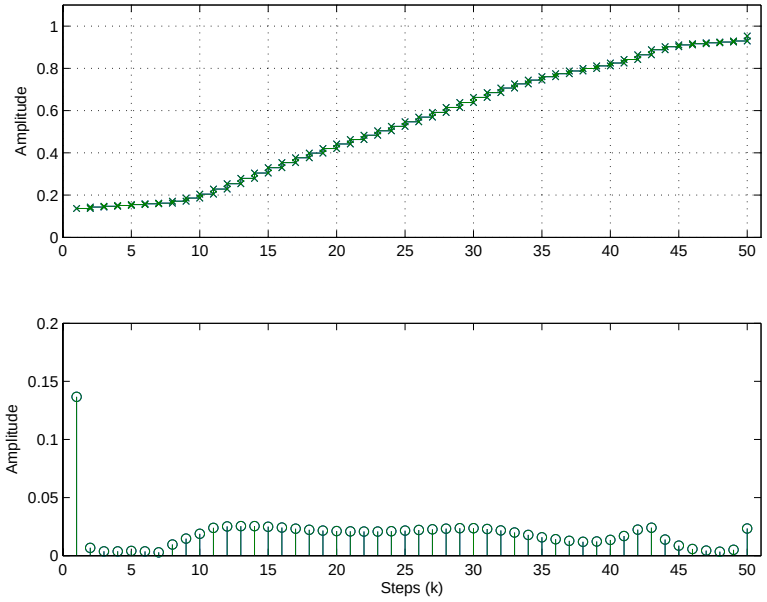

Figure 4.10: Input shaper impulses with ℓ_1 cost function.

Note that the input shaper designed with ℓ_1-norm cost function produced many, small impulses, instead of a few big ones. An attempt to encourage large impulses and suppress small ones by computing the optimization again with weights from reciprocal of original impulses is not very useful in cases like this since most impulses are small and of relatively same size. It may seem undesirable from the point of view of ℓ_0/ℓ_1-norm philosophy. However, the end result is actually very encouraging since input shapers like this has an effect of ramping step changes in input signals.

With ℓ_2-norm Cost Function

When ℓ_2-norm is used, input shaper design produces small impulses, gradually ramping up to the final value. The fact that impulses with ℓ_1 and ℓ_2 cost functions are very similar confirms that the physical intuition that gradual increase in actuation also saves energy.

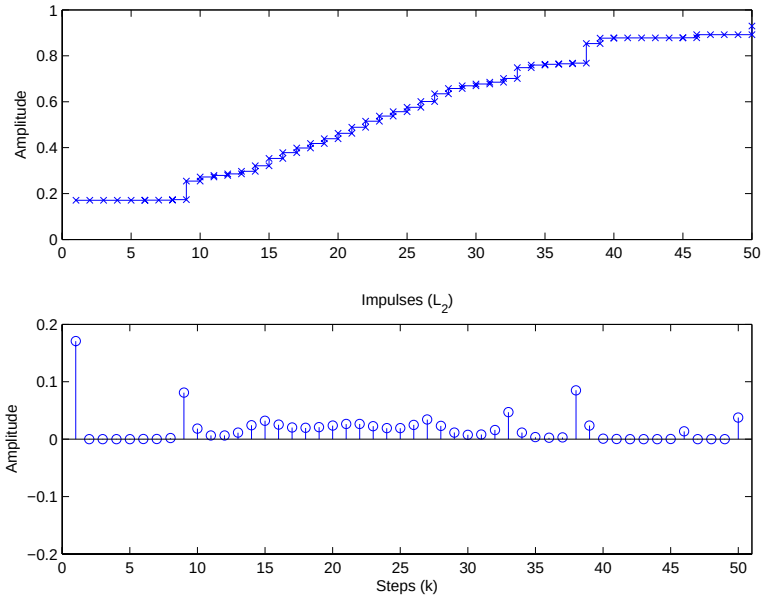

Figure 4.11: Input shaper impulses with ℓ_2 cost function.

4.5.2 Time Responses

Figures 4.12 and 4.13 show control efforts (u) for vehicles #2 through #9 in response to a step acceleration reference input. As step acceleration input enters the platoon, vehicles start to react to the signal over time. The effect shows up over time and grows stronger as the input signal progresses through the platoon. Also evident is the time that the vehicles start reacting to input signal as the input signal progresses through platoon. In other words, there is delay in vehicle response to reference signal.

Figures 4.14 and 4.15 show accelerations for vehicles #2 through #9. The results

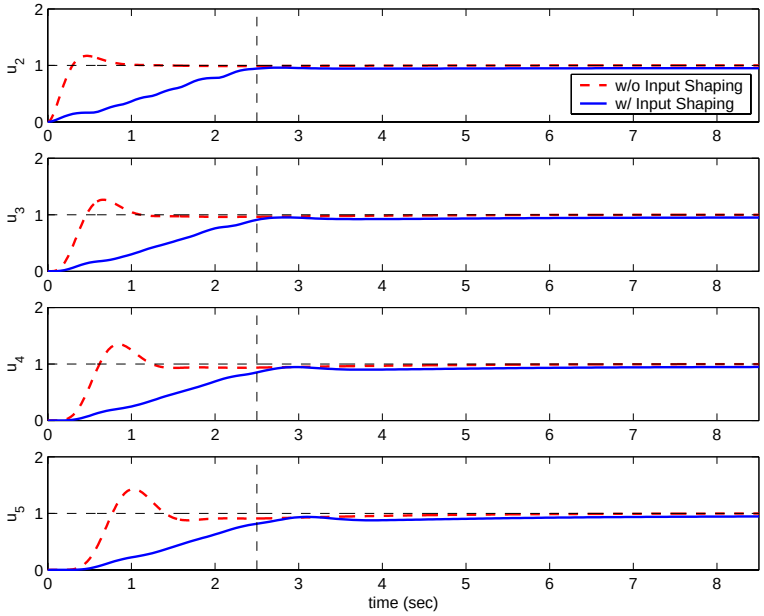

Figure 4.12: Controls (u_2 to u_5) to step acceleration input: ℓ_2 cost function.

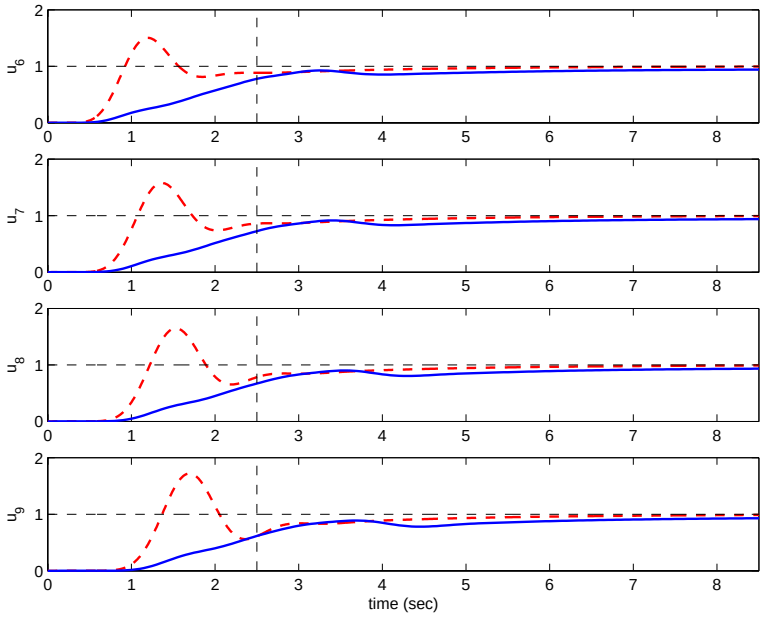

Figure 4.13: Controls (u_6 to u_9) with ℓ_2 cost function.

in these plots are almost identical to Figures 4.12 and 4.13 since the only difference in models between actuation and acceleration is a small, constant gain (no additional dynamics).

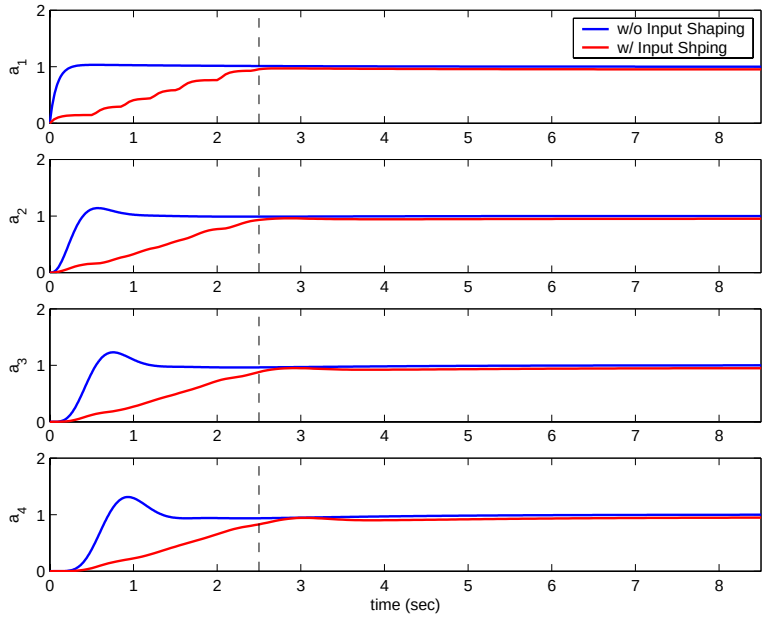

Figure 4.14: Accelerations (a_2 to a_5) with ℓ_2 cost function.

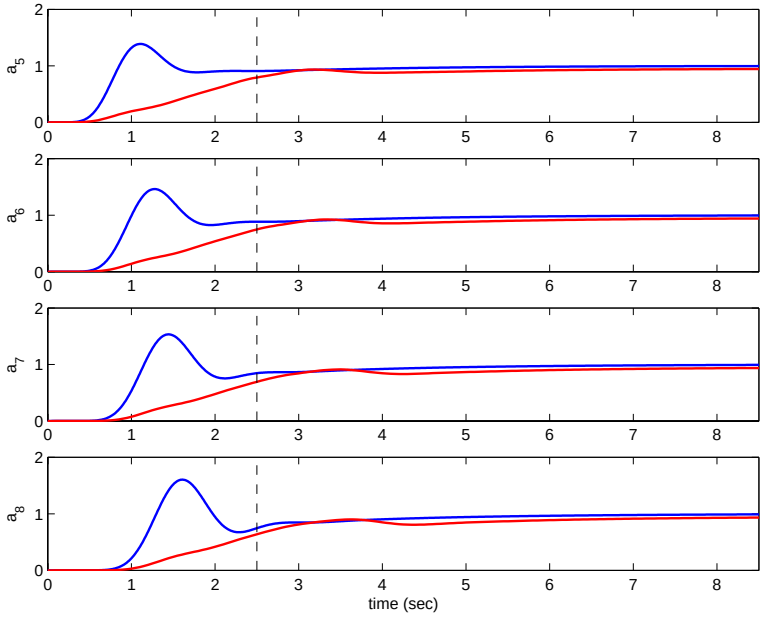

Figure 4.15: Accelerations (a_6 to a_9) with ℓ_2 cost function.

4.5.3 Frequency Responses

Figure 4.16 shows the magnitudes of the transfer function from reference acceleration command to actuation in #2 vehicle, unshpaed in green and shaped in red. The transfer function response of the input shaper is shown in blue/dotted with magenta line showing overall magnitude constraint. Figure 4.17 shows the transfer function

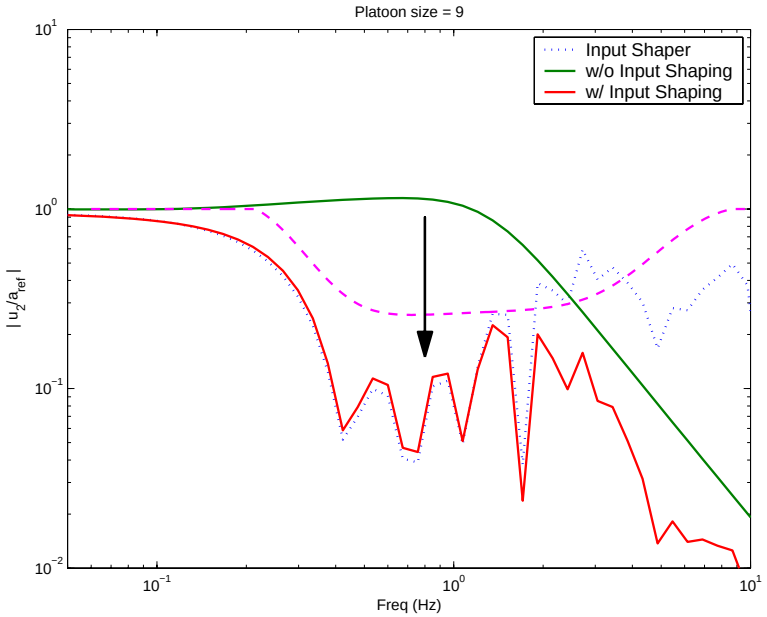

Figure 4.16: $|U_2(s)/A_{ref}(s)|$ with ℓ_2-norm cost function.

responses from reference acceleration command to actuation in #9 vehicle. Similar to results in time domain, Figures 4.18 and 4.19 are almost identical to Figures 4.16 and 4.17, respectively, since the only different in the frequency response of these transfer functions are a small, constant gain.

Recalling Figure 4.6, dynamics from vehicle #2 dominates higher frequency magnitude (about 2 Hz) while the highest peak at a lower frequency (below 2 Hz) is a function of vehicle #9. This explains that the magnitude of shaped transfer function responses is closer to the constraint line at a higher frequency and a lower frequency points for vehicle #2 and #9, respectively.

This characteristics can be easily seen in Figure 4.20 that demonstrates that the input shaper designed with time and frequency domain constraints indeed satisfy

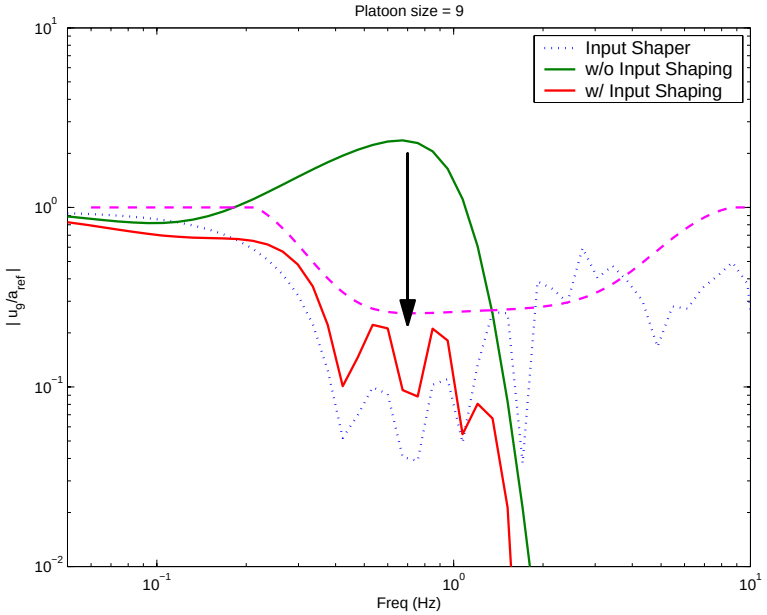

Figure 4.17: $|U_9(s)/A_{ref}(s)|$ with ℓ_2-norm cost function.

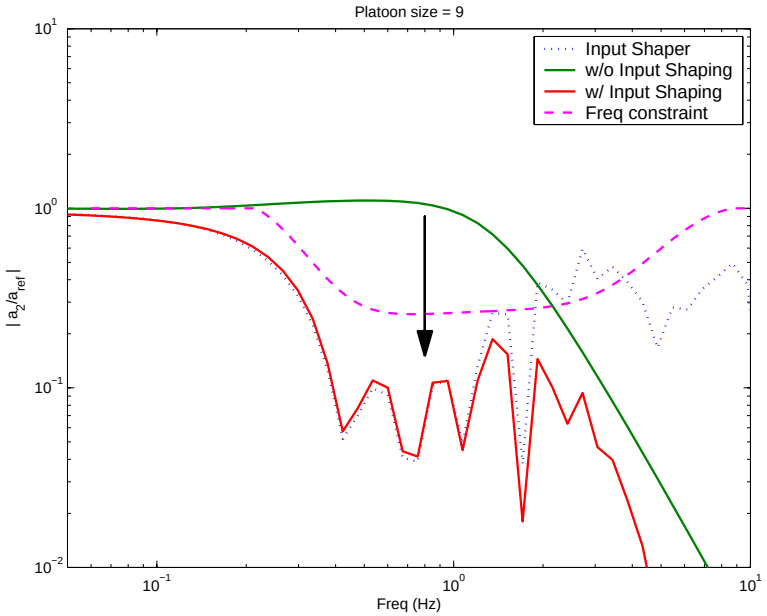

Figure 4.18: $|A_2(s)/A_{ref}(s)|$ with ℓ_2-norm cost function.

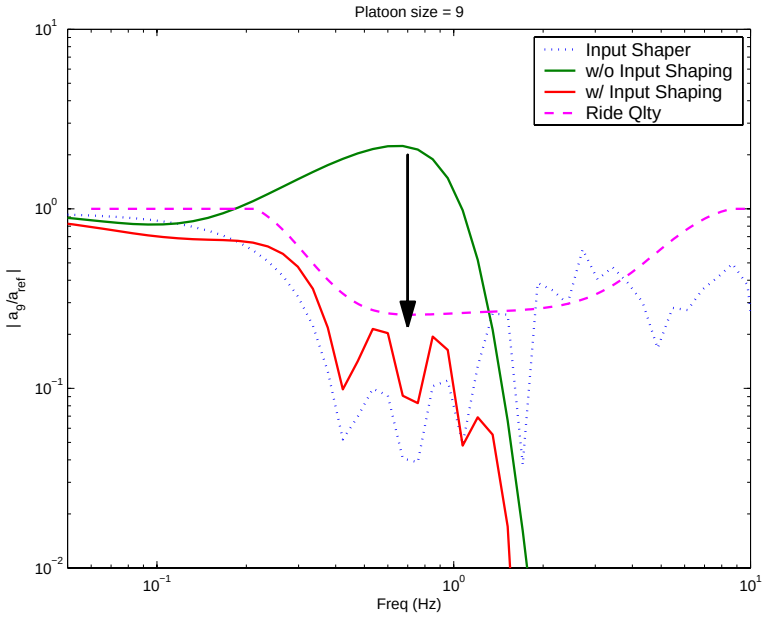

Figure 4.19: $|A_9(s)/A_{ref}(s)|$ with ℓ_2-norm cost function.

all of those constraints, including robustness for model uncertainty. As discussed earlier, some of the responses from vehicle #9 touches the overall gain constraint line (magenta) at lower frequencies while responses from vehicle #2 are the active constraints at higher frequencies.

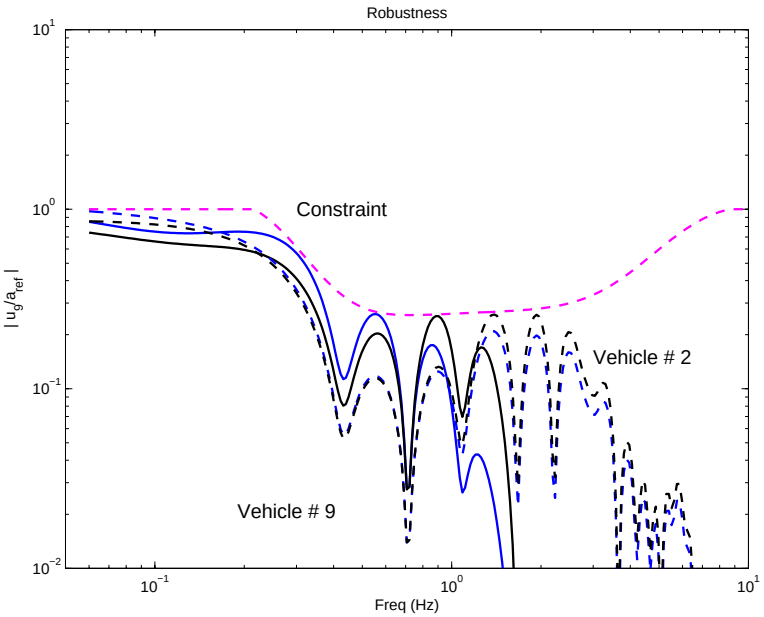

Figure 4.20: Explicit comparison of robust performance.

4.5.4 Input Shaper with Positive and Negative Impulses

As mentioned before, using both positive and negative impulses essentially allows more high frequency content. However, in most input shaping design cases, only the positive impulses have been used since having both positive and negative impulses may destabilize a system when the model used is uncertain at higher frequencies. On the other hand, the convex optimization input shaper design technique with frequency domain constraint developed in this work can explicitly address frequency shaping. Therefore, the extent to which an input shaper can handle in terms of frequency content is completely in the hands of a designer.

Figure 4.21 and 4.22 clearly show that the input shaper with both positive and negative impulses contain higher frequency content while the input shaper with only positive impulses has the effect of high frequency roll-off.

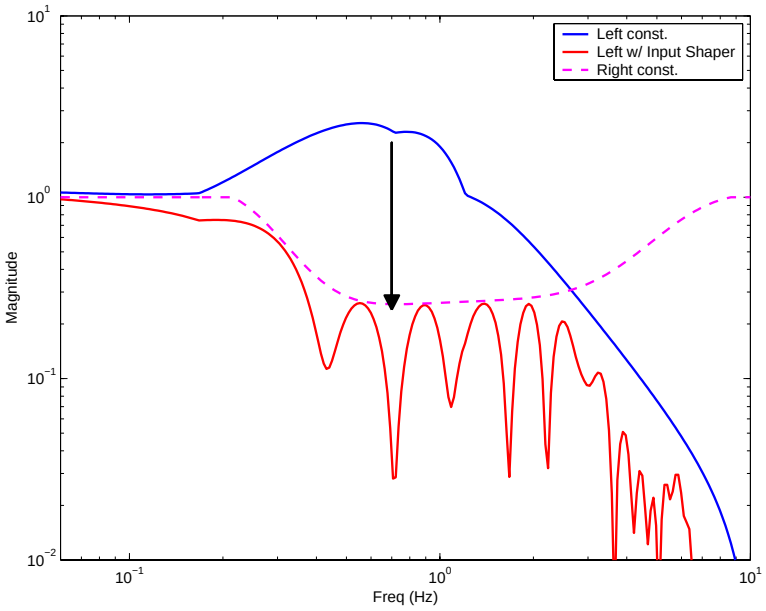

Figure 4.21: Positive only impulses have the effect of high frequency roll-off.

In Figure 4.23, the actual impulses are shown for the input shaper with positive and negative impulses. The fact that an input shaper with virtually any type of impulses can be designed in the convex optimization framework clearly shows that this input shaper design method is much easier and effective to include more constraints

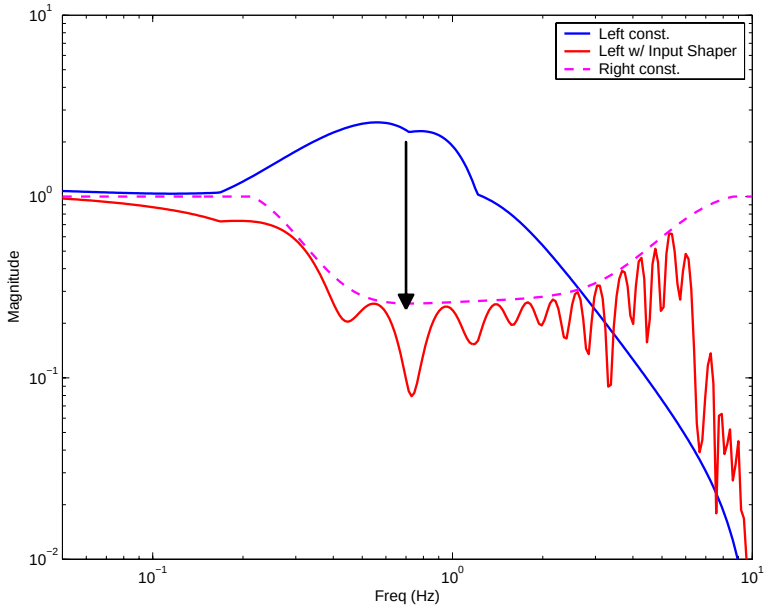

Figure 4.22: Positive and negative impulses allows more high frequency content.

as needed.

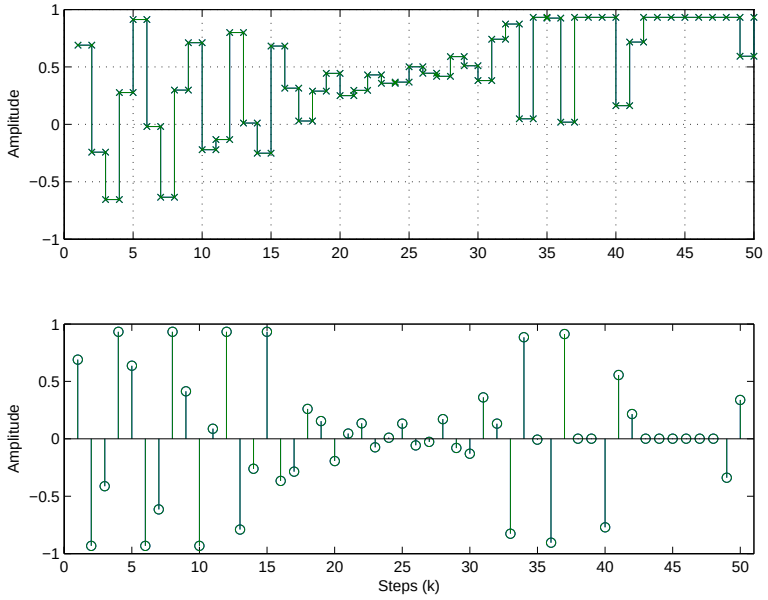

Figure 4.23: Input shaper with positive and negative impulses

4.5.5 Command Profile with Input Shaping

Figure 4.24 shows a realistic command scenario for a platoon. The first plot shows the command in acceleration with upper and lower bounds at 0.5 m/s^2 and -1 m/s^2, respectively. These bounds represent physical (static) limits of acceleration for a given platoon. The acceleration command is then input shaped (shown in red), which is now dynamically bounded as well ("ramping" effect).

In addition, vehicle #6 is weak in this example in the sense that its actuation limits are lower than others (hence, the weakest link in the platoon). Since the input shaper has been designed for robustness and this particular case is a subset of all possible cases, the results will show that the vehicle actuators do not saturate as expected.

The dynamic bounding from input shaping is necessary since the acceleration commands with static bounds may excite the actuation to saturate. In Figure 4.25, actuators in vehicle #6 are completely overwhelmed for much of the high acceleration and deceleration period. Actuators in other vehicles are also saturating for short period of time (shown as spikes). However, when the acceleration command is

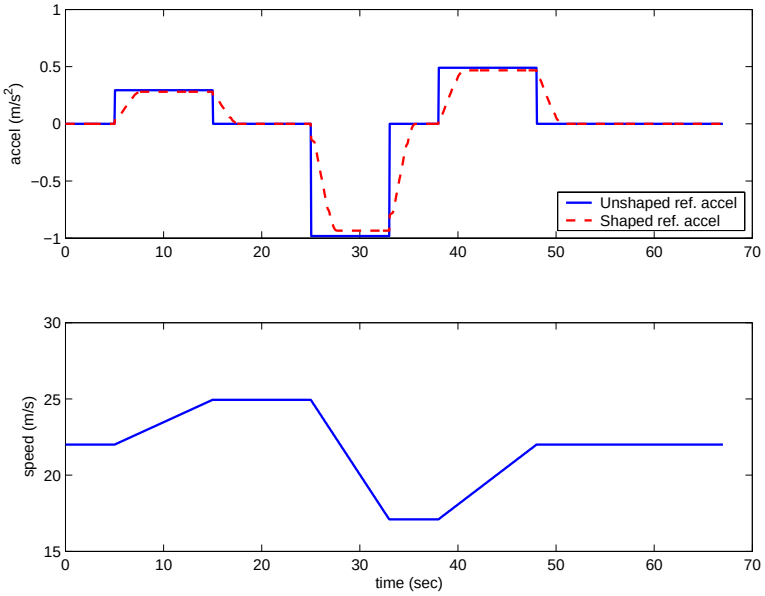

Figure 4.24: Unshaped, shaped reference acceleration and reference speed.

dynamically bounded as well, overshoot and saturation in actuation are eliminated, which makes the platoon maintain string stability (the right plot in Figure 4.30 and Figure 4.27).

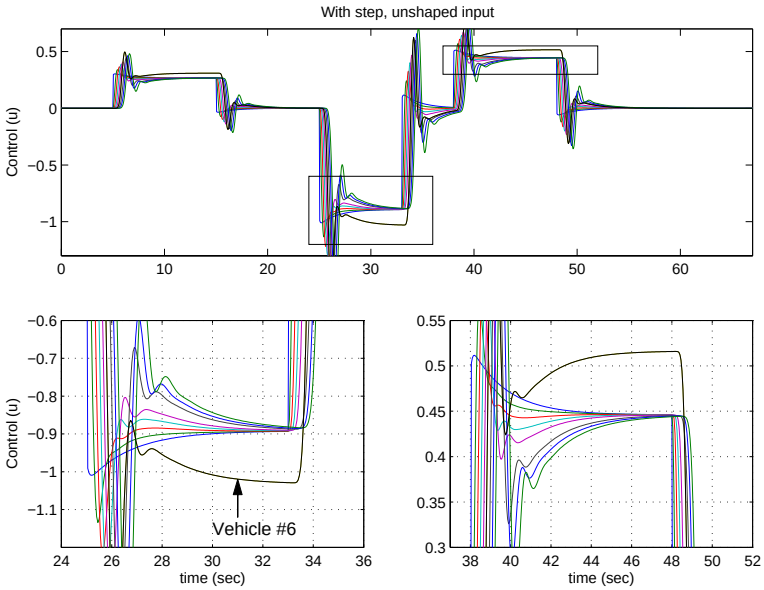

Figure 4.25: Unshaped (with step acceleration changes) control effort (u).

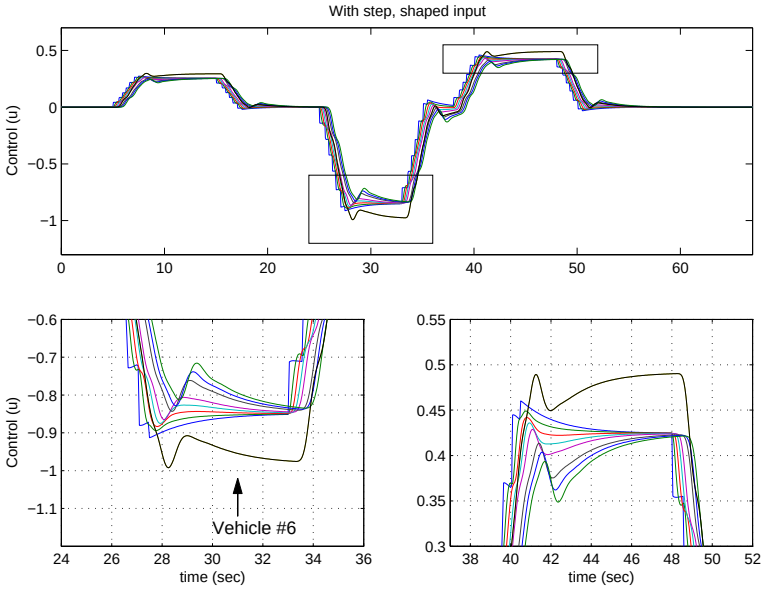

Figure 4.26: Shaped (with step acceleration changes) control effort (u).

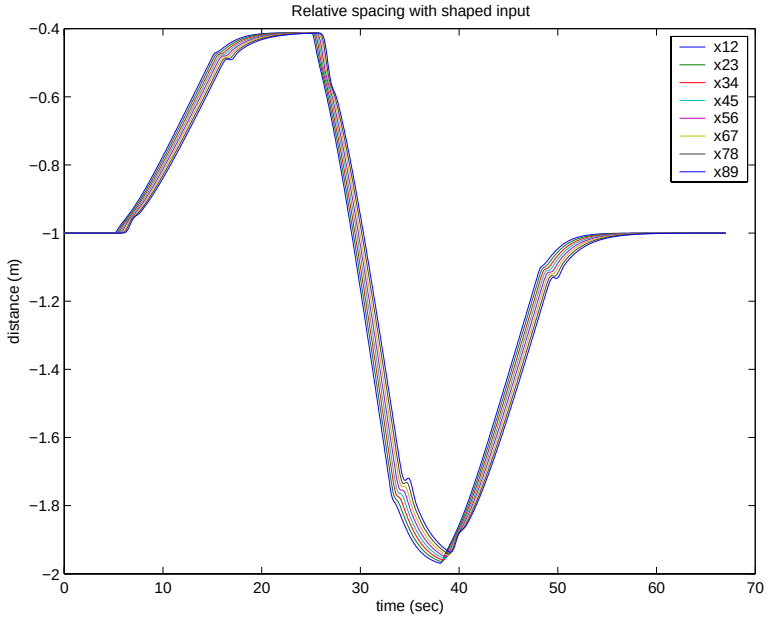

Figure 4.27: Relative spacing with shaped input.

4.6 Ramped Input Case

Instead of a series of step inputs, ramped input may be used such as commands in Figure 4.28. However, without a systematic design process, the desired characteristics in ramping is unclear such as how fast or slow to ramp the step signal given varying length and actuation capabilities of platoons. As in the previous section, robustness is also considered in that the actual mass for Vehicle #6 is 90% of "known" value while the rest is operating at 110% of assumed vehicle mass.

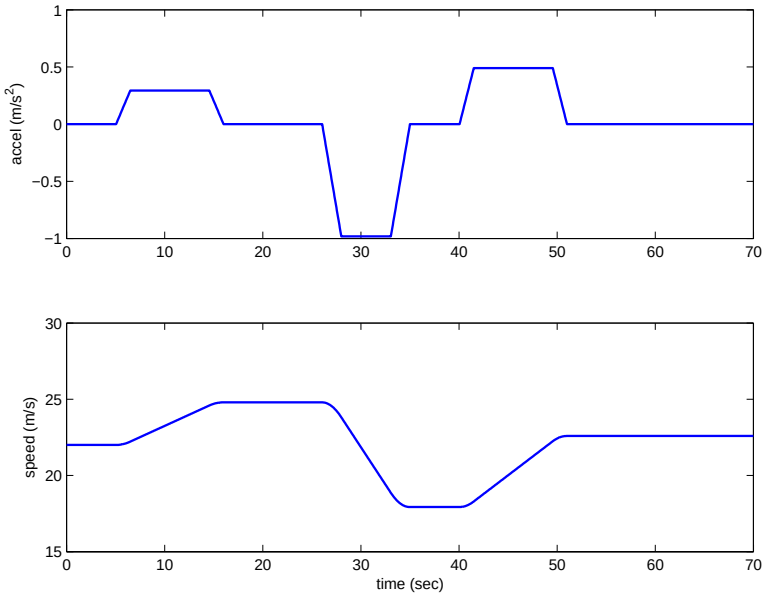

Figure 4.28: Unshaped, ramped reference acceleration and reference speed.

Figure 4.29 clearly shows that, without a systematic design process, the ramping effect was not enough to prevent actuator saturation. Input shaping design synthesis is a powerful tool to solve this problem.

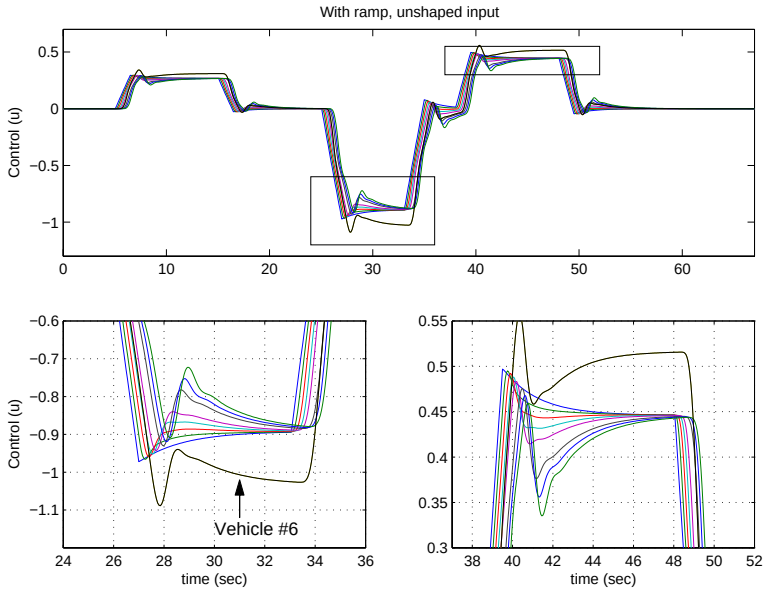

Figure 4.29: Unshaped (with ramp acceleration changes), shaped control effort (u).

4.7 Nonlinear Input Shaper Design

Techniques have been discussed in Section 4.3.5 to approximate the nonlinear magnitude expression with a linear expression since softwares for linear convex optimization are more readily available. However, some software packages can handle nonlinear convex optimization and this section describes how to formulate the problem to take advantage of nonlinear optimization.

Expressing Equation 4.17 in the frequency domain,

$$\begin{aligned} H(w) &= \sum_{i=0}^{N-1} h_i e^{-jw(iT_s)}, \quad j=\sqrt{-1} \\ &= \sum_{i=0}^{N-1} \{h_i \cos(iwT_s) - jh_i \sin(iwT_s)\} \qquad (4.63) \\ &= [\ 1 \quad \cos(wT_s) \quad \cos(2wT_s) \quad \cdots\ ]H \qquad (4.64) \\ &- \ j[\ 0 \quad \sin(wT_s) \quad \sin(2wT_s) \quad \cdots\ ]H \qquad (4.65) \end{aligned}$$

Rearranging for a more compact form,

$$|H(w_k)|^2 = \left\| \begin{bmatrix} 1 & \cos(w_kT_s) & \cos(2w_kT_s) & \cdots \\ 0 & \sin(w_kT_s) & \sin(2w_kT_s) & \cdots \end{bmatrix} H \right\|_2^2 \qquad (4.66)$$

This form can be directly used with software available in [8]. The results are shown in Figures 4.30 and 4.31.

An interesting fact is that the input shaper length with nonlinear optimization turns out to be almost as long as the linear optimization input shaper. This is an important observation that linear optimization software would be sufficient for most of input shaping design cases.

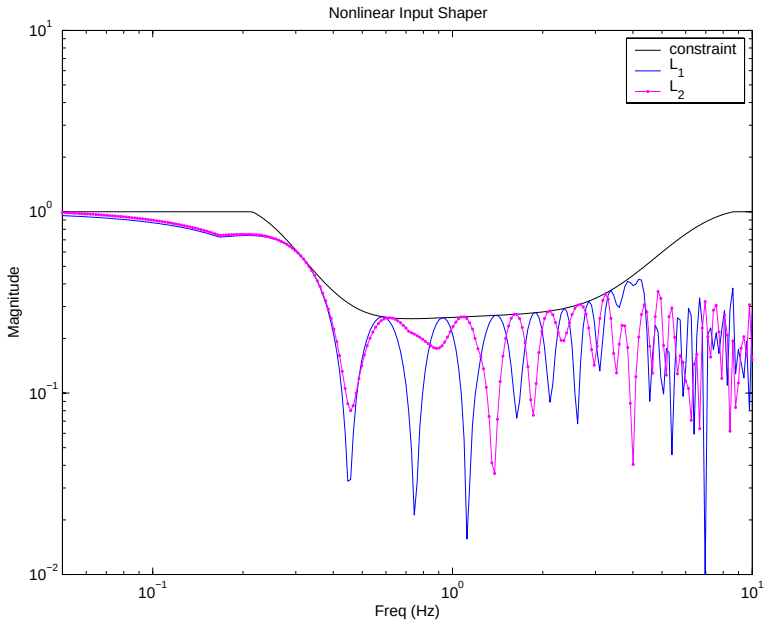

Figure 4.30: Frequency responses with nonlinear optimization.

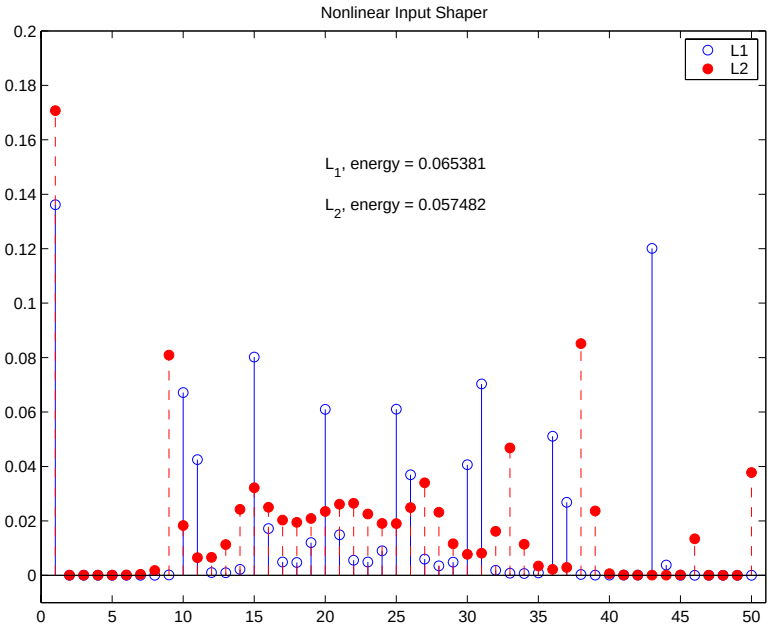

Figure 4.31: Impulses with nonlinear optimization.

4.7.1 ℓ_2-norm Cost Function

A quadratic cost function can also be used in SOCP formulation.

$$\begin{array}{rcll} \text{minimize} \quad \sqrt{u^T u} & \Leftrightarrow & \text{minimize} & ||C_u S_u H|| \\ & \Rightarrow & \text{minimize} & t \\ & & \text{subject to} & ||C_u S_u H|| \leq t \\ & \Rightarrow & \text{minimize} & f^T x \\ & & \text{subject to} & ||Ax|| \leq c^T x \end{array}$$

where x is the new variable to solve for, and

$$\begin{aligned} x &= \begin{bmatrix} H \\ t \end{bmatrix} \in \mathbf{R}^{N+1} \\ f^T &= \begin{bmatrix} 0_{1\times N} & 1 \end{bmatrix} \\ A &= \begin{bmatrix} C_u S_u & 0 \end{bmatrix} \\ c^T &= \begin{bmatrix} 0 & 1 \end{bmatrix} \end{aligned}$$

4.8 Summary

This chapter presented a new method for maintaining and improving string stability by preventing actuator saturation in automated vehicles on highways. Instead of relying on feedback controllers to deal with the issue of actuator saturation after the fact, reference commands are feed through an FIR filter called an input shaper so that harmful components in the reference commands are reduced or removed. Input shaping is a command modification technique in which a reference command to a system is modified or shaped through convolution with an FIR filter. Original (unmodified) reference signals are passed through the input shaper and the shaped (modified) signals are then fed to the system. The purpose of this modification is to remove frequency content from the reference command that can produce oscillations in the closed-loop system due to lightly damped, flexible modes. With properly chosen impulses, the effect can be very significant.

Automated highway systems can benefit from input shaping. A platoon of automated vehicles can be thought of as a series of spring-mass-damper systems where vibration must be controlled for stable operation. For such systems, acceleration can be used for reference commands, but ideal signals must be modified to reflect performance limitations of a platoon of vehicles. A convex optimization approach to input shaper design that can capture time domain constraints such as engine saturation or maneuver end-point is therefore quite useful.

These previous formulations for designing input shapers, however, have included only time domain constraints such as acceleration or position requirements. It is sometimes desirable to have constraints specified in the frequency domain, for instance limiting input shaper gain at high frequencies. In other cases, constraints can only be effectively expressed in the frequency domain. A good example in the context of automated highways is ride quality, which is strongly frequency dependent. This chapter showed how such constraints can be added to the convex optimization framework in a systematic way.

Input shapers designed with time and frequency domain constraints in convex optimization framework have been shown to prevent actuator saturation by dynamically bounding reference commands.

Chapter 5

Conclusion

Automated vehicles require sufficiently accurate system models in order to achieve a desired level of closed-loop performance in, for example, automated highways systems or smart cruise control systems. Parameters of the models are one of the important factors that determine the accuracy of system modeling and, eventually, the overall performance of the closed-loop system.

Current GPS sensing technology enables estimation of road grade and, consequently, simple treatment of parameter estimation from a static force balance. This work has demonstrated that road grade can be reliably estimated using synchronized two antennae GPS system or the vertical to horizontal velocity ratio from GPS speed measurements. While both methods provide similar performance in road grade estimation with comparable errors, the velocity-ratio based, single-antenna system is a better choice since it is more economical to implement than two-antenna system.

In addition, GPS is used to generate an accurate elevation and/or road grade maps for future reference. Results show that these maps are comparable in accuracy to offline maps. When combined with inertial navigation sensors through Kalman filtering, GPS may also be used for dead reckoning purpose. This GPS/INS integration has been demonstrated experimentally to eliminate the problem of GPS signal loss due to the difficulty associated with maintaining the line of sight to satellites inherent in GPS navigation around urban environment.

Accurate estimation of road grade enables the estimations of other important vehicle parameters. With reliable and accurate road grade estimates and the assumption of low frequency dynamics, the vehicle mass estimates have been shown to converge quickly within $\pm 2\%$ and $\pm 5\%$ of the measured values for a passenger car and a heavy truck, respectively. Sum of drag force and rolling resistance has also been reliably estimated. However, separate estimation of them proved less successful. Future work will include separation of drag coefficient and rolling resistance using more detailed models. Given accurate estimate of important vehicle parameters, high performance closed-loop systems are possible.

This work also presented a new method for maintaining and improving string stability by preventing actuator saturation in automated vehicles on highways. Instead of relying on feedback controllers to deal with the issue of actuator saturation after the fact, reference commands are fed through an FIR filter called an input shaper so that harmful components in the reference commands are reduced or removed. Input shaping is a command modification technique in which a reference command to a system is modified or shaped through convolution with an FIR filter. Original (unmodified) reference signals are passed through the input shaper and the shaped (modified) signals are then fed to the system. The purpose of this modification is to remove frequency content from the reference command that can produce oscillations in the closed-loop system due to lightly damped, flexible modes. With properly chosen impulses, the effect can be very significant.

Automated highway systems can benefit from input shaping. A platoon of automated vehicles can be thought of as a series of spring-mass-damper systems where vibration must be controlled for stable operation. For such systems, acceleration can be used for reference commands, but ideal signals must be modified to reflect performance limitations of a platoon of vehicles. A convex optimization approach to input shaper design that can capture time domain constraints such as engine saturation or maneuver end-point is therefore quite useful.

These previous formulations for designing input shapers, however, have included only time domain constraints such as acceleration or position requirements. It is sometimes desirable to have constraints specified in the frequency domain, for instance

limiting input shaper gain at high frequencies. In other cases, constraints can only be effectively expressed in the frequency domain. A good example in the context of automated highways is ride quality, which is strongly frequency dependent. This work showed how such constraints can be added to the convex optimization framework in a systematic way.

Input shapers designed with time and frequency domain constraints in convex optimization framework have been shown to prevent actuator saturation by dynamically bounding reference commands, and therefore, generating smooth trajectories that ultimately guarantee string stability.

Appendix A

Notations

Some specific sets

$\mathbf{R}$	Real numbers
$\mathbf{R}^n$	Real n-vectors ($n \times 1$ matrices)
$\mathbf{R}^{1\times n}$	n-row-vectors ($1 \times n$ matrices)
$\mathbf{R}^{m\times n}$	Real $m \times n$ matrices
$\mathbf{R}_+$	Nonnegative numbers
$\mathbf{R}_{++}$	Positive real numbers
$\mathbf{C}$	Complex numbers
$\mathbf{C}^n$	Complex n-vectors
$\mathbf{C}^{m\times n}$	Complex $m \times n$ matrices
$\mathbf{Z}$	Integers
$\mathbf{Z}_+$	Nonnegative ntegers
$\mathbf{S}^n$	Symmetric $n \times n$ matricies
$\mathbf{S}^n_+$	Symmetric positive semidefinite $n \times n$ matricies
$\mathbf{S}^n_{++}$	Symmetric positive definite $n \times n$ matricies

Vectors and matrices

$\mathbf{1}$	Column vector with all components one
I	Identity matrix
X^T	Transpose of matrix X

Norms and distances

$\|\|x\|\|_1$	l_1-norm of vector x, $\|\|x\|\|_1 = \|x_1\| + \cdots + \|x_n\|$
$\|\|x\|\|_2$	l_2- (or Euclidean) norm of vector x, $\|\|x\|\|_2 = (x_1^2 + \cdots + x_n^2)^{1/2}$
$\|\|x\|\|_\infty$	l_∞-norm of vector x, $\|\|x\|\|_\infty = \max\{\|x_1\|, \ldots, \|x_n\|\}$
$\|\|X\|\|_2$	Spectral norm (maximum singular value) of matrix X

Appendix B

Kalman Filter

A Kalman filter is composed of time update and measurement update steps [18]. In short, the system model is propagated for a time update step, taking advantage of higher update of inertial sensors. The measurement update is performed only when GPS is available and used to estimate the inertial sensor biases and zero out state estimate error.

Simple integration of inertial sensors is performed during time update since the GPS measurement is not available. In the discrete domain, the time update steps are

$$x_k = \Phi_{k-1} x_{k-1} + w_{k-1} \tag{B.1}$$

$$P_k(-) = \Phi_{k-1} P_{k-1}(+) \Phi_{k-1}^T + Q_{k-1} \tag{B.2}$$

where

$$\begin{aligned} \Phi_{k-1} &= \text{Discretized system dynamics matrix} \\ w_{k-1} &= \text{Process (state estimation) noise} \\ Q_{k-1} &= \text{Process noise covariance} \end{aligned}$$

Measurement update steps are

$$\hat{x}_k(+) = \hat{x}_k(-) + K_k[z_k - Hx_k(-)] \tag{B.3}$$

$$K_k = P_{k-1}(-)H_k^T[H_kP_k(-)H_k^T + R_k]^{-1} \tag{B.4}$$

$$P_k(+) = [I - K_kH_k]P_k(-) \tag{B.5}$$

where

$$\begin{aligned}
\hat{x}_k(-) &= \text{Prior estimate of system state at time } k \\
\hat{x}_k(+) &= \text{Updated estimate of system state at time } k \\
P_k(-) &= \text{Prior error covariance at time } k \\
P_k(+) &= \text{Update error covariance at time } k \\
K_k &= \text{Kalman gain at time } k \\
z_k &= \text{New measurement} \\
H_k &= \text{Observation matrix} \\
R_k &= \text{Measurement noise covariance}
\end{aligned}$$

Appendix C

Convex Optimization

This chapter contains useful background information and theories related to convex optimization.

C.1 Basic Optimization

The problem of finding an x that minimizes $f_0(x)$ among all x that satisfy $f_i(x) \leq 0, i = 1, \ldots, m$ and $h_i(x) = 0, i = 1, \ldots, p$ is written in a convenient form:

$$\begin{array}{ll} \text{minimize} & f_0(x) \\ \text{subject to} & f_i(x) \leq 0, \quad i = 1, \ldots, m \\ & h_i(x) = 0, \quad i = 1, \ldots, p \end{array} \tag{C.1}$$

The function $f_0(x) : \mathbf{R}^n \to \mathbf{R}$ is called the *objective* or *cost function* and $x \in \mathbf{R}^n$ called the *optimization variable*. The functions $f_i : \mathbf{R}^n \to \mathbf{R}$ and $h_i : \mathbf{R}^n \to \mathbf{R}$ are the *inequality constraint* and *equality constraint* functions.

The basic optimization problem becomes a *convex optimization* problem when the objective (f_0) and inequality functions (f_i) are convex, and the equality constraint functions (h_i) are affine. Convex optimization problems are particularly useful since finding a solution is essentially a feasibility test. If a solution exist, the solution is the global optimum; if a solution does not exit, the problem is not feasible under given

conditions.

C.2 Linear Program

When the objective and constraint functions are all affine, the prlbme is called a *linear program* (LP). A general linear program has the form

$$\begin{array}{ll} \text{minimize} & c^T x + d \\ \text{subject to} & \bar{G}x \preceq h \\ & Ax = b, \end{array} \tag{C.2}$$

where $G \in \mathbf{R}^{m \times n}$ and $A \in \mathbf{R}^{p \times n}$.

C.3 Quadratic Program

The convex optimization problem is called *quadratic program* (QP) if the objective function is (convex) quadratic and the constraint functions are affine.

$$\begin{array}{ll} \text{minimize} & (1/2)x^T P x + q^T x + r \\ \text{subject to} & \bar{G}x \preceq d \\ & Ax = b, \end{array} \tag{C.3}$$

where $P \in \mathbf{S}_+^n$, $G \in \mathbf{R}^{m \times n}$, and $A \in \mathbf{R}^{p \times n}$.

If the objective as well as the inequality constraint functions are (convex) quadratic, as in

$$\begin{array}{ll} \text{minimize} & (1/2)x^T P_0 x + q_0^T x + r_0 \\ \text{subject to} & (1/2)x^T P_i x + q_i^T x + r_i \leq 0, \;\; i = 1, \ldots, m \\ & Ax = b, \end{array} \tag{C.4}$$

where $P_i \in \mathbf{S}_+^n, i = 0, 1, \ldots, m$, the problem is called a *quadratically constrained quadratic program* (QCQP). In a QCQP, we minimize a convex quadratic function over a feasible region that is the intersection of (possibly degenerate) ellipsoids.

C.4 Second-Order Cone Program

C.4.1 Norm cone

The *norm cone* associated with the norm $||\cdot||$ is the set

$$C = \{(x,t) \mid ||x|| \leq t\}$$

The second-order cone is the norm cone for the Euclidean norm,

$$\begin{aligned} C &= \left\{(x,t) \in \mathbf{R}^{n+1} \mid ||x||_2 \leq t\right\} \\ &= \left\{ \begin{bmatrix} x \\ t \end{bmatrix} \;\middle|\; \begin{bmatrix} x \\ t \end{bmatrix}^T \begin{bmatrix} I & 0 \\ 0 & -1 \end{bmatrix} \begin{bmatrix} x \\ t \end{bmatrix} \leq 0, \quad t \geq 0 \right\} \end{aligned}$$

C.4.2 SOCP

A *second-order cone program* (SOCP) has the following form:

$$\begin{array}{ll} \text{minimize} & f^T x \\ \text{subject to} & ||A_i x + b_i||_2 \leq c_i^T x + d_i, \;\; i = 1, \ldots, m \\ & Fx = g, \end{array} \tag{C.5}$$

where $x \in \mathbf{R}^n$ is the optimization variable, $A_i \in \mathbf{R}^{n_i \times n}$, and $F \in \mathbf{R}^{p \times n}$.

The name comes from the *norm cone*. The *norm cone* associated with the norm $||\cdot||$ is the set

$$C = \{(x,t) \mid ||x|| \leq t\}.$$

For example, the second-order cone is the norm cone for the Euclidean norm,

$$\begin{aligned} C &= \left\{(x,t) \in \mathbf{R}^{n+1} \mid ||x||_2 \leq t\right\} \\ &= \left\{ \begin{bmatrix} x \\ t \end{bmatrix} \;\middle|\; \begin{bmatrix} x \\ t \end{bmatrix}^T \begin{bmatrix} I & 0 \\ 0 & -1 \end{bmatrix} \begin{bmatrix} x \\ t \end{bmatrix} \leq 0, \quad t \geq 0 \right\}. \end{aligned}$$

C.5 Norms

C.5.1 l_0-norm

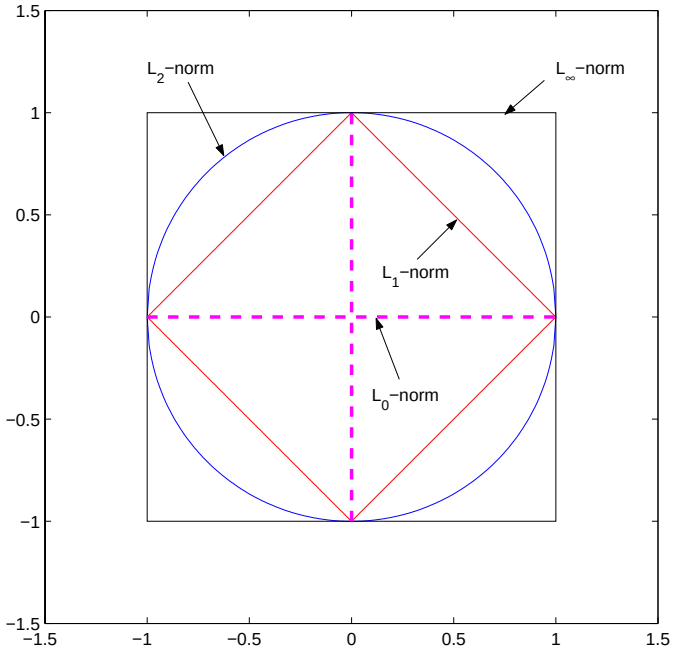

Figure C.1: Plot of $||x||_0, ||x||_1, ||x||_2, ||x||_\infty = 1, \ \ (x \in \Re^2)$.

Finding an input shaper with minimum number of non-zero elements is an l_0-norm optimization problem. The unit ball for the l_0-norm is $\cup_{i=1}^{N} E_i$ such that [32]

$$E_i = \{x \in \Re^N | x = \lambda e_i, |\lambda| \leq 1, e_i^T = [0, \cdots, \underbrace{1}_{i-th}, \cdots, 0]\}. \tag{C.6}$$

The l_0-norm's pictorial description is shown in Figure C.1 along with other norms. Strictly speaking, however, this is not a norm since it does not satisfy the homogeneous condition: $\|tx\|_0 \neq |t|\|x\|_0$. Nonetheless, the term *norm* is used according to the convention by the mathematics research community.

C.5.2 l_1-norm and Cardinality

The least l_1-norm problem,

$$\begin{array}{rl} \text{minimize} & ||x||_1 \\ \text{subject to} & \text{Ax} = \text{b} \end{array} \tag{C.7}$$

tends to produce a solution x with a large number of components equal to zero. In other words, the least l_1-norm problem tends to produce *sparse* solutions of $Ax = b$, often with m non-zero components.

The *cardinality* or *size* of a vector $x \in \Re^n$ is the number of non-zero components and denoted $\mathbf{card}(x)$. The function $\mathbf{card}$ is quasiconcave on $\Re^n_+$ (but not $\Re^n$). This follows immediately from the modified Jensen inequality

$$\mathbf{card}(x+y) \geq \min\{\mathbf{card}(x), \mathbf{card}(y)\}, \tag{C.8}$$

which holds for $x, y \succeq 0$.

C.5.3 ℓ_2-norm

Sometime, it's useful to have an Euclidean norm for the cost function, e.g. minimizing energy which is express in ℓ_2-norm form.

$$\begin{array}{rl} \text{minimize} & ||Ax-b||_2 \\ \text{subject to} & Fx \preceq g \end{array}$$

Since the norm is always non-negative, we can just as well solve the problem

$$\text{minimize} \quad ||Ax-b||_2^2 = (Ax-b)^T(Ax-b)$$

, in which we minimize the square of the Euclidean norm. The equivalent problem is then a *quadratic program* (QP) problem where the cost function is quadratic and the constraint functions are affine:

$$\begin{array}{rl} \text{minimize} & x^TA^TAx - 2b^TAx + b^Tb \\ \text{subject to} & Fx \preceq g \end{array}$$

If the constraint as well as cost functions are quadratic, it is called a *quadratically constraint quadratic program* (QCQP).

C.6 Convex Optimization Formulation in MATLAB

The constrained ℓ_1-norm approximation of

$$\begin{array}{rl} \text{minimize} & \|Ax-b\|_1 \\ \text{subject to} & Fx \preceq g \end{array}$$

can be written as

$$\begin{array}{rl} \text{minimize} & \mathbf{1}^T y \\ \text{subject to} & Ax-b \preceq y \\ & Ax-b \succeq -y \\ & Fx \preceq g \end{array}$$

In a MATLAB friendly format (`linprog.m`),

$$\mathbf{1}^T y \implies \begin{bmatrix} 0_{1\times n} & \mathbf{1} \end{bmatrix} \begin{bmatrix} x \\ y \end{bmatrix} \tag{C.9}$$

$$Ax-b \preceq y \implies \begin{bmatrix} A & -I_{n\times n} \end{bmatrix} \begin{bmatrix} x \\ y \end{bmatrix} \preceq b \tag{C.10}$$

$$Ax-b \succeq -y \implies \begin{bmatrix} -A & -I_{n\times n} \end{bmatrix} \begin{bmatrix} x \\ y \end{bmatrix} \preceq -b \tag{C.11}$$

$$Fx \preceq g \implies \begin{bmatrix} F & 0_{k\times n} \end{bmatrix} \begin{bmatrix} x \\ y \end{bmatrix} \preceq g \tag{C.12}$$

$$\tag{C.13}$$

Weighted input shaper design form,

$$\begin{array}{rl} \text{minimize} & \|WH\|_1 \\ \text{subject to} & FH \preceq g \end{array}$$

can be written as

$$\begin{array}{rl} \text{minimize} & \mathbf{1}^T y \\ \text{subject to} & WH \preceq y \\ & WH \succeq -y \\ & FH \preceq g \end{array}$$

Putting in a MATLAB format, cost function and constraints are

$$\mathbf{1}^T y \implies \begin{bmatrix} 0_{1\times n} & \mathbf{1} \end{bmatrix} \begin{bmatrix} H \\ y \end{bmatrix} \tag{C.14}$$

$$\left.\begin{array}{r} Ax - b \preceq y \\ Ax - b \succeq -y \\ FH \preceq g \end{array}\right\} \implies \begin{bmatrix} W & -I_{n\times n} \\ -W & -I_{n\times n} \\ F & 0_{k\times n} \end{bmatrix} \begin{bmatrix} H \\ y \end{bmatrix} \preceq \begin{bmatrix} 0_{n\times 1} \\ 0_{n\times 1} \\ g \end{bmatrix} \tag{C.15}$$

C.7 Convexity of SOCP

If a function f is convex, it satisfies the following inequality,

$$f(\alpha x + \beta y) \leq \alpha f(x) + \beta f(y) \quad where \quad \alpha + \beta = 1, \quad \alpha, \beta \geq 0$$

From the inequality constraint of SOCP problem, with $\alpha + \beta = 1, \quad \alpha, \beta \geq 0$,

$$\begin{aligned} f(x) &= \|Ax + b\|_2 - c^T x \\ \alpha f(x) + \beta f(y) &= \alpha(\|Ax + b\|_2 - c^T x) + \beta(\|Ay + b\|_2 - c^T x) \\ f(\alpha x + \beta y) &= \|A(\alpha x + \beta y) + b\|_2 - c^T(\alpha x + \beta y) \end{aligned}$$

Then,

$$\begin{aligned}
&\alpha f(x) + \beta f(y) - f(\alpha x + \beta y) \\
&\quad = \alpha\|Ax+b\|_2 - \alpha c^T x + \beta\|Ay+b\|_2 - \beta c^T x - \|A(\alpha x+\beta y)+b\|_2 + c^T(\alpha x+\beta y) \\
&\quad = \alpha\|Ax+b\|_2 + \beta\|Ay+b\|_2 - \|\alpha(Ax+b)+\beta(Ay+b)+b(1-\alpha-\beta)\|_2 \\
&\quad = \alpha\|Ax+b\|_2 + \beta\|Ay+b\|_2 - \|\alpha(Ax+b)+\beta(Ay+b)\|_2 \\
&\quad \geq 0
\end{aligned}$$

Therefore, the inequality constraint function in SOCP is convex. In multiple appearances of l_2-norms,

$$\begin{aligned}
f(x) &= \|Ax+b\|_2 + \|Fx+g\|_2 - c^T x \\
\alpha f(x) + \beta f(y) &= \alpha(\|Ax+b\|_2 + \|Fx+g\|_2 - c^T x) + \beta(\|Ay+b\|_2 + \|Fy+g\|_2 - c^T x) \\
f(\alpha x + \beta y) &= \|A(\alpha x+\beta y)+b\|_2 + \|F(\alpha x+\beta y)+g\|_2 - c^T(\alpha x+\beta y)
\end{aligned}$$

Then,

$$\begin{aligned}
&\alpha f(x) + \beta f(y) - f(\alpha x + \beta y) \\
&\quad = \alpha(\|Ax+b\|_2 + \|Fx+g\|_2 - c^T x) + \beta(\|Ay+b\|_2 + \|Fy+g\|_2 - c^T x) \\
&\qquad - \|A(\alpha x+\beta y)+b\|_2 - \|F(\alpha x+\beta y)+g\|_2 + c^T(\alpha x+\beta y) \\
&\quad = \alpha(\|Ax+b\|_2 + \|Fx+g\|_2) + \beta(\|Ay+b\|_2 + \|Fy+g\|_2) \\
&\qquad - \|\alpha Ax+\beta Ay+b\|_2 - \|\alpha Fx+\beta Fy+g\|_2 \\
&\quad = \alpha(\|Ax+b\|_2 + \|Fx+g\|_2) + \beta(\|Ay+b\|_2 + \|Fy+g\|_2) \\
&\qquad - \|\alpha(Ax+b)+\beta(Ay+b)+b(1-\alpha-\beta)\|_2 \\
&\qquad - \|\alpha(Fx+g)+\beta(Fy+g)+g(1-\alpha-\beta)\|_2 \\
&\quad = \alpha\|Ax+b\|_2 + \beta\|Ay+b\|_2 - \|\alpha(Ax+b)+\beta(Ay+b)\|_2 \\
&\qquad + \alpha\|Fx+g\|_2 + \beta\|Fy+g\|_2 - \|\alpha(Fx+g)+\beta(Fy+g)\|_2 \\
&\quad \geq 0
\end{aligned}$$

Therefore, generalizing to n number of norms in the inequality constraint,

$$f(x) = \sum_{k=1}^{n} \|A_k x + b_k\|_2 - c^T x$$

is also convex.

C.8 Formulating QCQP in SOCP

Let us consider the general convex quadratically constrained quadratic program (QCQP).

$$\begin{array}{ll} \text{minimize} & x^T P_0 x + 2q_0^T x + r_0 \\ \text{subject to} & x^T P_i x + 2q_i^T x + r_i \leq 0, \quad i = 1, \ldots, p, \end{array} \tag{C.16}$$

where $P_0,\ P_1,\ \ldots,\ P_p \in \mathbf{R}^{n \times n}$ are symmetric and positive semidefinite. We will assume for simplicity that the matrices P_i are strictly positive definite, although the problem can be reduced to an SOCP in general. This allows us to write the QCQP (C.16) as

$$\begin{array}{ll} \text{minimize} & ||P_0^{1/2} x + P_0^{-1/2} q_0|| + r_0 - q_0^T P_0^{-1} q_0 \\ \text{subject to} & ||P_i^{1/2} x + P_i^{-1/2} q_i|| + r_i - q_i^T P_i^{-1} q_i \leq 0, \quad i = 1, \ldots, p, \end{array}$$

which can be solved via the SOCP with $p + 1$ constraints of dimension $n + 1$

$$\begin{array}{ll} \text{minimize} & t \\ \text{subject to} & ||P_0^{1/2} x + P_0^{-1/2} q_0|| \leq t \\ & ||P_i^{1/2} x + P_i^{-1/2} q_i|| \leq (q_i^T P_i^{-1} q_i - r_i)^{1/2}, \quad i = 1, \ldots, p, \end{array} \tag{C.17}$$

where $t \in \mathbf{R}$ is a new optimization variable. The optimal values of (C.16) and (C.17) are equal up to a constant and a square root. More precisel, the optimal values of (C.16) is equal to $p^{*2} + r_0 - q_0^T P_0^{-1} q_0$, where p^* is the optimal value of (C.16).

As a special case, we can solve a convex quadratic programming problem (QP)

$$\begin{array}{ll} \text{minimize} & x^T P_0 x + 2q_0^T x + r_0 \\ \text{subject to} & a_i^T x \leq b_i, \quad i = 1, \ldots, p, \end{array}$$

($P_0 > 0$) as an SOCP with one constraint of dimension $n + 1$ and p constraints of dimension one:

$$\begin{array}{rl} \text{minimize} & t \\ \text{subject to} & ||P_0^{1/2}x + P_0^{-1/2}q_0|| \leq t \\ & a_i^T x \leq b_i, \quad i = 1, \ldots, p, \end{array}$$

where the variables are x and t.

C.9 Uncertainty Representation in Convex Optimization

Consider a linear program,

$$\begin{array}{rl} \text{minimize} & c^T x \\ \text{subject to} & a_i^T x \leq b_i, \quad i = 1, \ldots, m, \end{array} \tag{C.18}$$

in which there is some uncertainty or variation in a_i. If a_i is known to lie in given ellipsoids:

$$a_i \in \mathcal{E}_i = \{\overline{a}_i + P_i u \mid ||u||_2 \leq 1\} \tag{C.19}$$

where $x, a_i, u \in \mathbf{R}^n$ and $P_i \in \mathbf{R}^{n\times n}$. If P_i is singular we obtain 'flat' ellipsoid, of dimension **rank** P_i; $P_i = 0$ means that a_i is known perfectly.

For robustness, the constraints should be satisfied for all possible values of the parameters, a_i,

$$\begin{array}{rl} \text{minimize} & c^T x \\ \text{subject to} & a_i^T x \leq b_i \text{ for all } a_i \in \mathcal{E}_i \quad i = 1, \ldots, m, \end{array} \tag{C.20}$$

The robust linear constraint, $a_i^T x \leq b_i$ for all $a_i \in \mathcal{E}_i$, can be expressed as

$$\sup\{a_i^T x \mid a_i \in \mathcal{E}_i\} \leq b_i, \tag{C.21}$$

the left hand side of which can be written as

$$\begin{aligned} \sup\{a_i^T x \mid a_i \in \mathcal{E}_i\} &= a_i^T x + \sup\{u^T P_i^T x \mid \|u\|_2 \leq 1\} && \text{(C.22)} \\ &= \overline{a}_i^T x + ||P_i^T x||_2. && \text{(C.23)} \end{aligned}$$

Thus, the robust linear constraint can be expressed as

$$\overline{a}_i^T x + ||P_i^T x||_2 \leq b_i, \tag{C.24}$$

which is evidently a second-order cone constraint. Therefore, the robust linear programming in Equation (C.20) can be expressed as the SOCP

$$\begin{array}{ll} \text{minimize} & c^T x \\ \text{subject to} & \overline{a}_i^T x + ||P_i^T x||_2 \leq b_i, \quad i = 1, \ldots, m, \end{array} \tag{C.25}$$

The additional norm term act as *regularization terms*; they prevent x from being large in directions with considerable uncertainty in the parameters a_i.

C.10 Inequality Constraints with Sum of Norms

Suppose an optimization problem with the following contraint:

$$\|Ax\|_2 + \|Bx\|_2 + \cdots \leq c^T x + d \tag{C.26}$$

The question rises since the MOSEK software (or, probably other SOCP software packages) assumes the only one norm in inequality constraint form as in Equation (C.5). It is easy to show that the form in Equation (C.26) can be rearranged into the form in Equation (C.5). Without loss of generality, let's assume we have two l_2-norms:

$$\|Ax\|_2 + \|Bx\|_2 \leq c^T x + d \tag{C.27}$$

By introducing a slack variable t, Equation (C.27) is

$$\|Ax\|_2 \leq c^T x + d - t \tag{C.28}$$
$$\|Bx\|_2 \leq t \tag{C.29}$$

By defining a new optimization variable $[\ x \quad t\ ]^T \in \mathbf{R}^{n+1}$, the problem becomes

$$\left\| \begin{bmatrix} A & 0 \end{bmatrix} \begin{bmatrix} x \\ t \end{bmatrix} \right\|_2 \leq \begin{bmatrix} c^T & -1 \end{bmatrix} \begin{bmatrix} x \\ t \end{bmatrix} + d \tag{C.30}$$
$$\left\| \begin{bmatrix} B & 0 \end{bmatrix} \begin{bmatrix} x \\ t \end{bmatrix} \right\|_2 \leq \begin{bmatrix} 0 & 1 \end{bmatrix} \begin{bmatrix} x \\ t \end{bmatrix} \tag{C.31}$$

which is exactly in the form of Equation (C.5). In case of m l_2-norms in the constraint, with a slack variable vector

$$t = [\ t_1 \quad t_2 \quad \cdots \quad t_{m-1}\ ]^T \in \mathbf{R}^{m-1}$$

, the problem is,

$$\begin{aligned} \|A_0 x\|_2 &\leq c^T x + d - \mathbf{1}^T t \\ \|A_1 x\|_2 &\leq t_1 \\ &\vdots \\ \|A_{m-1} x\|_2 &\leq t_{m-1}. \end{aligned}$$

Defining a new optimization variable $[\ x \quad t\ ]^T \in \mathbf{R}^{n+m-1}$, the problem becomes

$$\left\| \begin{bmatrix} A_0 & 0_{n\times(m-1)} \end{bmatrix} \begin{bmatrix} x \\ t \end{bmatrix} \right\|_2 \leq \begin{bmatrix} c^T & -\mathbf{1}^T \end{bmatrix} \begin{bmatrix} x \\ t \end{bmatrix} + d \tag{C.32}$$

$$\left\| \begin{bmatrix} A_1 & 0_{n\times(m-1)} \end{bmatrix} \begin{bmatrix} x \\ t \end{bmatrix} \right\|_2 \leq \begin{bmatrix} 0 & \mathbf{1}_1^T \end{bmatrix} \begin{bmatrix} x \\ t \end{bmatrix} \tag{C.33}$$

$$\vdots$$

$$\left\| \begin{bmatrix} A_{m-1} & 0_{n\times(m-1)} \end{bmatrix} \begin{bmatrix} x \\ t \end{bmatrix} \right\|_2 \leq \begin{bmatrix} 0 & \mathbf{1}_{m-1}^T \end{bmatrix} \begin{bmatrix} x \\ t \end{bmatrix} \tag{C.34}$$

where

$$\mathbf{1}_k^T = [\ 0 \quad \cdots \quad 0 \ \underbrace{1}_{k\text{-th}}\ 0 \quad \cdots \quad 0\ ]_{1\times(m-1)}$$

C.11 Input Shaper and Its Magnitude

It's been known that an input shaper with only positive (or only negative, to be mathematically complete) impulses has maximum magnitude of 1 while another with positive AND negative impulses produces amplification [27][1]. Here's why.

Given the input shaper constraint (DC gain constraint in Equation 4.40),

$$h_0 + h_1 + h_2 + \cdots + h_{N-1} = 1$$

An input shaper can be written as

$$h(t) \ = \ h_0 + \sum_{i=1}^{N-1} h_i \delta(t - iT_s)$$

[1]While this fact has been mentioned in numerous publications, no analytical proof was found, perhaps, because it's too simple to call it a proof. A simple analysis is given here for completeness.

Laplace transformed,

$$\begin{aligned} H(w)|_{s=jw} &= h_0 + \sum_{i=1}^{N-1} h_i e^{-s(iT_s)} \\ \|H(w)\| &= \|h_0 + \sum_{i=1}^{N-1} h_i e^{-s(iT_s)}\| \\ &\leq \|h_0\| + \sum_{i=1}^{N-1} \|h_i\| \|e^{-s(iT_s)}\| \\ &\leq \|h_0\| + \sum_{i=1}^{N-1} \|h_i\| \\ &= \sum_{i=0}^{N-1} \|h_i\| \end{aligned}$$

Therefore,

$$\|H(w)\| \leq \sum_{i=0}^{N-1} \|h_i\| = 1 \quad if \quad h_i \geq 0.$$

If h_i can be positive or negative, there is no bound on $\|H(w)\|$, and therefore, the can be larger than 1.

Bibliography

[1] *Automotive Handbook*. SAE Society of Automotive Engineers, Warrendale, PA, 3 edition, 1993.

[2] Annual Mobility Report. Technical report, Texas Tranportation Institute, 1999.

[3] Hong S. Bae and J. Christian Gerdes. Parameter estimation and command modification for longitudinal control of heavy vehicles. In *Proceedings of the International Symposium on Advanced Vehicle Control (AVEC)*, pages 114–121, 2000.

[4] Hong S. Bae and J. Christian Gerdes. Command modification using input shaping for automated systems with heavy trucks. In *Proceedings of the 2003 American Control Conference*, pages 54–59, 2003.

[5] Hong S. Bae, J. Ryu, and J. Christian Gerdes. Road grade and vehicle parameter estimation for longitudinal control using GPS. In *IEEE Conference on Intelligent Transportation Systems*, pages 166–171, 2001.

[6] S.P. Bhat and D. K. Miu. Precise point-to-point positioning control of flexible structures. *ASME Journal of Dynamic Systems, Measurement, and Control*, 112(4):667–674, December 1990.

[7] J. B. Bidwell. The Car-Road Complex Theory of Traffic Flow. In *Theory of Traffic Flow*, New York, 1961. Elsevier Publishing Co.

[8] S. Boyd. Ee364 convex optimization with engineering applications, 2003.

[9] Mireille Broucke and Varaiya Pravin. The Automated Highway System: A Transportation Technology for the 21st Century. In *Proceedings of the 13th World Congress of the International Federation of Automatic Control (IFAC)*, pages 141–146, 1996.

[10] R. J. Caudill and W. L. Garrard. Vehicle follower longitudinal control for automated transit vehicles. *ASME Journal of Dynamic Systems, Measurement, and Control*, 99(4):241–248, 1977.

[11] X. Chen and T. W. Parks. Design of FIR filters in the complex domain. *IEEE Transactions on Acoustics, Speech and Signal Processing*, 35(2):144–153, 1987.

[12] C. Chien and P. Ioannou. Automatic vehicle following. In *Proceedings of the 1992 American Control Conference, Chicago, IL*, pages 1748–1752, 1992.

[13] M. Druzhinina, L. Moklegaard, and A. Stefanopoulou. Compression braking control for heavy-duty vehicles. In *Proceedings of the American Control Conference*, pages 2543–2547, 2000.

[14] M. Druzhinina, L. Moklegaard, and A. Stefanopoulou. Speed gradient approach to longitudinal control of heavy duty vehicles equipped with variable compression brake. In *Proceedings of the International Symposium on Advanced Vehicle Control (AVEC)*, pages 98–105, 2000.

[15] S. Fiorentin. Sensors in automobile applications. research activity in the european prometheus program. In *Fisica e Tecnologia*, volume 12, pages 3–22, Turin, Italy, 1989. Electronic Systems, FIAT Research Centre. In Italian.

[16] W. L. Garrard, R. J. Caudill, A. L. Kronhauser, D. MacKinnon, and S. J. Brown. State-of-the-art of longitudinal control of automated guideway transit vehicles. *High Speed Ground Transportation Journal*, 12(4):35–68, 1968.

[17] W. L. Garrard and A. Kornhauser. Use of state observers in the optimal feedback control of automated transit vehicles. *ASME Journal of Dynamic Systems, Measurement, and Control*, 95(2):220–227, 1973.

[18] Arthur Gelb. *Applied Optimal Estimation.* Analytic Science Corporation, Cambridge, MA, 1974.

[19] Thomas D. Gillespie. *Fundamentals of Vehicle Dynamics.* Society of Automotive Engineers, Warrendale, PA, 1992.

[20] K. Glashoff and K. Roleff. A new method for Chebyshev approximation of complex-valued functions. In *Mathematics of Computation*, volume 36, pages 233–239, 1981.

[21] Hammache, Nick Stabile, Stefano Frascaroli, and Frederick Browand. Aerodynamic forces on truck models, including two trucks in tandem. Technical report, California PATH, Berkeley, California, 2001.

[22] J. K. Hedrick, V. K. Narendran D. H. McMahon, and D. Swaroop. Longitudinal vehicle controller design for ivhs systems. In *Proceedings of American Control Conference*, pages 3107–3112, 1991.

[23] J. K. Hedrick, M. Tomizuka, and P. Varaiya. Control issues in automated highway systems. In *IEEE Control Systems Magazine*, volume 14, pages 21–32, 1994.

[24] R. Herman and R. B. Potts. Single-Lane Traffic Theory and Experiment. In *Theory of Traffic Flow*, New York, 1961. Elsevier Publishing Co.

[25] R. Horowitz and P. Varaiya. Control design of an automated highway system. In *IEEE Proceedings*, volume 88, pages 913–925, 2000.

[26] International Organization for Standardization. *ISO 2631-1:1997 Evaluation of human exposure to whole-body vibration.*

[27] B. Whitney Rappole Jr., Neil C. Singer, and Warren P. Seering. Input shaping with negative sequences for reducing vibrations in flexible structures. In *Proceedings of the American Control Conference*, pages 2695–2699, 1993.

[28] Elliott D. Kaplan. *Understanding GPS: principles and applications.* Artech House, Inc., Boston, 1996.

[29] K. Koide and K. Kitoh. Trends of Automobile Information and Communication Systems. In *Systems, Control and Information*, volume 33, pages 321–328, 1989. In Japanese.

[30] Frank Lattemann, Konstantin Neiss, Thomas Connolly, and Stephan Terwen. The predictive cruise control. Technical report, DaimlerChrysler Research and Technology North America, Inc, 2003.

[31] Jack D. Leatherwood, Thomas K. Dempsey, and Sherman A. Cleveson. Design tool for estimating passenger ride discomfort within complex ride environment. *Human Factors*, 22(3):291–312, 1980.

[32] S. Y. Lim, H. D. Stevens, and J. P. How. Input shaping design for multi-input flexible systems. *ASME Journal of Dynamic Systems, Measurement, and Control*, 121(3):443–447, 1999.

[33] Dragos B. Maciuca and J. K. Hedrick. Brake dynamics effect on ahs lane capacity. In *SAE Systems and Issues in ITS (SP-1106)*, pages 81–86, 1995. SAE Paper No. 951929.

[34] D. H. McMahon, J. K. Hedrick, and S. E. Shladover. Vehicle modelling and control for automated highway systems. In *Proceedings of the 1990 American Control Conference, San Diego, CA*, pages 297–303, 1990.

[35] California State Department of Transportation. *Highway Design Manual*. Analytic Science Corporation.

[36] J. Ryu, E. J. Rossetter, and J. C. Gerdes. Vehicle Sideslip and Roll Parameter Estimation Using GPS. In *Proceedings of the International Symposium on Advanced Vehicle Control (AVEC)*, pages 373–380, 2002.

[37] S. Sheikholeslam and C. A. Dssoer. Longitudinal control of a platoon of vehicles. In *Proceedings of American Control Conference*, pages 291–297, 1990.

[38] S. E. Shladover. Longitudinal control of automated guideway transit vehicles within platoons. In *ASME Journal of Dynamic Systems, Measurement, and Control*, pages 302–310, 1978.

[39] S. E. Shladover. Longitudinal control of automotive vehicles in close-formation platoons. *ASME Journal of Dynamic Systems, Measurement, and Control*, 113:231–241, June 1991.

[40] N. Singer and W. Seering. An extension of command shaping methods for controlling residual vibration using frequency sampling. In *IEEE International Conference on Robotics and Automation*, volume 1, pages 800–805, 1992.

[41] N. Singer and W. Seering. Vibration reduction using multi-hump extra-insensitive input shapers. In *Proceedings of the 1995 American Control Conference, Seattle, WA*, volume 5, pages 3830–3834, 1995.

[42] N. Singer, W. Singhose, and E. Kriikku. An input shaping controller enabling cranes to move without sway. In *American Nuclear Society 7th Topical Meeting on Robotics and Remote Systems*, volume 1, pages 225–231, 1997.

[43] N. C. Singer and W. P. Seering. Preshaping command inputs to reduce system vibration. *ASME Journal of Dynamic Systems, Measurement, and Control*, 112:76–82, 1990.

[44] T. Singh and S. R. Vadali. Robust time-optimal control: A frequency domain approach. *AIAA Journal of Guidance, Control and Dynamics*, 17(2):346–353, Mar.-Apr. 1994.

[45] W. E. Singhose, W. P. Seering, and N. C. Singer. Residual vibration reduction using vector diagrams to generate shaped inputs. *Journal of Mechanical Design*, 116(2):654–659, June 1994.

[46] Society of Automotive Engineers, Warrendale, PA. *Vehicle Dynamics Terminology*, July 1976.

[47] Roy L. Streit and Albert H. Nuttall. A note on the semi-infinite programming approach to complex approximation. In *Mathematics of Computation*, volume 40, pages 599–605, 1983.

[48] D. V. A. H. G. Swaroop. *String Stability of Interconnected Systems: An Application to Platooning in Automated Highway Systems*. PhD thesis, University of California at Berkeley, 1994.

[49] M. Tomizuka. Advanced vehicle control systems (AVCS) research for automated highways systems in california path. In *Vehicle Navigation and Information Systems Conference*. IEEE, 1994.

[50] M. Tomizuka and J. K. Hedrick. Automated vehicle control for ivhs systems. In *Proceedings of the 12th Triennial World Congress of the International Federation of Automatic Control (IFAC)*, pages 109–112, 1994.

[51] T. D. Tuttle and W. P. Seering. A zero-placement technique for designing shaped inputs to suppress multiple-mode vibration. In *Proceedings of American Control Conference*, pages 2533–2537, 1994.

[52] Anthony Tzes and Stephen Yurkovich. An adaptive input shaping control scheme for vibration suppression in slewing flexible structures. *IEEE Transactions on Control Systems Technology*, 1(2):114–121, 1993.

[53] A. Vahidi, M. Druzhinina, A. Stefanopoulou, and H. Peng. Simultaneous mass and time-varying grade estimation for heavy-duty vehicles. In *Proceedings of the 2003 American Control Conference*, pages 4951–4956, 2003.

[54] Pravin Varaiya. Smart Cars on Smart Roads: Problems of Control. In *IEEE Transactions on Automatic Control*, volume 38, pages 195–207, 1993.

[55] Charles Vlcek, Patricia McLain, and Michael Murphy. GPS/Dead Reckoning for Vehicle Tracking in the Urban Canyon Environment. In *IEEE-IEE Vehicle Navigation & Information Systems Conferences*, pages A34–A41, 1993.

[56] Rudi Vuerinckx. Design of high-order Chebyshev FIR filters in the complex domain under magnitude constraints. *IEEE Transactions on Signal Processing*, 46(6):1676–1681, 1998.

[57] D. E. Whitney and M. Tomizuka. Normal and emergency control of a string of vehicles by fixed reference sampled-data control. In *IEEE Transactions on Vehicular Technology*, volume VT-21, pages 128–138, 1972.

[58] B. Wie, R. Sinha, and Q. Liu. Robust time-optimal control of uncertain structural dynamic systems. *AIAA Journal of Guidance, Control and Dynamics*, 16(5):980–983, Sep.-Oct. 1993.

[59] S. Wu, S. Boyd, and L. Vandenberghe. FIR filter design via semidefinite programming and spectral factorization. In *IEEE Conference on Decision and Control*, volume 1, pages 271–276, 1996.

[60] M. Wurtenberger, St. Germann, and R. Isermann. Modeling and parameter estimation of nonlinear vehicle dynamics. *ASME Transportation Systems*, 44:53–63, 1992.

[61] D. Yanakiev and I. Kanellakopoulos. Speed tracking and vehicle follower control design for heavy-duty vehicles. *Vehicle System Dynamics*, 25:251–276, 1996.

[62] D. Yanakiev and I. Kanellakopoulos. Nonlinear spacing policies for automated heavy-duty vehicles. *IEEE Transactions on Vehicular Technology*, 47(4):1365–1377, 1998.

[63] Michael Zabat, Nick Stabile, Stefano Frascaroli, and Frederick Browand. The aerodynamic performance of platoons: Final report. Technical Report UCB-ITS-PRR-95-35, California PATH, Berkeley, California, 1995.